

493573

JPL Publication 92-29

The Goldstone Solar System Radar

A Science Instrument for Planetary Research

J. D. Dvorsky
N. A. Renzetti
D. E. Fulton

(NASA-CR-192793) THE GOLDSTONE
SOLAR SYSTEM RADAR: A SCIENCE
INSTRUMENT FOR PLANETARY RESEARCH
(JPL) 128 p

N93-22478

Unclass

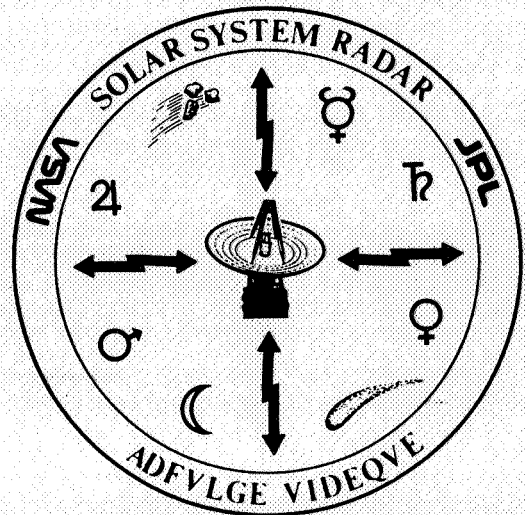
G3/32 0154768

December 15, 1992



National Aeronautics and
Space Administration

Jet Propulsion Laboratory
California Institute of Technology
Pasadena, California



The Goldstone Solar System Radar

A Science Instrument for Planetary Research

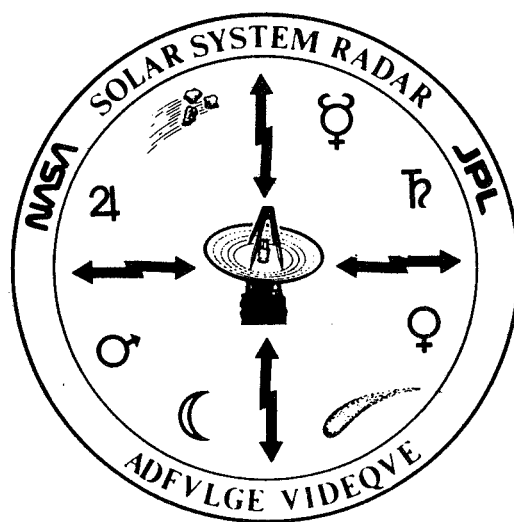
J. D. Dvorsky
N. A. Renzetti
D. E. Fulton

December 15, 1992



National Aeronautics and
Space Administration

Jet Propulsion Laboratory
California Institute of Technology
Pasadena, California



The research described in this publication was carried out by the Jet Propulsion Laboratory, California Institute of Technology, under a contract with the National Aeronautics and Space Administration.

Reference herein to any specific commercial product, process, or service by trade name, trademark, manufacturer, or otherwise, does not constitute or imply its endorsement by the United States Government or the Jet Propulsion Laboratory, California Institute of Technology.

Preface

This report describes the current status of the radar instrument as it is being operated for planetary research: what is there, how it works, and what the products are. It also describes how these products are used by planetary researchers in increasing our knowledge of the objects of the solar system. Finally, there is a complete bibliography of papers presented by principal investigators whose research depended on data from this instrument. These papers have been published in open literature in refereed journals.

Acknowledgements

This author is grateful to the following JPL and contractor personnel: N. A. Renzetti, for initiating the project, defining the contents, guidance, and general support; M. A. Slade, for providing much source material, guidance, and editing help; D. Fulton, for many helpful suggestions for the writing and final form of the report; R. F. Jurgens, for helpful discussions and editing of Chapters III and IV—Section VI.2 is based on his work; S. J. Ostro, for much source material and editing help on Chapter V; and D. Hills for guidance, interesting discussions, and an orientation to Goldstone. L. Robinett helped with Chapter VI; D. Howard explained GSSR ranging system software designs in Chapter IV; P. Priest wrote source material for Chapters IV and VI; H. Cox was helpful with specifications; the Radio Astronomy and Radar Group at the Mars station, including R. Genzmer, R. Winkler, and P. Dendrenos, explained workings of the instrument while actually tracking an asteroid. T. Tesarek and R. Rose at the Goldstone site were helpful. I am grateful to V. Piette for help in network computing and L. Rivas, J. Hoeptner, and D. Worthington for secretarial help; C. Waff kindly provided access to his DSN historical library. Others in the Telecommunications and Data Acquisition (TDA) organization were very helpful in providing explanations and answering many questions.

J. D. Dvorsky
November, 1992

Abstract

The Goldstone Solar System Radar (GSSR) station at NASA's Deep Space Communications Complex in California's Mojave Desert is described. A short chronological account of the GSSR's technical development and scientific discoveries is given. This is followed by a basic discussion of how information is derived from the radar echo and how the raw information can be used to increase understanding of the solar system. A moderately detailed description of the radar system is given, and the engineering performance of the radar is discussed. The operating characteristics of the Arecibo Observatory in Puerto Rico are briefly described and compared with those of the GSSR. Planned and in-process improvements to the existing radar, as well as the performance of a hypothetical 128-m-diameter antenna radar station, are described. A comprehensive bibliography of refereed scientific and engineering articles presenting results that depended on data gathered by the instrument is provided.

Contents

I. Introduction	1
II. Evolution of the GSSR	4
II.1 General	4
II.2 The First Goldstone Deep Space Station	4
II.3 The Echo Deep Space Station	5
II.4 The Beginnings of Radar Astronomy	5
II.5 Early Radar Contacts with Venus	6
II.5.1 Considerations in Making the Attempt	6
II.5.2 First Venus Radar Experiments Attempted	7
II.5.3 Results of the First Venus Experiments	8
II.5.4 Early Venus Experiments Continue	9
II.6 Construction of the Research and Development Station	10
II.7 Design, Construction, and Development of the 64-m Antenna Station	10
II.8 Further Improvements to the Radar	11
II.9 Further Observations of Venus	12
II.10 Observations of Mars	13
II.11 Observations of Mercury	14
II.11.1 The Physical Planet	14
II.11.2 Mercury and Tests of Theory	15
II.12 Observations of Jupiter and the Galilean Satellites	16
II.13 Observations of Titan and the Rings of Saturn	16
II.14 Observations of Asteroids	17
III. Application of Radar to the Observation of Solar System Objects	19
III.1 General	19
III.2 Parameters of the Radar Echo that are Examined	21
III.2.1 Amplitude	21
III.2.2 Doppler Frequency	24
III.2.3 Time Delay (Range)	28
III.2.4 Polarization	31
III.2.5 Radar Cross Section σ	33
III.2.5.1 General	33
III.2.5.2 Directivity	34
III.2.5.3 Backscatter Function	35
III.2.5.4 Reflectivity and the Dielectric Constant	35
III.3 Applications of the Measured Data	36
III.3.1 Ephemerides	36
III.3.2 Surface Characteristics, Topography, and Radar Maps	39
III.3.3 Bulk Density and Porosity	39
III.3.4 Spin Vectors	40
III.3.5 Observations of Multiparticle Systems	42

IV. GSSR Present Capabilities and Performance	44
IV.1 General	44
IV.2 Modes of Operation	46
IV.2.1 Continuous Wave	46
IV.2.1.1 Continuous Wave, Narrow Bandwidth	47
IV.2.1.2 Continuous Wave, Medium Bandwidth	47
IV.2.1.3 Continuous Wave, Wide Bandwidth	48
IV.2.2 Binary Phase Coded	48
IV.2.3 Monostatic	48
IV.2.4 Bistatic and Multistatic Operation	48
IV.2.4.1 General	48
IV.2.4.2 Echo Station	50
IV.2.4.3 Venus Station	50
IV.2.5 Goldstone/Very Large Array Collaboration	50
IV.3 Transmitter	51
IV.3.1 Exciter	51
IV.3.2 Final Amplifier	54
IV.3.3 Power Supply	57
IV.3.3.1 Motor Generator	57
IV.3.3.2 Transformer/Rectifier	57
IV.3.3.3 Filter	57
IV.3.3.4 Crowbar	57
IV.3.4 Heat Exchanger	57
IV.4 Antennas	58
IV.4.1 General	58
IV.4.2 Main Reflector	59
IV.4.3 Subreflector	60
IV.4.4 Antenna Pointing Subsystem	60
IV.5 Receiver	61
IV.5.1 Receiver Subsystem	61
IV.5.2 Microwave Subsystem (Receive)	61
IV.5.3 Front-End Modules	65
IV.5.4 Intermediate Frequency Stages	66
IV.5.5 Ephemeris Tuning and Local Oscillators	67
IV.5.6 Instrumentation	68
IV.6 Data Acquisition Subsystem	68
IV.6.1 General	68
IV.6.2 Monitor and Control	70
IV.6.3 Complex Mixers	70
IV.6.4 Programmable Local Oscillator Frequency Setting	70
IV.6.5 Binary Phase-Coded Modulation and Demodulation	72
IV.6.5.1 Generation and Use of Binary Phase-Coded Signals	72
IV.6.5.2 Demodulation (Ranging)	73
IV.6.6 Frequency Hopping	75
IV.6.7 Signal Processing	75
IV.6.7.1 Low-Pass and Band-Pass Filtering	75
IV.6.7.2 Analog-to-Digital Conversion	76

IV.6.7.3 Range Gate Processing	76
IV.6.7.4 Doppler Processing	77
IV.6.8 Data Display	78
IV.6.9 Data Recording	78
IV.6.9.1 VAX	78
IV.6.9.2 Personal Computer	79
IV.7 Frequency and Time References	79
V. The Arecibo Observatory: Performance and Comparison with the GSSR	82
V.1 General	82
V.2 Location	82
V.3 Main Antenna	82
V.4 Transmitter and Receiver	84
V.5 Data Acquisition System	85
V.6 Interferometry	85
V.7 Comparison with GSSR	85
VI. Future Capabilities	88
VI.1 Planned and Possible Upgrades to the Existing Radar Instrument	88
VI.1.1 General	88
VI.1.2 Single-Horn Switch	88
VI.1.3 Megawatt Transmitter at 3.5-cm Wavelength	90
VI.1.4 Data Acquisition System Upgrade	90
VI.1.5 GSSR Receiver Upgrade	90
VI.1.6 Programmable Local Oscillator	91
VI.2 Stand-Alone Radar System	92
VI.2.1 General	92
VI.2.2 Antenna	93
VI.2.3 Transmitter	94
VI.2.4 Receiver	95
VI.2.4.1 Sensitivity	95
VI.2.4.2 Bandwidth	95
VI.2.5 Data Acquisition System	96
VI.2.5.1 Continuous Wave	96
VI.2.5.2 Delay-Doppler Mapping	96
VI.2.6 Time Stability	97
VI.2.7 Frequency Stability	98
VI.2.8 Phase Stability	98
VI.2.9 Optimal Wavelength of Operation	99
VII. Conclusion	100
VIII. References	101
IX. Bibliography	105

IX.1 Mercury	105
IX.2 Venus	105
IX.3 Moon	109
IX.4 Mars	109
IX.5 Asteroids	112
IX.6 Jupiter and the Galilean Satellites	114
IX.7 Saturn's Rings and Moons	114
IX.8 Comets	114
IX.9 General	115

Tables

1. Goldstone Deep Space Station Inventory	3
2. System Parameters for the First JPL Radar Detection of Venus	8
3. Observations by GSSR	18
4. Echo Station Performance (34-m Antenna)	50
5. Venus Station Performance (26-m Antenna)	51
6. Transmitter Performance	54
7. Antenna Performance	58
8. Receiver Performance	62
9. Data Acquisition Subsystem Performance	71
10. Pseudonoise Code Example	74
11. Radar Parameters: Arecibo and Goldstone	86
12. Existing and Proposed Radar Systems Performance	93

Figures

1. The Goldstone 70-m Antenna	2
2. Inferior and Superior Conjunctions	7
3. Tricone Assembly	11
4. Radar Observables	22
5. Specular and Diffuse Echoes	24
6. Constant Doppler Regions	25
7. Polar and Equatorial Aspects	26
8. Tracking a Surface Feature	27
9. Ranging	28
10. Constant Range Rings	29
11. North-South Ambiguity	30
12. Echoes in Two Polarizations	31
13. GSSR System Functions and Interfaces	45
14. Interferometry	49
15. Very Large Array	52
16. Transmitter Subsystem Functions and Interfaces	53
17. The 3.5-cm-Wavelength Klystron	55
18. Final Amplifier Control Panel	56

19. Cassegrain Configuration	59
20. Microwave Subsystem Functions and Interfaces	63
21. The 3.5-cm-Wavelength Maser Under Test	64
22. Radar Control Room	69
23. Complex Mixer	72
24. Transmitter Modulation	73
25. Autocorrelation	75
26. Butterfly	78
27. Data Reduction and Analysis at JPL	79
28. The Arecibo Observatory	83
29. Single-Horn Switch	89

I. Introduction

The Goldstone Solar System Radar (GSSR), managed by the Jet Propulsion Laboratory of the California Institute of Technology, is one of the most sensitive radar installations in the world. It shares some of the equipment and facilities of the Goldstone Deep Space Communications Complex, one of the three complexes of the Deep Space Network. This Network provides Earth-based two-way communications capabilities for all of NASA's lunar, planetary, and interplanetary spacecraft, and in recent years, for those of the European, Japanese, and Russian space agencies. The Goldstone Complex is located in the Mojave Desert in Southern California, about 72 km north of Barstow on land leased from the U.S. Army on the Ft. Irwin military reservation.

The GSSR originated in 1958 with initiation of the space program under NASA. In particular, NASA funded a technology development program recognizing that planetary research would require a state-of-the-art two-way communications capability on Earth. This technology development by JPL, universities, and industry made use of natural solar system objects to advance such elements of communication technology as low-noise amplifiers, high-power transmitters, and signal processing equipment. In carrying out field experiments at Goldstone, technology development had the benefit of the antennas required by the Deep Space Network for such efforts as Project Echo, which required a high-power transmitter to perform its experiment. The NASA Office of Tracking and Data Acquisition, now known as the Office of Space Communications, provided the funding for this technology development; for many years this made it possible for the Deep Space Stations to achieve the state of the art of telecommunications. One of the natural targets for this development was the Planet Venus. Many radar installations around the world competed to be the first to detect an echo from Venus; however, it was the Goldstone radar that achieved this first.

Over the next few years subsequent to these experiments, it became obvious to the NASA science community that this instrument could provide some of the information needed to design spacecraft missions to the planets, their satellites, and comets. As sensitivity of the instrument grew, asteroids were added to the list of targets. NASA began to fund scientific investigators who, in turn, brought continuing requirements for new capabilities; these will be discussed in Chapter VI. Thus, radar observations of the objects of our solar system have become an integral part of NASA's exploration program. In addition to sponsoring Goldstone, NASA in the early 1970s funded the implementation of radar capability for planetary research at the Arecibo Observatory in Puerto Rico, and this installation will be discussed in Chapter V.

The center of planetary radar activity at Goldstone is the Mars station, which consists of a 70-m-diameter parabolic reflector antenna (Figure 1), two high-power transmitters, sensitive receivers, and recording and signal processing equipment. The 70-m station can be used alone as a radar telescope, or it can be used in conjunction with other stations at the Goldstone complex that are within tens of miles (Table 1) to perform radar interferometry experiments. The station also can be used with other observatories including the National Radio Astronomy Observatory's Very Large Array in Socorro, New Mexico; the National Astronomy and Ionosphere Center's Arecibo Radio Observatory; or the Owens Valley, California, facility of Caltech.

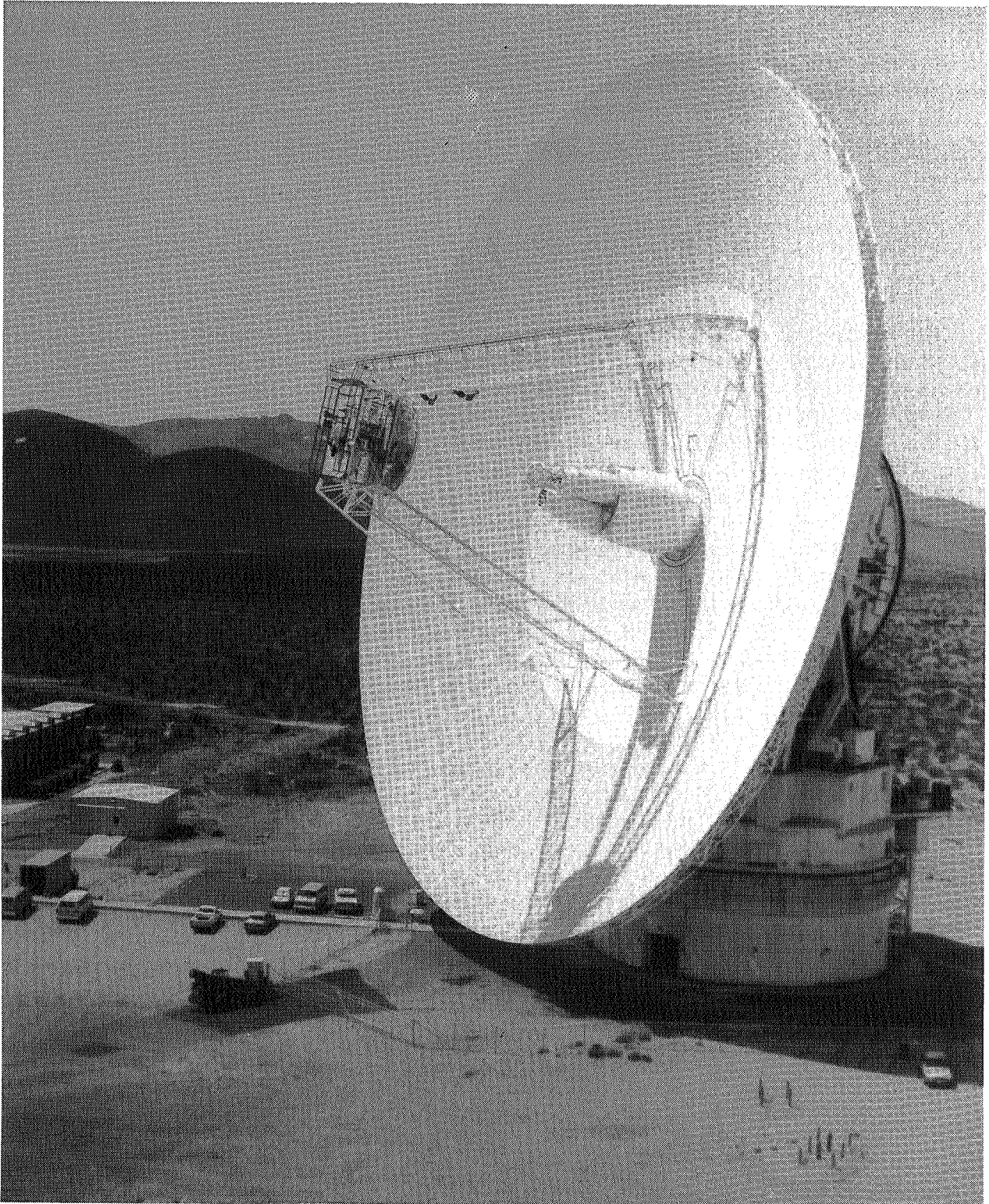


Figure 1. *The Goldstone 70-m Antenna*

Table 1. Goldstone Deep Space Station Inventory

Deep Space Station number (name)	Antenna diameter, m (ft)	Mount
12 (Echo) ^a	34 (111)	Equatorial
13 (Venus standard) ^a	26 (85)	Azimuth-elevation
13 (Venus beam waveguide) ^a	34 (111)	Azimuth-elevation
14 (Mars)	70 (230)	Azimuth-elevation
15 (Uranus) ^b	34 (111)	Azimuth-elevation

^aUsed as a receive-only station for interferometry.
^bUsed for near-Earth Orbital Debris Radar (Subsection IV.2.1.1).

In addition to use of the equipment and facilities while at the Goldstone Complex, experimenters can conduct experiment design and antenna pointing at JPL in Pasadena or at the home institution of the principal investigator (PI). Because an experiment performed at Goldstone culminates in data recorded on magnetic tape, analyses of these data also can be carried out at JPL, Pasadena, or at the home institution of the PI.

NASA and JPL encourage the use of the GSSR for radar astronomy in making direct contributions to our knowledge of the solar system objects and for contributing to the design of spacecraft to be deployed to the vicinity of these objects. To enable this activity, the JPL staff includes a Friend of the Radar who, while personally carrying out radar observations, is available to assist guest investigators with technical advice and support. Also, the Operations Organization includes a radar astronomy support staff to assist with the preparation of proposals, scheduling of the experiments, and assignment of Goldstone staff to aid the PI in conducting his experiment.

In addition to providing certain elements of the radar instrument at Goldstone, the Deep Space Network, itself, is a world-class scientific instrument in the following fields: radio astronomy, celestial mechanics, tests of general relativity, and the detection of gravitational waves. Also, because the Network sites include Global Positioning System instrumentation and very long baseline interferometry instrumentation, it makes direct contributions to Earth science—namely, data in support of plate tectonic models of the Earth.

II. Evolution of the GSSR

II.1 General

Continual evolution and the pursuit of higher performance characterize the GSSR, which is on the frontier of technology and will continue this tradition in the future. The discoveries of the GSSR since its inception in 1961 are numerous, and only a few are mentioned here; Chapter IX provides a greater list of sources.

II.2 The First Goldstone Deep Space Station

The beginning of the Goldstone Deep Space Station complex was the direct result of a decision by the Advanced Research Projects Agency (ARPA) in the spring of 1958 to launch several Pioneer spacecraft to the Moon by the end of that year. The U. S. Army had overall responsibility for the newly founded Pioneer Program and turned to its long-time contractor, JPL, for the payloads and the tracking and data acquisition facilities.

The signal from the Pioneer spacecraft would be weak because its flight path would carry it 240,000 mi from Earth. For this reason, the key piece of equipment required to successfully track and receive signals from the spacecraft on its way to the Moon was a large, paraboloidal antenna. Goldstone was the site selected for the location of this antenna station, which was named the Pioneer Station.

Because of the accelerated schedule of Pioneer, JPL searched for an existing design of a very large paraboloidal antenna that could be erected quickly, i.e., within 6 months. The search was successful; an antenna very similar to the one needed had been under development for more than 5 years. The design concept started at the Naval Research Laboratory, with assists from the Carnegie Institute and the Associated Universities, and had already been completed by the Blaw-Knox Company. The existing design was intended for application to the field of radio astronomy, a discipline that was rapidly expanding in the 1950s.

Since the antenna was to be used for the precise tracking of interplanetary spacecraft, several important modifications to the existing radio-astronomy antenna were required. The antenna's sidereal drive, useful for tracking celestial objects with slow angular movement, was replaced with a closed-loop continuous-tracking system required for the faster angular motions of spacecraft. Furthermore, a feed system had to be installed, and the antenna had to be "ruggedized" to operate continuously for many hours under high desert winds and temperatures. Finally, a system of antenna-pointing feedback in the form of digitized angles had to be provided; these would, in turn, be teletyped to a waiting computer in Pasadena for trajectory computations.

When setting up the overall communications system for Pioneer, an important choice was the frequency of operation. The frequency range of 950 to 10,000 MHz is desirable for operation of satellite communications systems because the galactic background noise is lowest in this range. Furthermore, use of the higher frequencies yields improved performance, such as increased antenna gain and narrower beamwidths. Experience

gained from the Explorer satellites reinforced this concept. An operating frequency of 960 MHz, compatible with the existing antenna design, was chosen.

In June 1958, construction began on an antenna with a 26-m (85-ft) diameter, a paraboloidal shape, an hour-angle/declination mount, a surface contour tolerance of ± 0.32 cm, and a narrow beamwidth of 0.1 deg. By December, the first Deep Space Station at Goldstone, the Pioneer Station, was complete. The station tracked and acquired telemetry from several Pioneer spacecraft.

The station was used for many other purposes until its deactivation in 1981, and has been designated a National Historic Landmark by the U. S. Department of the Interior.

II.3 The Echo Deep Space Station

A decision was made in the late 1950s that JPL would participate in the Echo communications research project, which was to establish a communications link from Bell Telephone Laboratories in Holmdel, N. J., to Goldstone via an orbiting, 30.5-m, reflecting balloon. A new ground-based, high-power transmitter was required.

Hence, a second Goldstone tracking station, designated Echo, was designed to include a 13-kW, 2388-MHz transmitter and a 26-m parabolic antenna with an azimuth-elevation mount for additional flexibility. The station was to be located about 11 km from the existing Pioneer tracking station where it would be isolated from the Pioneer Station by hills. Construction of the new station was completed in December 1959. A 2388-MHz receiver was added to the Pioneer Station, and a ground-based microwave link was set up between the Pioneer Station and the Echo Station. This two-station configuration formed a bistatic radar (Subsection IV.2.4.1), and the system began operation in April 1960 (Renzetti, 1971).

The first of two Echo orbiting balloons was launched on August 12, 1960, and experiments soon began. The Echo Station beamed signals to the balloon and both the Pioneer Station and Holmdel received echoes. This was the first use of Goldstone radar for a scientific purpose.

In 1961, the Echo antenna was moved to a new area at Goldstone, the Venus Research and Development Station. As a replacement, a new 26-m-diameter antenna with equatorial mount and high tracking rate was constructed at the Echo site where it remains to this day.

II.4 The Beginnings of Radar Astronomy

In 1926, the first radar ionospheric soundings were performed, six years before Karl G. Jansky, an American who is considered the father of radio astronomy, discovered radio signals of extraterrestrial origin (Green and Pettengill, 1960).

On January 10, 1946, the U. S. Army Signal Corps used radar technology developed during World War II to detect echoes with a 2.5-s delay from the Moon at a distance of 240,000 mi (Dewitt and Stodola, 1949). The transmitter at the Evans Signal Laboratory

in New Jersey used a frequency of about 111.5 MHz and transmitted pulses with a peak power of 3000 W. A group in Hungary also performed similar experiments and detected echoes on February 6, 1946 (Bay, 1947). These experiments used a pulsed radar with a peak power of 3000 W at 2.5-m wavelength.

The investigators were puzzled by a rapid fading of the echoes. This was later discovered to be the result of changing interference from simultaneous echoes from different regions on the Moon (multipath). They also noticed a slower fading, where the signal disappeared for minutes at a time, and observed that the fading was dependent on the signal's polarization. This fading was found to be the result of Faraday rotation as the signal passed through Earth's ionosphere (Subsection III.2.4).

The technical capability to detect lunar echoes had been demonstrated; however, its only application during the years 1946 through 1956 was the experimental use of the Moon as a passive reflector in communication systems. It was not until the mid-1950s that the radar was used for purely scientific lunar experiments.

In 1952, an Australian radio astronomer wrote the first serious technical discussion of planetary radar (Kerr, 1952). In April 1959, a team headed by V. R. Eshelman at Stanford University detected radar echoes from the Sun.

II.5 Early Radar Contacts with Venus

II.5.1 Considerations in Making the Attempt

Even though echoes from the Moon had been detected in 1946, it was not until 1961 that radar systems had improved enough to obtain echoes from a planet. Construction of a sufficiently large antenna was the delaying factor. Venus is the closest target after the Moon and for this reason was the first planet observed by radar. There were many unanswered questions about Venus because its surface is always obscured by a dense cloud cover, and optical observations of surface features are impossible.

Even at its closest approach to Earth, Venus is still 100 times more distant than the Moon and 10 million times more difficult to detect than the Moon, based on distance alone.

Scientists realized that a significant factor in detection was the time at which an observation was made because the planets are moving targets and the distance varies. The relative positions of the planets in their orbits are important to radar detection because the strength of the echo depends on the inverse fourth power of the planet's distance (Section III.1). Venus is in inferior conjunction (Figure 2) with the Earth about every 19.2 months; the planet is roughly 1000 times more difficult to detect at its furthest point than at inferior conjunction.

While the most important parameter for determining detectability of a radar target is distance, other factors affect detectability. For instance, a larger target produces a stronger echo: the diameter of Venus is $3\frac{1}{2}$ times that of the Moon, so the ratio of the reflecting areas of the two bodies is 10:1. However, the atmosphere of Venus is

absorptive of the radar signal, and this effect increases with increasing frequency.

At about the time the Echo Station was constructed at Goldstone, it was realized that the requirements for a system for spacecraft telecommunications and data acquisition are very similar to those for a planetary radar system: large-aperture antennas, high-efficiency/low-noise feeds, very low-noise receivers, very high-power transmitters, signal processing technology, ultrastable frequency and time references, and ranging systems.

In planning interplanetary spacecraft missions for the early 1960s, JPL recognized that accurate knowledge of the *astronomical unit* (AU, the mean distance from the Sun to the Earth) and predictions of the positions of the planets (*ephemerides*) would be essential to spacecraft navigation. With this in mind, JPL investigated upgrading the Pioneer and Echo Stations to allow indirect AU and ephemerides measurements by conducting radar experiments with Venus. Most of the needed capability was already in place.

II.5.2 First Venus Radar Experiments Attempted

Other scientific groups were also working on the problem. After extensive analysis, Lincoln Laboratory of the Massachusetts Institute of Technology decided that an attempt to transmit and detect radar echoes was justified. On February 10 and 12, 1958, the attempt was made; at first it was thought that a weak detection, barely exceeding the noise, was achieved. Similar attempts were made in March of 1959, but no echoes were detected (Pettengill, 1965). Evans and Taylor of Jodrell Bank Experimental Station of the University of Manchester, England, reported a successful detection during 1959 that agreed with the Lincoln Laboratory 1958 result. However, it was later determined that these results were spurious (Pettengill, 1965).

Venus was again in inferior conjunction in the spring of 1961, and back at Goldstone, the 12.6-cm wavelength bistatic radar was turned toward the planet. The first interplanetary radar system of JPL consisted of the 2388 MHz, 13-kW transmitter at the Echo Station and a receiver operating at the same frequency at the Pioneer Station. A signal was transmitted on March 10, and unmistakable echoes were detected; from these echoes, the range to the planet was determined to within ± 500 km, and the frequency shift due to Doppler effect was measured. Also, the overall radar cross section was determined to be 11% (Subsection III.2.5.1). In 1961, JPL's radar could track Venus for only several months out of 19 months; better performance was required to reach superior conjunction. The specifications of JPL's first planetary radar are given in Table 2.

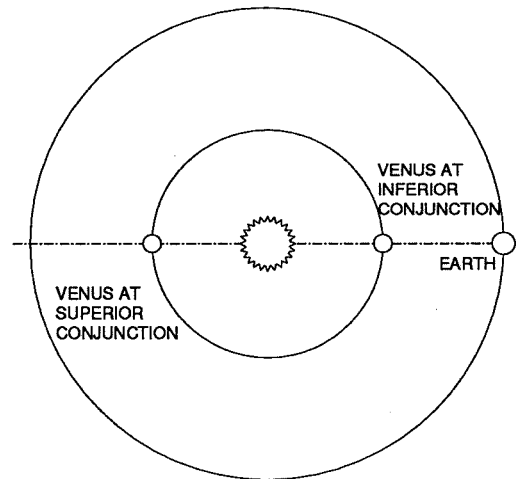


Figure 2. Inferior and Superior Conjunctions

Table 2. System Parameters for the First JPL Radar Detection of Venus

Parameter	Value
Transmitter power, kW	13
Transmitter antenna gain, dB ^a	53.4
Receiver noise temperature, K	64
Receiver postdetection integration time, s	68
Power intercepted by Venus, dBm	40.5
Distance to Venus, km	58×10^6
Typical receiver input, W	10^{-20}
Frequency, MHz	2388
Antenna diameter, m	26
Receiver antenna gain, dB	53.4
Receiver threshold, dBm	-181
Typical signal-to-noise ratio, dB	11

^aA quantity or ratio expressed in *decibels (dB)* is $10 \log_{10} (x/y)$ and is a convenient way to express ratios of extremely large or small numbers.

During these experiments, continuous-wave mode (Subsection IV.2.1) was used with a radiometer (Subsection III.2.1), spectrum analyzer, amplitude-modulated ranging, and ephemeris tuning (Subsection IV.6.4). A pseudorandom binary code was used for ranging, in contrast to the ranging used by some other investigating groups, which preferred pulsed radar (Subsection IV.6.5.1). In one set of observations, the radar system was used in a manner similar to that of a switched radiometer of the type used in radio astronomy, except that the transmitter and not the receiver was switched on and off. This enabled the experimenters to measure the difference between noise and signal plus noise, thus cancelling systematic errors.

Other scientific groups were also ready in 1961 and radar observations of Venus were made by Lincoln Laboratory, Jodrell Bank Observatory, a USSR tracking station in the Crimea, and RCA Corporation.

II.5.3 Results of the First Venus Experiments

In addition to measuring time delay and Doppler shift, a radar wave polarization reversal test was performed. By examining the echo power returned at the same and opposite polarizations and comparing these data with those from the Moon, scientists were able to determine that the surface variability and roughness of Venus were

comparable to those of the Moon. From these early data, it was concluded that the smoothest surfaces yield the strongest echo.

During the 1961 Venus experiments, JPL was the only one of the five radar observatories to use two antennas. This was an advantage because the transmitter was not shut down during listening periods and thus in a given time provided twice the amount of data obtainable with a single antenna system.

In the course of the 1961 experiments, the figure of merit, C (Equation (1)), was developed as a way to evaluate radar systems.

$$C = \frac{PGA}{T\sqrt{F}} \quad (1)$$

where

P = transmitter power, W

G = antenna gain

A = receiver aperture, m^2

T = system temperature, K

F = frequency, MHz

For the first Venus radar experiments, $C = 3 \times 10^8$. As a comparison, the figure of merit was $C = 100$ for the radar system used by the Army Signal Corps for the first Moon detections.

The most important new result from the 1961 experiments, besides showing that contact could be made, was the determination of the AU from radar measurements of the range and Doppler shift of the Venus echoes. The AU was determined to be 98,500 km greater than the accepted, optically measured value of about 149,500,000 km. If the optically measured value had been used to navigate the Mariner 2 spacecraft to Venus in 1962, no encounter with the planet would have occurred; the GSSR range and Doppler measurements contributed to the success of this mission.

II.5.4 Early Venus Experiments Continue

JPL continued the Venus radar observations at the next inferior conjunction, and in November 1962, the Goldstone Deep Space Instrumentation Facility (DSIF), as the Goldstone Complex was now called, needed one of the 26-m antennas to track Mariner 2 to Venus. The figure of merit for the radar was $C = 6 \times 10^8$; computer processing was used, and delay-Doppler maps were formed. From October to December 1962, almost 2000 runs were made. (A "run" is a sequence consisting of the transmitter *on* for the round-trip light time, followed by the receiver *on* for the same time.) Estimates of the spin rate of the planet were made, leading to the surprising discovery that the rotation was slow and retrograde (opposite to that of Earth) with a period of roughly 240 days.

In anticipation of higher performance requirements for spacecraft telecommunications systems, technical improvements were being implemented at Goldstone. By 1964, stable rubidium atomic time references were available at all Goldstone antenna stations; stable time and frequency references are necessary for navigation of spacecraft. Also significant is that before the end of 1965, all operations had adopted the 12.6-cm wavelength.

II.6 Construction of the Research and Development Station

The Venus 26-m-diameter antenna station (built around the antenna moved from the Echo site) was operational in August of 1962, and final construction was complete in November of that year. The primary purpose of this station was (and still is) to serve as a laboratory for the development of advanced communications systems, rather than a telecommunications and data acquisition link with spacecraft.

Before the end of 1963, a 100-kW transmitter was operating at 12.6-cm wavelength at the Venus site. Functioning as a monostatic radar, this 26-m-antenna station has been used to observe the planets. The station also has been used as a receiving site in bistatic and tristatic experiments.

II.7 Design, Construction, and Development of the 64-m Antenna Station

The 26-m-diameter antennas in use at the Pioneer and Echo Stations were adaptations of antennas originally designed for radio astronomy. In about 1960, NASA along with JPL began studies to determine the size and performance requirements for an antenna specifically designed for deep space tracking and data communications. The types of antennas considered were steerable paraboloids, fixed dishes with moveable feeds, and numerous small dishes connected so that their signals could be added. The result of the trade-off studies, known as the Advanced Antenna System (AAS), showed that antenna diameters in the 55- to 75-m-diameter range were the most cost effective and near optimum for communications with spacecraft within the solar system.

In 1962, JPL released to industry a proposal for a 64-m-diameter antenna. Blaw-Knox performed the conceptual design, while Rohr Corporation did the detailed design and began construction at the Goldstone Mars site in late 1963. The first signals detected by the 64-m antenna were from the Mariner 4 spacecraft on its way to Mars; this detection occurred on March 16, 1966. Formal dedication of the antenna came on April 29, 1966. The new antenna was fully operational in May and provided support for the Pioneer VII spacecraft, launched into a heliocentric orbit in August 1966.

The 64-m antenna, built with a focal-length-to-diameter ratio of 0.42, was by design a more rigid structure than the usual radio-astronomy antenna. The construction was rigid and precise enough to be effective at 15 GHz, unusual for an antenna of this size. Rigidity is important because antennas used for spacecraft communications must be ready to send commands to the spacecraft for crucial mission events, such as navigation maneuvers, regardless of wind and weather conditions. Another basic difference between radio-astronomy antennas and the 64-m dish is the dish's fast slew rate—usually unnecessary in radio astronomy, where the antenna need only track the relatively slow target motion caused by the Earth's rotation. These features increase the value of the

spacecraft-antenna stations for planetary radar use, because the rigidity maintains antenna performance in windy conditions, and a higher slew rate is advantageous for certain radar functions, such as switchover from communications to radar operation.

Although there are commonalities, some equipment at the station is user specific, i.e., planetary radar requires hardware different than that needed for DSN communications. Initially, the changeover from one use to another was accomplished by a time-consuming removal and replacement of the equipment in the feedcone.

In the late 1960s, a need to accelerate the slow changeover process gave rise to the concept of the *tricone*—three conical structures at the center of the antenna dish, each containing user-specific equipment, such as the transmitter and low-noise receiver (Figure 3). The switch from one wavelength to another, or from planetary radar use to DSN use, could now be done by moving the subreflector via a motorized drive, thus completing the switch in much less time (Subsection IV.4.3). A tricone containing a new 400-kW transmitter was constructed at the Mars Station in 1970.

The Mars Station became the center of planetary radar activity at Goldstone. Because of its high performance, the antenna was in demand for telecommunications and data acquisition with the most distant interplanetary spacecraft, for radio astronomy, and for planetary radar.

II.8 Further Improvements to the Radar

By 1982, Mercury, Venus, Mars, the Galilean satellites of Jupiter, Saturn's rings, and a dozen asteroids had been observed by GSSR. By the same year, sensitivity had increased by 10^{12} over the first lunar radar experiment performed by the Army Signal Corps, this due to larger antenna sizes and tighter surface tolerances, lower noise receiving systems, more powerful transmitters, and superior digital signal processing.

From September 1987 to May 1988, the 64-m antenna was upgraded to a 70-m diameter, resulting in a 4-dB performance improvement. In the spring of 1991, the 3.5-cm wavelength transmitter was upgraded by installing two new 250-kW klystrons, resulting in a continuous power output of 465 kW. The new klystrons have been used successfully in combination with the Very Large Array

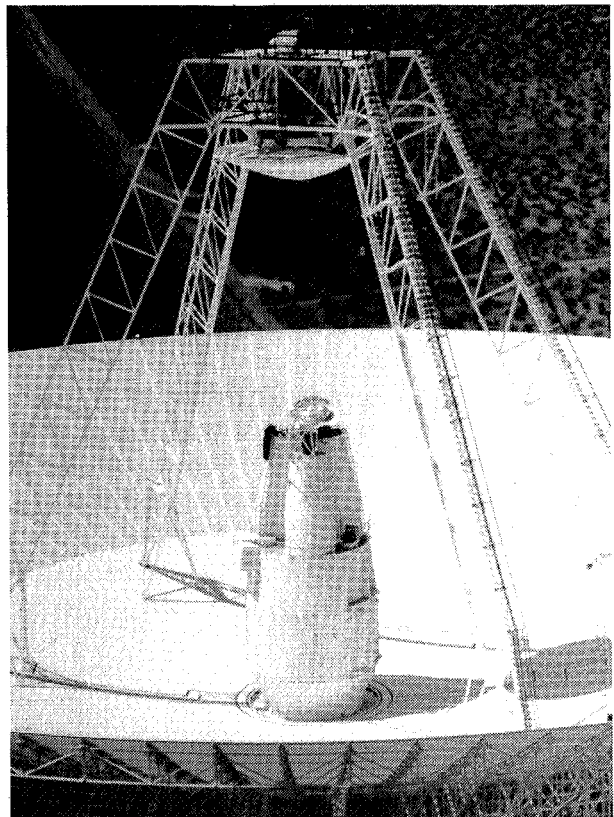


Figure 3. *Tricone Assembly*

(VLA) for observations of Saturn's moon Titan and also for Asteroid 1991 JX observations in May and June of 1991.

Software and data acquisition system improvements at the Mars Station have been ongoing. During the period 1982 through 1985, the data acquisition system was replaced by a digital system with totally new software. The capability for real-time verification was added. This capability can provide a useful feedback during a radar track, for if the radar data are simply recorded upon magnetic tape for later analysis, a malfunction could not be detected and corrected in real time. At the Venus site, a 34-m *beam waveguide* antenna was constructed adjacent to the veteran 26-m antenna, and this new instrument was completed in 1991. The beam waveguide routes the signal to the environmentally controlled room at the base of the antenna by using microwave mirrors rather than conventional waveguide, enabling any of a variety of feed systems to be used. Surface accuracy is 0.40 mm rms.

II.9 Further Observations of Venus

During the 1964 inferior conjunction with Venus, scientists used the improved radar at the Goldstone research and development site to study Venus. The radar parameters were a 100-kW transmitter at 2388 MHz, two-way antenna gain of 108.5 dB, receiver system noise temperature of 33 K, and data acquisition system time step of 125 μ s with a distance resolution of 18 km.

The experimenters detected two bright spots, one named Alpha in the southern hemisphere and another named Beta in the northern hemisphere. The prime meridian (longitude = 0 deg) was selected to pass through Alpha. Much more surface detail was to be revealed in later experiments. The radar cross section was 0.1 to 0.2, and the data showed that Venus was smoother than the Moon. The spin was estimated at -250 ± 9 days, and the direction of the spin axis was also estimated. These measurements were refined in later years as the experiments continued with improved radar. Today, about 243 days retrograde is an accepted value, with right ascension about 272.8 deg and declination about 67.2 deg (Slade et al., 1990).

In 1967, observations of Venus were made with the receiver, 100-kW transmitter, and 26-m-diameter antenna at the Venus site; bistatic observations were performed by using the Venus-site equipment in combination with the 64-m-antenna and receiver at the Mars site. Experiments continued, and in November of 1970, the radar system operating at 12.6-cm wavelength had been improved to provide two-way antenna gain of 124 dB, system temperature of 25 K, and transmitter power of 400 kW. With this refined radar and the use of both Doppler and range gating, Alpha and Beta were now observed with higher signal-to-noise ratios. (The features were first discovered using only Doppler.) Further details of the shapes and sizes of the features were obtained. Polarization studies showed the areas to be rough (Goldstein and Rumsey, 1972). During the June 1972 inferior conjunction, both monostatic and bistatic modes were used to perform altimetry measurements on part of the Venusian surface.

In the 1970s, radar maps of the Venusian surface were greatly improved through better instruments and image-enhancement techniques. The data showed a heavily

cratered surface. The characteristics of Venus as a radar target were favorable to the technique of delay-Doppler interferometry (Subsection IV.2.4.1), and this was performed in the 1970s. In 1977, tristatic (three-receiving-station) radar experiments yielding high quality altimetry were performed, with resolution of 8×10 km in equatorial regions. The surface feature Maxwell showed high contrast to its surroundings.

Venus multiwavelength experiments using 3.5-cm signals as one of the wavelengths are useful for atmospheric studies because the higher frequencies are absorbed more by the atmosphere. By comparing the 3.5-cm-wavelength return with the returns of the longer wavelengths, signal loss in the atmosphere can be estimated. Various scientific studies of the atmosphere were proposed. For example, a search of the Venusian cloud layers for sulfuric-acid rain was made but none was found.

In 1990, in anticipation of the Magellan mission and to obtain a calibrated map of Venus with same-sense polarization (Subsection III.2.4), the combination of the 70-m antenna at Goldstone transmitting a circularly polarized signal with the VLA receiving the *same* sense of polarization was used to image Venus. The signal processing and system performance were such that complete maps of the entire Venusian disk with a resolution of 45×45 km were made in a single day.

II.10 Observations of Mars

Mars is a more difficult radar target than Venus because it is about one-third again further away (the round-trip light time is 11 minutes) and has a higher spin rate; a Mars echo is 100 times weaker than a Venus echo, and the spectrum is more dispersed in frequency by a factor of 200 (Subsection III.2.2). Improvements in the radar were made, however, and Mars was first detected in 1963 using the 12.6-cm wavelength radar at the 26-m Venus Station. The studies reported that both smooth and rough surfaces were present (Goldstein and Gillmore, 1963). Initial Mars radar cross-section measurements varied in the range of 2 to 6% with the region observed. The GSSR also showed Mars has much more height variation than Venus.

By February 1965, the radar had improved: the transmitter power was at 100 kW, the frequency was 2388 MHz, the product of transmit and receive antenna gains was 108.5 dB, and the receiver system temperature was 27 K.

The signal from the Martian limbs was not strong enough to be seen, and most of the power was received from the sub-Earth point. The total bandwidth of the echo at the 12.6-cm wavelength was 7670 Hz, and this spectrum was measured with a bandwidth of 3700 Hz (Goldstein, 1965). The spectrograms were averaged, and the data set was reduced to a set of spectra for each 10-deg increment in Mars longitude. Strong, narrow-band reflections were noted in the region Trivium Charontis at 200 to 210 deg longitude.

In the 1970s, ranging was done at the subradar point; the Hagfors model for backscattering (Subsection III.2.5.3) fits these data very well.

The GSSR searched for suitable landing sites for the Mars Viking Lander in the mid-1970s. Before final selection, several sites were observed to be rougher than thought

from the Mars Viking Orbiter observations. Mars radar altimetry was performed to 100-m accuracy near the south part of Arsia Mons. The final landing-site selection was based on GSSR observations of the potential sites.

The Goldstone 64-m dish has been used to measure Martian topography. During the 1971 opposition, for example, the surface topography was explored, and many craters of 1- to 2-km depth were seen in the 50- to 100-km-diameter range. These data complemented photos from the Mariner 9 spacecraft launched in 1971, photos that did not yield accurate measures of crater depths.

During the inferior conjunctions in 1988 and 1990, a cooperative effort of the GSSR and the Arecibo Observatory performed dual-polarization measurements of Mars. This experiment was the first multiwavelength study (GSSR used 3.5-cm and Arecibo 12.6-cm wavelengths) to include the entire echo in both circular polarizations. The data are used to study the spatial variation and wavelength dependence of the echo (Harmon et al., 1992).

II.11 Observations of Mercury

II.11.1 The Physical Planet

Mercury is the innermost planet and has several inferior conjunctions every year. Because of its distance from Earth, it was not detectable when the first Venus radar experiments were performed in 1961. After increasing the performance of the radar, a weak detection was obtained by the GSSR during a 1963 opportunity. The measurements indicated the radar cross section was about 6%, similar to that of the Moon.

One of the goals of planetary scientists was reliable determination of the spin rate of Mercury. Before the advent of radar, astronomers attempted to bracket the spin rate using their optical telescopes. According to the 1882 observations by Giovanni Schiaparelli, 88 days was believed to be the correct rotation rate of Mercury, and this rate would make the rotation synchronous with its orbit. This incorrect result was accepted until radar remeasured the rotation. GSSR data gathered during the 1963 opportunity provided spin information (Carpenter and Goldstein, 1963) because there was enough sensitivity at that time to gather echoes from the limbs. In the spring of 1965, scientists at the Arecibo Observatory performed the first proper measurement of the spin of Mercury, with a result of about 59 days (Dyce, et al., 1967). In 1968, the spin rate was measured to be 59 ± 3 days. Later GSSR observations confirmed the result.

The investigators found Mercury rough at the 12.6-cm wavelength. In 1969, radar data showed that the surface of the planet consisted of several large rough features and one very smooth area. Later, in 1972, radar probes at 2388 MHz revealed the existence of hills and valleys with 1-km relief. The data also suggested craters with 50-km diameters and depths of 700 m. The Mariner 10 flybys confirmed these findings.

In 1991, the combination of Goldstone 70-m-antenna transmission with VLA reception obtained full-disk (rather than only subradar-strip) images of Mercury. The

technique of aperture synthesis was used. Maps were produced of areas not already studied by Mariner 10.

II.11.2 Mercury and Tests of Theory

Observations of Mercury are used for important tests of gravitational theory, Einstein's general theory of relativity, and other tests in physics. The theory of general relativity predicts that a light beam will be deflected and slowed by gravity as it passes near a massive object; the maximum delay occurs in the strongest gravitational field. Mercury and Venus are the planets closest to the Sun and therefore experience strong gravitational fields.

In a simplified discussion, the classical system model (nonrelativistic) consists of gravitational theory and laws of motion with a constant speed of light as described by Isaac Newton; the general relativity model, however, uses Einstein's theory for gravity and motion along with a speed of light that is influenced by gravity. Experiments that look for relativistic effects have to be carefully designed because the differences between classical and relativistic predictions are extremely small, and electromagnetic waves can be slowed for other reasons. One such reason is the passage of the waves through the solar corona, but this effect diminishes with frequency, and multiwavelength radar experiments should be able to isolate coronal slowing from gravitational slowing.

An experimental test of general relativity involves the advance of the perihelion of Mercury (Shapiro, 1968). In celestial mechanics, the perihelion is the point along the planet's orbit that is closest to the Sun. If relativity holds, the perihelion will drift across the solar longitude at a very slow rate (a small fraction of one degree per century) rather than cross the classically predicted solar longitude on every revolution around the Sun. This test is performed by careful radar measurement of Mercury's orbit. A history of measurements has been established, and these data are compared with predictions to test the hypothesis.

Another test of general relativity is the search for an increased delay of the echo return times of radio signals reflected from Mercury or Venus (Shapiro, et al., 1971). The experiment is performed near superior conjunction so the radar beam passes close to the Sun, where it will be slowed the most. The relativistic slowing is independent of radar wavelength, and the predicted delay is about 200 μ s for a Mercury experiment. The ultimate accuracy of this type of test depends on the stability of the frequency and time reference of the radar system. The slowing of radar waves as they pass near the Sun is confirmed by radar, and these results tend to verify the theory of relativity.

Gravitational theories, including the hypothesis that the gravitational constant changes with time, are tested by measuring closure points, e.g., by repetitive high-precision ranging to the same region on the surface of Mercury and removal of topographical time delay variations by differencing. Another test of this hypothesis seeks to determine the Sun's oblateness, i.e., the deviation of the shape of the Sun from that of a sphere.

II.12 Observations of Jupiter and the Galilean Satellites

Jupiter was thought to have a deep atmosphere that would absorb radar signals, and therefore it was expected to return very little echo power. However, in the fall of 1963, Jupiter was apparently detected by GSSR at a signal-to-noise ratio of 8. To produce an echo of this strength, a very high radar cross section of 0.6 was required (Goldstein, 1964a). A very shiny spot appeared with a width greater than 1200 km; this return was not an echo from the Great Red Spot. Further experiments by JPL and other groups did not repeat this detection. Later experiments with equipment orders of magnitude more sensitive have not confirmed the detection, and it is concluded that the 1963 observation was probably spurious.

Ganymede, Callisto, Europa, and Io, the four Galilean satellites of Jupiter, have all been observed by the GSSR. Ganymede, the largest of these, was first observed by the GSSR at 12.6-cm wavelength in 1974. The first three of these moons are good radar reflectors. The surfaces are believed to be very rough. The radar echoes are extremely unusual when the polarization properties of the radar return are compared with those of the typical solar system echo. In later years, observations were made at 3.5-cm wavelength.

II.13 Observations of Titan and the Rings of Saturn

To date, the furthest objects detected by the GSSR are the rings of Saturn and Saturn's moon Titan. (Saturn itself, like Jupiter, is thought to have a deep atmosphere that is very absorptive of radar waves, and for this reason it returns no echo.) The GSSR made the first detection of the rings in a series of experiments begun in December 1972 and completed in January 1973; the radar used the 64-m antenna with a 400-kW transmitter at the 12.6-cm wavelength. This time period was chosen for the tests because the rings were then at a high angle of inclination, and thus more visible than if they were viewed edge on. The round-trip light time was 2 hours and 15 minutes, and Saturn was at a distance of 1.2×10^9 km (Goldstein and Morris, 1973). Upon analysis of the data, it was concluded that the particles that make up the rings were efficient reflectors of the 12.6-cm waves, indicating that they were probably rough objects a meter or more in diameter, and were certainly larger than a radar wavelength. Before these first radar results, the particles were thought to be much smaller.

The rings were observed again in late 1974 by a bistatic radar configuration in a cooperative effort with Arecibo Observatory. Arecibo transmitted at the 12.6-cm wavelength, and Goldstone received with the 64-m antenna (Goldstein et al., 1977). Linear polarization was used. GSSR then carried out monostatic observations at the 3.5-cm wavelength using circular polarization. These observations showed that the echo strength did not have great dependence on wavelength. To take advantage of possible synergisms, studies were made to correlate Voyager space probe images with these ground-based data.

In 1989, Saturn's moon Titan was observed in an experiment with the 70-m antenna at Goldstone transmitting at the 3.5-cm wavelength and the VLA receiving; the echoes were definitely from a solid surface. This detection, and subsequent detections in 1990,

1991, and 1992, exclude the widely accepted theory that Titan is covered by a global ocean of ethane.

II.14 Observations of Asteroids

The object 1566 Icarus became the first asteroid detected by planetary radar on June 14, 1968. Both JPL's Goldstone and MIT's Haystack facilities succeeded in making contact. As of 1970, a total of only five asteroids out of thousands in existence had been detected by the world's radio telescopes. As of 1991, about 66 asteroids of all types had been detected by all radio observatories; a list of the asteroids and other objects observed by GSSR is given in Table 3.

Table 3. Observations by GSSR

Object	Year of observation
Venus	1961
Moon	1961
Mercury	1963
Mars	1963
Rings of Saturn	1973
Asteroids	
1566 Icarus	1968
1685 Toro	1972
433 Eros	1975
1986 JK	1986
1981 Midas	1987
3908 (1980 PA)	1988
1580 Betulia	1989
1917 Cuyo	1989
1989 JA	1989
1989 PB (4769 Castalia)	1989
1990 MF	1990
1990 OS	1990
194 Prokne	1990
324 Bamberga	1991
1991 EE	1991
7 Iris	1991
1991 JX	1991
3103 (1982 BB)	1991
1992 UQ	1992
4 Vesta	1992
Galilean Satellites of Jupiter	
Ganymede	1974
Callisto	1987
Europa	1988
Io	1992
IRAS-Araki-Alcock (comet)	1983
Phobos	1988
Saturn's moon Titan	1989

III. Application of Radar to the Observation of Solar System Objects

III.1 General

The objective of any solar system radar experiment is to detect a recognizable echo from a solar system body. The radio telescope is a ground-based sensing instrument designed to accomplish this demanding task. A radar experiment is conducted by beaming 450 kW of precisely controlled radio frequency energy at a target millions of kilometers away. The radar signal's interplanetary round trip requires from about 30 seconds (2.5 seconds for the Moon) to several hours (for Saturn) at the speed of light; upon arrival at Earth, the radar echo has been attenuated to a billionth of a trillionth of a watt or even less. The signal received by the antenna is amplified, converted to video frequencies, and filtered. The resultant electrical signal contains the target's *radar signature*—the distortion or changes in the radio signal caused by the reflection.

The parameters of the echo that contain scientific data are its strength (Subsection III.2.1), Doppler shift (Subsection III.2.2), time delay (Subsection III.2.3), and polarization (Subsection III.2.4). Equation (2) is the *radar range equation*, giving the strength of the echo power, and Equation (3) defines the experimental *radar cross section*, which is obtained by solving Equation (2) for σ .

$$P_r = \frac{P_t G^2 \lambda^2}{4\pi(4\pi R^2)^2} \sigma \quad (2)$$

$$\sigma(f, t) = \frac{P_r 4\pi(4\pi R^2)^2}{P_t G^2 \lambda^2} \quad (3)$$

where

- P_r = echo power, W
- P_t = transmitted power, W
- G = antenna gain
- λ = wavelength of radar signal, m
- R = distance to target, m
- σ = radar cross section, m²

When expressed as a function of time and frequency as in Equation (3), σ is the radar scattering function; measurement and analysis of this function are central to the science of radar astronomy. The radar scattering function depends on the size and surface material of the object, incidence angle, radar reflectivity of the surface, viewing direction, and rotational speed of the object.

The strength of the echo depends primarily on the distance between Earth and the target body. Typically, the scattering properties are normalized by multiplying by R^4 in an attempt to remove all systematic effects; those that remain are truly characteristic of the surface.

There are two dimensions to the radar data, frequency of the returned signal and time delay of the signal's round trip, with polarization as an added constraint. Often, a *delay-Doppler* map (Subsection III.2.3) is formed from these two dimensions. Multistatic (more than one receiving antenna location) experiments add another dimension to the observations. The jump from radar signature to physical characteristics is in principle straightforward but in practice complex and depends greatly upon what is known a priori.

The science return that can be achieved depends on the resolution and precision of the measurements, and the resolution is in turn dependent on the signal-to-noise ratio. From measured differences between received and transmitted frequencies (Doppler shifts) and the round-trip time delays, improved ephemerides of the target are obtained. Time delay and Doppler measurements are extremely powerful tools, useful in the precise orbit determination of planets, asteroids, and comets.

What information can be gained from a radar experiment depends in part upon the goals of the experimenter and the transmitted waveform. When investigating multiparticle systems or the properties of surface and subsurface layers, it is useful to conduct scientific experiments at the 3.5-cm wavelength alone or in combination with the 12.9-cm wavelength. The instrument can be used to investigate physical properties, size distributions, and spatial distributions of such multiparticle systems as Saturn's rings and cometary clouds. One method compares radar reflectivities at different wavelengths to test hypotheses about near-surface structure and composition.

A search for subsurface water or permafrost layers on Mars, or a search for metallic content of asteroids, are other examples of investigative goals. Another goal is to investigate surface roughness at different structural scales. The instrument can be used to explore subsurface structure: porosity gradients, layering, and rock populations at different scales and to different depths. Ground-based radar has been used to probe Venus, and the radar data have set an upper limit on the size of the droplets in the planet's atmosphere. The experimenter should acquire echoes at many rotational phases of any object to get a complete view; this may span hours, days, or, in the case of Mercury and Venus, even years. Mars also presents different latitudes to the Earth-based observer over a 16-year cycle.

Radar measurements have a number of advantages over optical studies. Radar can be used in the daytime when optical telescopes are not useful, if the object is not too close to the Sun in angular position; the illumination of the Moon can also obscure an optical observation. Radar can see through bad weather and clouds on Earth and elsewhere. Before the 1961 JPL radar experiments gathered scientific data from Venus, the planet's surface was a mystery because it is perpetually covered with clouds. Radar is the only known method of remotely studying the surface of Venus. Another advantage of radar is locating metal concentrations, because of metal's high radar reflectivity. Radar is an active process where the experimenter precisely controls the illumination properties such as wavelength, polarization, transmitted waveform, and power level; light- or infrared-based observations, however, rely on passive, incoherent illumination. Whereas optical measurements are controlled by the first microns of an object's surface, radar reflections are influenced by surface and subsurface materials to depths of centi-

meters to meters or deeper. Information from this larger scale is useful for many objectives.

Radar provides a complementary data type to optical telescopic observations. Light-gathering telescopes can measure angular position and optical brightness (magnitude), while distance, velocity, and polarization are measured with radar to very high precision. A principal advantage of optical and infrared, however, is that spectrographic measurements are very much more diagnostic of minerals. Radar observations supplemented by photoelectric light curves and stellar occultation timing data will enable the most complete view of a solar system object to be gained. Radar investigation of the planets is an iterative process of constraining linear dimensions, pole direction, spin period, topography, and composition, using radar data *and* other data types. The combination of ground-based radar observations with optical and infrared studies and data from spacecraft missions yields valuable insights into the nature and evolution of the solar system.

Using the fringe patterns from *bistatic* or *tristatic* radar modes (two or three receiving antenna locations, respectively) enables altimetry information to be obtained from areas away from the subradar region. (At the target, the subradar point is the termination of a straight line from the antenna to the closest point on the target.) Certain ambiguities present in data taken with monostatic observations can be resolved with multistatic experiments. The two different angles of view used in multistatic operation allow angular separation of surface features. When the combination of the Goldstone 70-m antenna and the Very Large Array is used, system sensitivity can be increased by a factor of 2.5.

III.2 Parameters of the Radar Echo that are Examined

The transmission of a pure sinusoid waveform at radio frequencies, spectral analysis, and often range gating and polarization separation at the receiver have proven to be a fruitful combination for gaining knowledge of our solar system. The parameters of the radar echo, or *radar observables*, will now be discussed. The physical information extracted from the radar echo is shown in Figure 4.

III.2.1 Amplitude

The amplitude (strength) of the signal returning from a solar system target has been diminished by the signal's round trip of interplanetary distances. Some echoes cannot even be discerned individually without extensive computer processing. Depending on their bandwidth, many echoes may have to be added together (integrated) for hours before they can be recognized.

As can be seen from Equation (2), the amplitude of the received signal depends on distance, transmitter power, antenna gain, and how much of the incident energy the target reflects back to the Earth station. The most significant factor influencing the detectability of a target is distance. This is because the received signal strength varies inversely as the fourth power of distance and is the primary reason that solar system radar requires the highest power transmitters, largest antenna apertures, and most sensitive receivers.

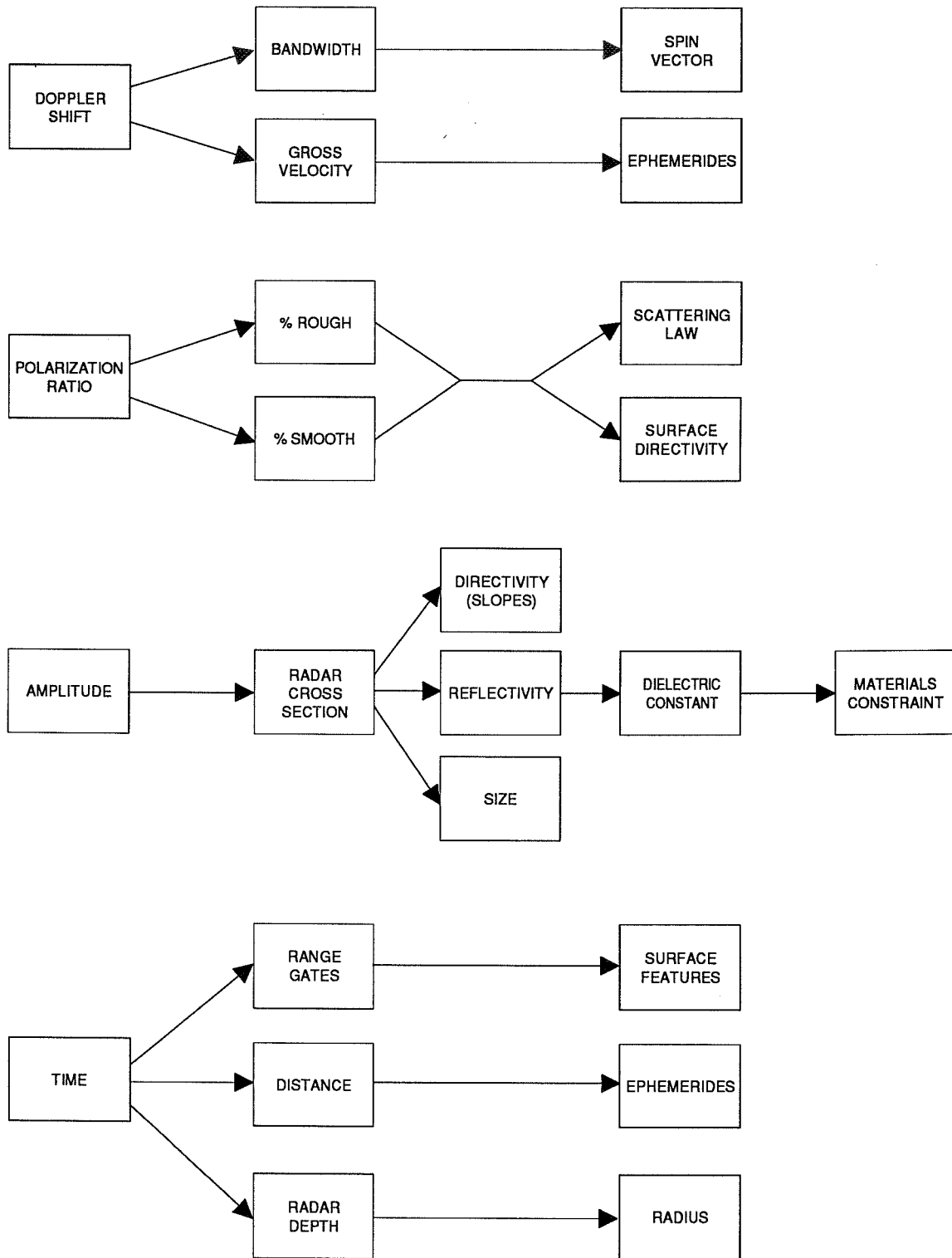


Figure 4. Radar Observables

What is the minimum strength needed for the echo? A 3:1 signal-to-noise ratio is usually the minimum required for reliable detectability. As of this writing, the rings and moons of Saturn are the furthest solar system entities detected. Amplitude determines whether the target can be seen at all, and the echo strength influences the quality of the conclusions and also the ultimate resolution. In terms of the target, detectability is a function of distance, size or cross-sectional area, reflectivity (albedo), and the direction and magnitude of the target's spin vector. The *albedo* of a radar target is the fraction of radar energy striking the target that has been scattered back to the observer. The product of the albedo and the size of the target gives the target's net radar reflectivity. In addition to a strong dependence on distance, the strength of the return signal depends on the characteristics of the surface and subsurface material, and the topographic relief or shape of the surface features. Since the hardware parameters of the radar system have been accurately measured, the expected echo strength can be estimated from Equation (2) if the distance to the target is at least approximately known. Given constraints on distance and size—perhaps from optical observations—the strength of the return signal can be predicted even more accurately. Usually, the subradar point has the strongest amplitude because the general orientation of the surface is perpendicular to the line of sight, so the radar wave is reflected directly to the Earth station.

When analyzing radar data as brightness maps, there are light and dark areas. A surface may be "radar dark" even though it is smooth and a good reflector, only because it is sloped so that the incident wave reflects into space away from Earth; or the area may be dark because it is very absorptive of radio waves at the wavelength used. A surface may be bright because it has just the right slope to reflect the wave back to Earth and because the material is smooth and highly reflective, possibly with a high concentration of metal. Smooth areas give echoes that look like a sharp spike, and rough areas produce diffuse echoes (Figure 5). Studies have been made to correlate areas of varying reflectivity at radio frequencies to light and dark areas from optical data. In addition to the slope, roughness, and material, the state of the same material may change with temperature, influencing the radar signature. Water and water ice reflect differently, for example. On Mars, the reflectivity of the Solis Lacus region was measured at several seasons during the Martian year, and characteristic changes in the radar signature indicate the possible presence of near-surface liquid water (Zisk and Mougins-Mark, 1980).

Jupiter's Galilean satellites have excited the curiosity of planetary radar scientists because of their bizarre radar signatures, which are unlike any in the solar system. The radar echoes from Europa, Ganymede, and Callisto are very strong and have extraordinary polarization (Subsection III.2.4). They have unexpectedly high geometric albedo relative to most other solar system objects, with Europa reflecting nearly as much energy (in one polarization) as that of a metal sphere (Ostro, 1992).

Very often, the radar signature is analyzed by forming its frequency spectrum, whose ordinate is power spectral density. The area under the graph of the signal's spectrum is the received power (Figure 5). In early experiments, the *radiometer* was used to measure received signal strength. The radiometer was developed by radio astronomers to measure the strength of noiselike signals emanating from celestial sources; it is a power measuring device. When it is connected to a receiver and antenna, it forms a radio telescope. An improvement in the basic radiometer is the switched or "Dicke" radiometer. The switched

radiometer improves the signal-to-noise ratio as the square root of measurement time. The instrument alternately listens to signal plus noise, and then noise only, to detect the small resulting change in output. Thus equipment drifts in gain and phase do not affect the celestial-source measurement because they are subtracted. Systematic errors are eliminated in this way. Some of the very earliest radar astronomy experiments measured total echo power from extraterrestrial sources using a technique similar to that of the Dicke radiometer; however, for practical reasons, the transmitter rather than the low-noise receiver was switched on and off.

III.2.2 Doppler Frequency

Doppler frequency shift ("Doppler") is the change in frequency from the transmitted to the received signal. Spectrally pure, single-frequency waves are transmitted to the target. When the radar signal is reflected from an object in relative motion to the Earth-based radar station, its frequency changes and its frequency spectrum broadens. For a given wavelength, the amount of change depends on the relative velocity along the line of sight. The relative velocity vector includes Earth rotation, the difference in orbital velocities (gross motion) between Earth and the planet, and rotational motion of the object. The radar echo really consists of multiple reflections from the visible parts of the celestial object. By virtue of the fact that different parts of the surface present a different component of velocity to the Earth-based observer, these areas can be resolved.

Doppler shift is usually analyzed by forming its frequency spectrum, which resolves the *dispersion*—the difference between the highest and lowest frequencies—into frequency cells or bins. The echo spectral shape alone provides information about the target. Assuming a spherical target, the spectrum often appears to have a central peak and left and right "skirts" (Figure 6). Spectrum bandwidth is measured from skirt edge to skirt edge. As will be explained later, Doppler spectra can be formed of two orthogonal senses of polarization, to study the mix of smooth and rough regions.

The center frequency gives the Doppler shift of the subradar point and so the line-of-sight velocity or gross motion. The frequency spread is caused by target rotation. The Doppler shift is greatest at the limbs, or extremities, of the target and minimum along a meridian passing through the subradar point parallel to the apparent spin axis. Large, fast-rotating objects have a large radial velocity component and therefore a wide band-

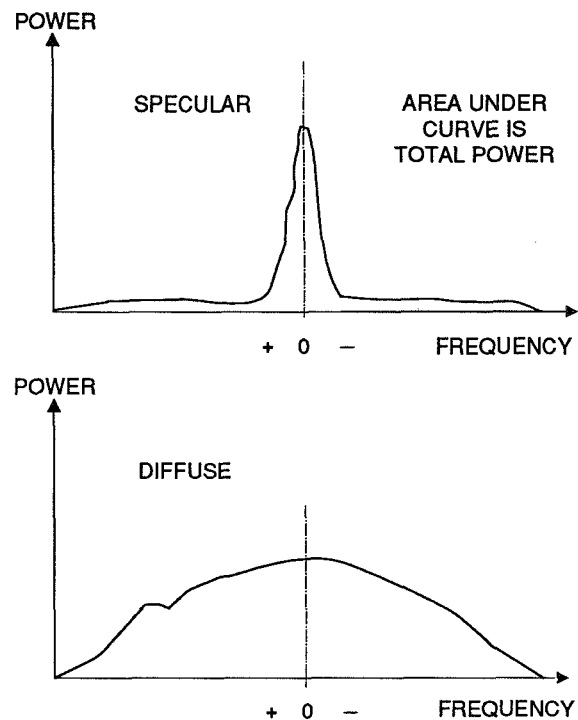


Figure 5. *Specular and Diffuse Echoes*

width, while slower rotators have a narrow frequency spread. Doppler shift information can be extracted from the echo using even the most basic radar configurations. Doppler measurements enable investigators to make extremely accurate orbital velocity measurements; on the order of 1 or 2 cm/s is not unusual accuracy. The ephemerides of the objects can be refined from this data.

Equation (4), the Doppler equation, predicts the amount of overall frequency shift in the echo, and Equation (5) describes the bandwidth of the signal.

$$\Delta f = \frac{2\vec{v} \cdot \vec{r}}{\lambda} \quad (4)$$

$$B = \frac{4\pi D}{\lambda P} \sin \alpha \quad (5)$$

where

- Δf = Doppler shift, Hz
- \vec{v} = relative velocity along the line of sight to the radar, m/s
- \vec{r} = unit vector along the line of sight to the radar
- λ = wavelength, m
- B = bandwidth of Doppler spread, Hz
- D = the width, measured normal to the line of sight, of the object's polar silhouette, m
- α = the aspect angle, between the line of sight and the apparent spin vector, rad
- P = target rotation period, s

The spectrum width depends on object size, apparent spin period, wavelength, and the angle of the pole with respect to the line of sight from the target to the radar. If viewed parallel with the pole or spin axis (polar silhouette), Doppler broadening would be zero; it is maximum when viewed perpendicular to the apparent spin axis. When looking at dispersions, it is significant that the limb-to-limb bandwidth is only the *projection* of the radial velocity, not the actual velocity. To obtain actual velocity, the viewing geometry is important. Figure 7 shows the extreme aspect angles of 0 deg and 90 deg. The line of sight must be perpendicular to the equator (90 deg) to get the peak bandwidth. A further complication is that the orbital motion causes an apparent spin that algebraically adds to the actual rotation. This effect can be quantified and removed.

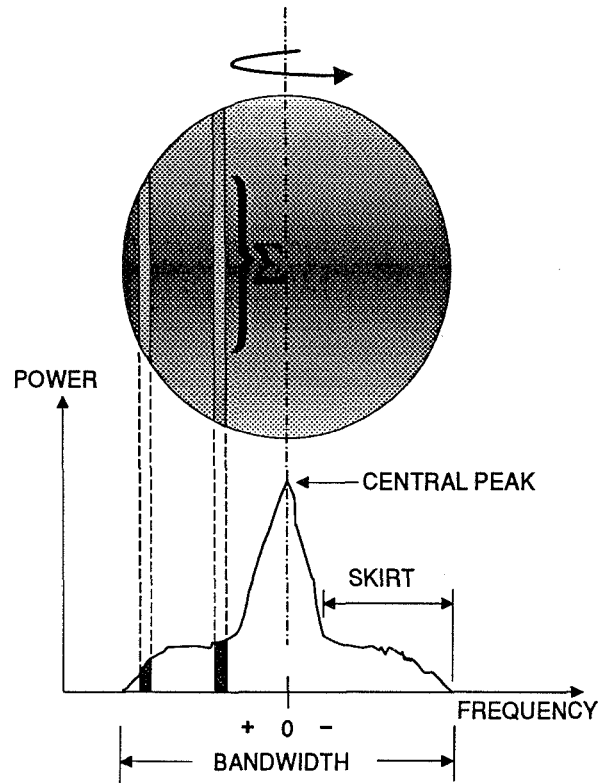


Figure 6. Constant Doppler Regions

A region of constant Doppler (Figure 6) is a strip parallel to the apparent spin axis; the part of the sphere approaching has a positive Doppler shift (increasing frequency), while the receding part has a negative frequency shift. Viewing a Doppler strip is a one-dimensional inspection that corresponds to a view through a vertical slit. During simple, monostatic, continuous-wave observations, any one point in frequency represents the summation of all reflected energy from a vertical strip parallel to the spin axis.

Some information is given by examining the whole frequency spectrum. If the target were a smooth sphere and highly reflective, a very bright return would be expected at the subradar bounce point, with very little energy returned from the limbs. This type of target produces a spectrum with a sharp central peak. Figure 5 shows single-polarization spectra of smooth and rough regions. An alternate model of a planet is a rough dielectric sphere, or Lambert scatterer. If the half-power points are wide apart, rather than appearing like a sharp spike, or if the skirts are thick, the planet may be rough. The reason is that a rough surface does not have as strong a dependence on the angle of incidence at regions near the limbs.

One can actually observe features moving through Doppler frequency spectra, if a series of time-contiguous frames is examined. Although a given point on a frequency spectrum represents the sum of all energy reflected from a vertical strip, the latitude of major surface features can be resolved by noting the passage of the features as they traverse the frequency spectrum with planet rotation. This is shown in Figure 8. The span of the left-to-right movement in the spectrum depends on the latitude of the anomalous reflection. Features present in the equatorial regions will be observed traversing the complete limb-to-limb span, but polar features will move only near the center of the spectrum.

The combination of a very stable transmit frequency and stable receiver tuning is necessary to prevent blurring or smearing the Doppler bins, especially if an object is a small, slow rotator or if high frequency resolution is required. Since an "ephemeris-tuned" receiver (Subsection IV.5.5) is used, the echo's central peak position, left to right, indicates the error in ephemerides. In the 1960s, Dr. Richard Goldstein of JPL conducted planetary radar experiments at 12.5 cm using the Goldstone facility. The ephemeris-tuned receivers then in use kept the frequency within 1/4 Hz. The frequency

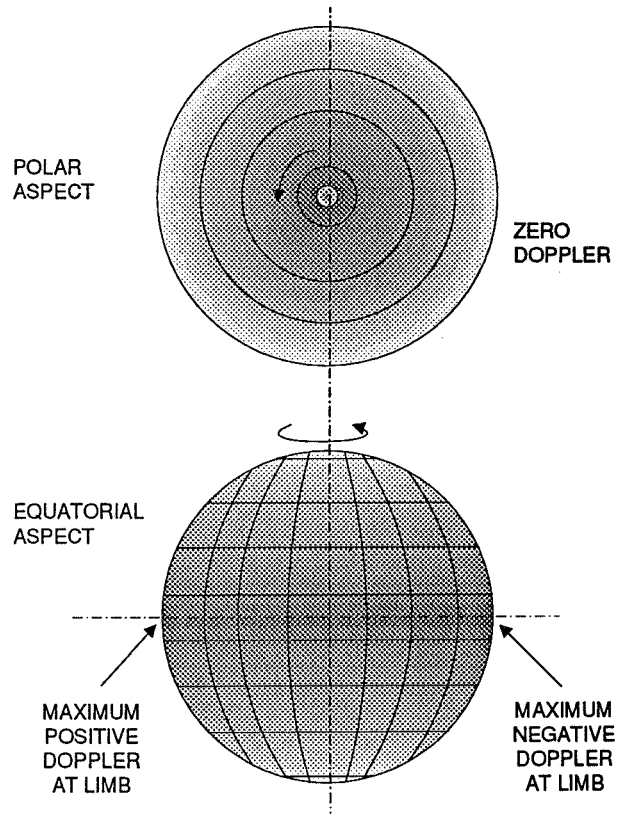


Figure 7. Polar and Equatorial Aspects

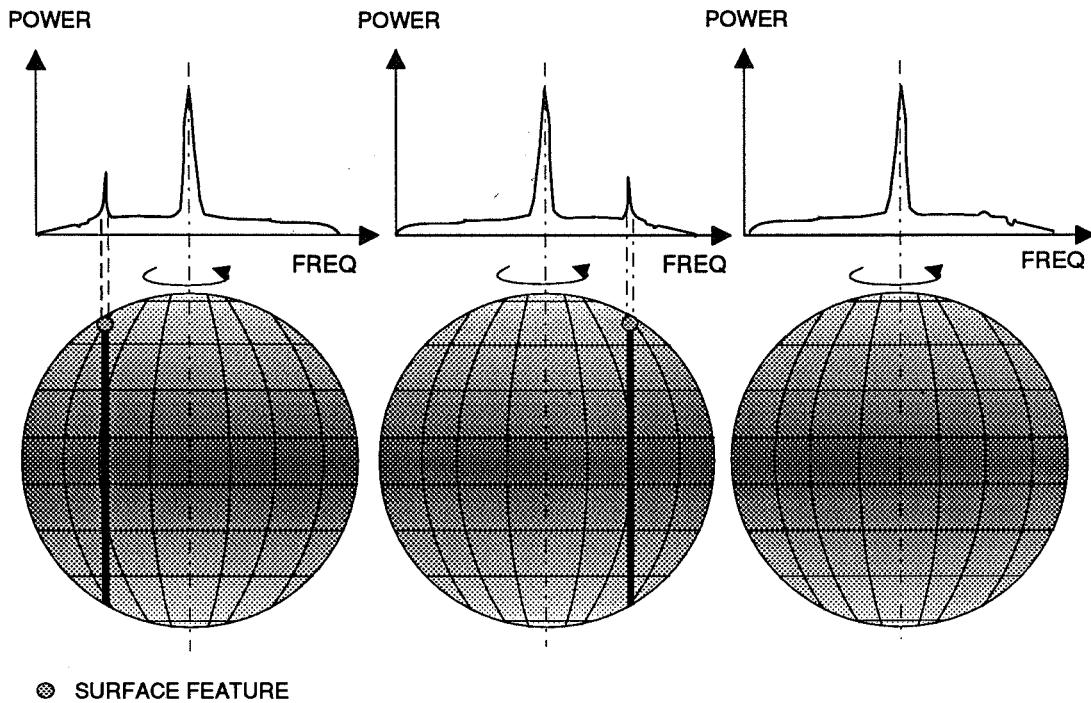


Figure 8. *Tracking a Surface Feature*

resolution of the receivers' local oscillators was as fine as $1/32$ Hz. Given the narrow bandwidth of some targets, it can be seen that extraordinarily stable frequency references are needed to avoid blurring the frequency data. Venus has a bandwidth of only about 30 Hz at 12.9-cm wavelength, depending on when it is measured, and if this dispersion is divided into 100 frequency bins 0.3 Hz wide, a frequency stability of about several parts in 10^{11} is needed to avoid smearing the data. Stable tuning is also required to keep the signal within the very narrow range of frequencies that the receiver will pass. Doppler shift and antenna pointing ephemerides are major unknowns at first observation, especially for newly discovered objects.

The rotation of a planet during one observation time (one round-trip light time) is significant if the angular velocity is high. In this case, the subradar point shifts slightly during one transmit-receive cycle. High spin rates can produce blurred spectral images like those of camera snapshots of fast motion taken with too long an exposure. The choice of measurement time for a specific target is influenced by this phenomenon. This is an important consideration relative to the radar's Data Acquisition System (Section IV.6). The round-trip light time for Mars, for example, is about 11 minutes, which is also significant in choosing the echo integration time. Mars can be a problem target, since it rotates relatively fast at 0.25 deg of longitude per minute; Venus and Mercury, however, rotate more slowly. On Venus, the longitude of the subradar point changes by only 0.85 deg per day. This means that the echoes from the subradar strip can be integrated for minutes or longer without blurring. Thus a trade-off exists: on one hand,

there are long integration times and better signal-to-noise ratios and, on the other, there is high resolution along the frequency axis.

Mars is a difficult target also because the echo power is spread out over a large bandwidth, resulting in weak spectral densities. For purposes of comparison, there is a 200:1 ratio in Venus-to-Mars bandwidth. Even if the total power of the Mars echo were the same as that of one from Venus, an echo from Mars would have a worse signal-to-noise ratio (weaker power spectral density). The Mars limb-to-limb bandwidth is about 8,000 Hz at 12.5-cm wavelength and 30,000 Hz at 3.5-cm wavelength.

III.2.3 Time Delay (Range)

Typically, a radar experiment is done by transmitting to the target for the round-trip light time, and then listening for the echo with the receiver for a similar time. Because an individual signal is weak, many such cycles are usually repeated, and the echoes are added together to increase their strength. This overall process is one *observation*. Radar ranging measures the round-trip light time to the target, and from this measurement the distance R can be calculated using the speed of light c , and time t :

$$R = \frac{ct}{2} \quad (6)$$

The measurement is made from the time the signal leaves the transmitter to the time it arrives at the receiver (Figure 9). The overall time of flight can be predicted in advance, given an accurate ephemeris. For the closest target in the solar system, the Moon, the round-trip light time is 2.5 seconds, while for the furthest detectable target, the rings of Saturn, the time is at least 2.5 hours. The distance of various points on the planet's surface can be determined by measuring the corresponding echo time. Each radar installation has a reference point for precise time measurements. The antennas for planetary radar are so large and the time so accurately measured that an arbitrary specific point, such as the top of an antenna feedcone, is designated the reference point.

On a spherical target, an area of constant range is a ring or annulus concentric with the subradar point. (This can be visualized as a bull's-eye with the subradar point in the center, as in Figure 10.) Note that as the time resolution increases to the order of several microseconds, the region of constant range no longer is a set

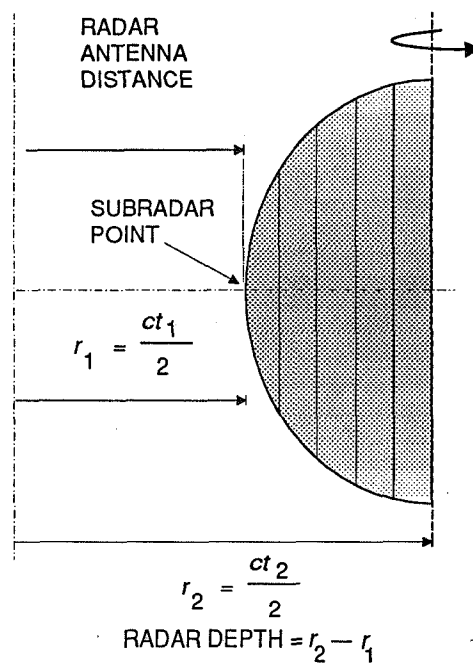


Figure 9. Ranging

of exact concentric circles, but is defined by the topography.

Signals with various delays are organized into range gates. A range gate is a device that accepts or passes signals from one range or time delay and rejects all others. For spherical targets such as the planets, the signal in one range gate is the summation of all energy reflected from a constant range ring. The overall distance to the surface is measured by the earliest range gate, the one corresponding to the radar bounce point. Later range gates measure reflections from constant range rings successively farther back from this point. Near the subradar region, the range-Doppler cells give poor resolution in latitude and longitude, but good resolution in altitude.

In early experiments, the transmitter was keyed off and on so that the radio-quiet background noise level could be measured. It was against this extremely low-level of cosmic background noise that a change in noise level was noted, indicating target detection. Current practice is to apply time modulation to the transmit waveform to perform ranging. If a 1- μ s pulse were transmitted, the resolution would be 150 m. But the energy in only one transmitted pulse may not be sufficient for detection. Usually, the echoes are added together or integrated; both coherent and incoherent integrations are used. The signal-to-noise ratio improves because the signals add coherently, but the noise does not. Radar astronomers modulate the transmitted signals with binary phase-coded (Subsection IV.6.5) continuous waveforms that change only in phase, and often the transmitter remains switched on for nearly the round-trip light time so maximum energy can be collected. At the end of the round-trip light time, the antenna is switched to the receiver to listen for the echo, and the signal is demodulated by looking for a replica of the transmitted waveform at the receiver. When the echo matches, the signal has peaked and this is considered the instant when the signal has been received. The time delay of the radar signal is measured precisely, using Goldstone's ultrastable hydrogen maser time reference. The speed at which the radar wave travels through vacuum is well known. The result is the distance to the point of reflection measured with great accuracy.

The subradar point has the shortest time delay. The difference between the shortest and longest delays is the *range dispersion*, and the corresponding distance should match well with the radius of the planet. In practice, the strength of the signal at the subradar range gate is usually much greater than the signals from gates corresponding to points

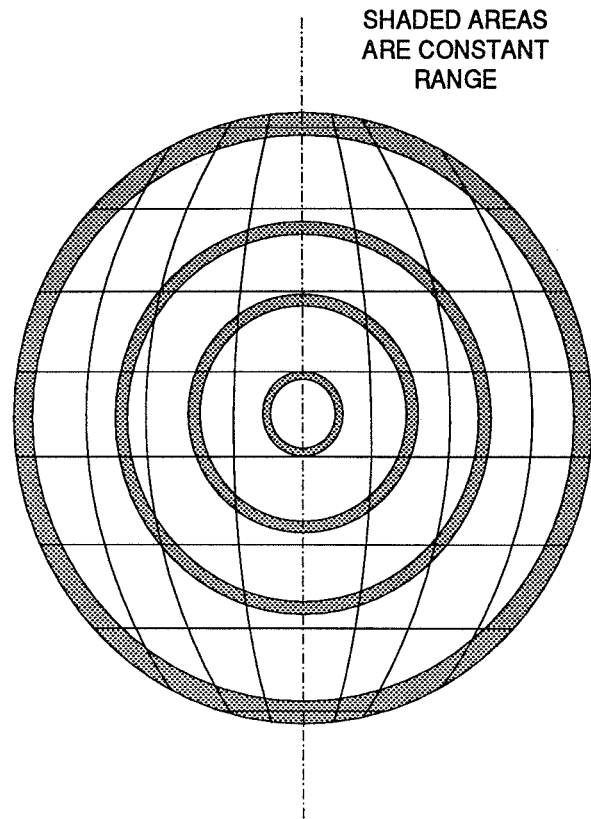


Figure 10. Constant Range Rings

further away. Generally, this is explained by backscattering. Near the limbs, the average angle of the surface is such that the radar wave is predominantly reflected into space away from Earth, except for reflections from rough areas.

The beamwidth of the antenna, a function of the antenna pattern, usually illuminates the entire visible hemisphere of the planet, and many of these areas return echoes. The echoes from each surface patch have an amplitude, direction, polarization, delay, and phase that depend on the orientation, composition, and location of the surface patch. Performing a Fourier transform on range gates produces a frequency spectrum; from this, delay-Doppler maps are created. Forming delay-Doppler maps is a way to resolve the composite return signal in terms of the latitude and longitude of the target.

For near-spherical targets, it is seen that concentric rings are regions of constant delay. Echoes from one of these rings fall into one range gate, that is, energy from all points on the ring is combined into one composite quantity. Generally, it is not possible to resolve points along the ring, if only time is considered. (It is possible to partially resolve the points if observations from different viewing angles are used; however, the technique is cumbersome and time-consuming, requiring several viewing opportunities and much computation in processing the data.)

Using both time delay and frequency provides two dimensions and resolves the ring of constant delay and the constant Doppler strip. A *delay-Doppler cell* is the intersection of a concentric ring with a strip parallel to the spin axis (Figure 11), and many of these cells combine to form a *delay-Doppler map*. Since both positive and negative Doppler shift can be uniquely identified, a surface patch is resolved except for a *north-south hemispherical ambiguity* (Figure 11); points in the northern hemisphere have conjugate points in the southern hemisphere. The reflections from both of these surface points fall in the same delay-Doppler cell. It is not possible to resolve the source of the echo with only one monostatic observation, but the areas can be resolved if the viewing geometry changes. Several other ways to resolve the ambiguity are presented in Subsection III.3.2.

A target is *overspread* to radar if the product of the time dispersion and frequency dispersion is greater than 1. Mars and the rings of Saturn are overspread, while most asteroids, Venus, and Mercury are not. If a target is overspread, frequency-stepped continuous waveforms may be used, but pulsed or random binary phase-coded transmit waveforms cannot be used. A trade-off usually exists between

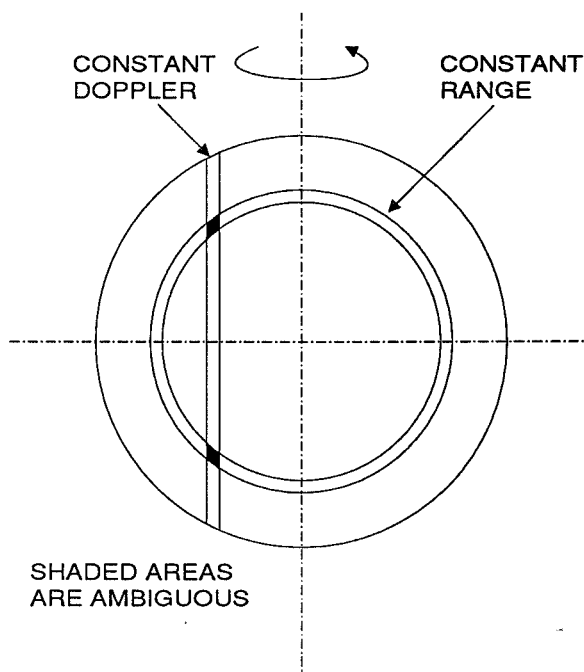


Figure 11. North-South Ambiguity

the delay resolution and the Doppler resolution. Multistatic observations are also a way to resolve this problem.

Present interplanetary time-delay measurements have been used to test Einstein's theory of relativity. Measurements of the orbit of Mercury tend to verify the theory that echoes from radar waves passing near the Sun have extra delay caused by the Sun's gravitational distortion of space. In the 1960s, the first JPL radar studies of the time delay to Venus were important in establishing the value of the astronomical unit (the mean radius of the Earth's orbit), some 150 million km. The precision of the measurement was on the order of microseconds, giving an accuracy of better than 1 km. This was an order of magnitude improvement over the optical-based data then available; subsequent radar data refined the measurement by an additional factor of one hundred. Measurement of the astronomical unit to such great accuracy allowed refinement of planetary ephemerides (Subsection III.3.1), which are essential for interplanetary spacecraft navigation. One simplifying assumption useful in early experiments was that the planets were spherical. However, real planets are not exactly spherical, but slightly oblate, and they have varied topography. In accurate ranging experiments, the topography of a planet is accounted for, if possible.

III.2.4 Polarization

Analysis of the *polarization* of planetary radar signatures can add insights into the nature of the surface and near surface. Usually, Goldstone transmits a radio wave that is completely right-circularly polarized. This is set by the radar's antenna system. Circularly polarized waves reverse their sense upon reflection from a smooth surface. If right-circular polarization is transmitted, left-circular will be received after reflection. These polarizations are conventionally described as same sense (SC) for the same sense as that transmitted, and opposite sense (OC), for the opposite sense to that transmitted.

A relatively smooth reflecting surface, designated a *quasi-specular* reflector, will reflect almost all the energy in the opposite sense (Figure 12), while a rough reflector will reflect considerable energy in the same sense. If both the same and opposite polarization sense components of the echo are measured simultaneously, the amount of near-surface roughness on the order of a radar wavelength can be estimated. This quantity is called the

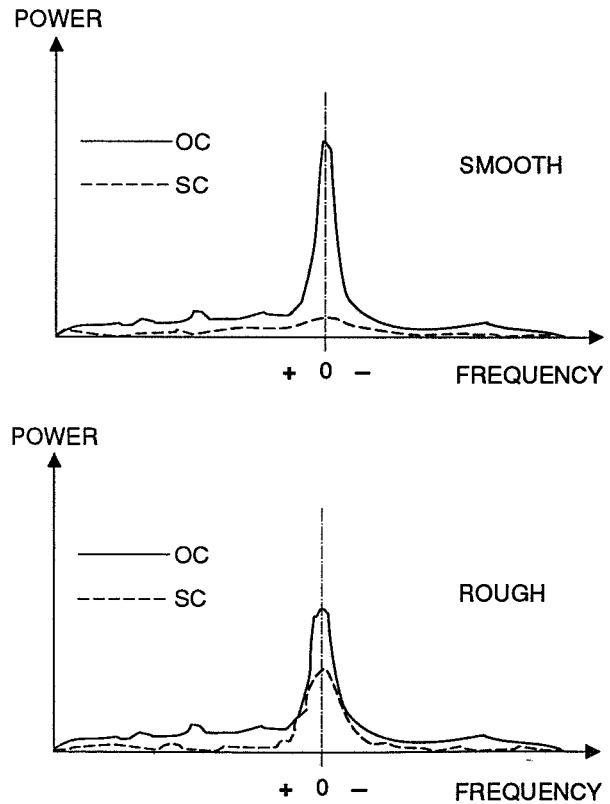


Figure 12. Echoes in Two Polarizations

polarization ratio μ_c and is formed from the radar cross sections of same sense (SC) and opposite sense (OC) polarizations:

$$\mu_c \equiv \frac{\sigma_{sc}}{\sigma_{oc}} \quad (7)$$

Low μ_c (near zero) means reflections from smooth-surface elements are the dominant source of the echo; a ratio near one or larger means a very rough surface on the order of a radar wavelength. In between are the quasi-specular reflectors. From experience, most echoes have both a specular and a diffuse component. The polarization ratio can be calculated at each point in the frequency spectrum, adding further value to the range-Doppler matrix. It may be possible, for example, to localize the smooth and rough areas from their position in the frequency spectrum, because the center or zero Doppler is at the subradar point, and the edges of the spectrum are near the limbs. Certain features on Mercury have the ability to depolarize waves (i.e., cause waves to be randomly polarized) more than adjacent areas; these are the rougher areas. Using the Goldstone Solar System Radar, JPL scientists have found that on Mercury, rough features are more frequent at middle latitudes than near the polar regions. On Venus, the bright regions Alpha and Beta were found to be depolarized regions; that is, they are rough regions and good reflectors. This type of observation would not be possible without two simultaneous receive channels, one for each polarization; polarization diversity alone is not sufficient.

The resolution of two circularly polarized channels to provide a gross estimate of surface roughness is achieved through a four-parameter Stokes vector of circular polarization. The circular polarization is obtained from two simultaneous antenna outputs, one left-circularly polarized and the other right. Both outputs must be in complex form; that is, they must have been resolved into their I and Q components. (The mathematical expressions for this vector and its components are found in Evans and Hagfors, 1968.) The four parameters necessary for the vector are the sum of the left and right received polarized power, the excess of left over right, and two quantities that result from a cross correlation of the left and right outputs. These four Stokes parameters enable resolution of the two circularly polarized channels into polarized and depolarized components, which in turn provide the degree of polarization, which is the ratio of received polarized power to received total power. From the degree of polarization, the estimate of surface roughness of a hard target can be made.

The typical circular polarization ratio for solid solar system objects is about 0.1. Recent Goldstone/VLA imaging of Mercury has shown the circular polarization ratio, μ_c , of the north polar region to be about 1.0 to 1.4 (Slade et al., 1992), a value similar to that for icy regions observed elsewhere in the solar system. The radar observations are interpreted as water ice.

When a radio wave leaves or returns to Earth and passes through the ionosphere and terrestrial magnetic field, it experiences *Faraday rotation* of its polarization. This effect is dependent on the square of frequency and is small at the 3.5-cm wavelength. The Faraday rotation effect on linearly polarized waves changes their polarization. With circular polarization, the effect of Faraday rotation is avoided.

III.2.5 Radar Cross Section σ

III.2.5.1 General

The *radar cross section* σ is a measure of how well a target reflects radio waves. A target that is a good "mirror" to radio waves will have a high radar cross section (RCS). More exactly, the radar cross section is the total power scattered in the direction of the receiver divided by the total incident power. The RCS depends only on the target; it is a disk-integrated quantity—it depends on the summation of all echoes from all points on the surface. Since the transmitter power, antenna gain, wavelength, and usually the distance are known, Equation (3) (Section III.1) can be used to determine the *experimental* RCS.

Measurement of the actual RCS demands accurate determination of the radar system characteristics, because the absolute echo power is used to calculate RCS. (The area under the frequency spectrum curve, as in the graph of Figure 5, represents total echo power.) The strength of the echo, after the other parameters have been accounted for, depends only on how well the target reflects the radar wave. The RCS can vary with the wavelength and polarization of the transmitted radar signal. Generally, the RCS can be further resolved into several components, all of which are functions of target geometry and composition:

$$\sigma = \pi R^2 g \rho \quad (8)$$

where

- σ = radar cross section, m^2
- R = radius of target, m
- g = the directivity or gain of the surface (slope)
- ρ = reflectivity (dependent on target materials)

For example, in 1961 it had been determined by JPL investigators that the RCS ratio of Venus is about 11% (Goldstein, 1964b). This means Venus reflects back to the radar station 11% of the 12.5-cm radar energy that impinges upon it. In another early study, JPL radar astronomers using the Goldstone facilities determined the reflectance of Mars to be 3.2% (Goldstein and Gillmore, 1963). To a first approximation, the energy not received was either absorbed by the target as a wave transmitted into the medium of the near surface (or absorbed by the target atmosphere), or reflected into space in a direction away from the receiving antenna. The RCS is further dependent on the basic size of the object (a large target will return more energy than a small one), the surface slope and roughness, and the type of surface and near-surface material.

While the goal of a radar experiment is to learn as much as possible about the physical properties and surface features of a solar system object, the data acquired are the product of several factors (Equation (8)) rather than that of an isolated factor. Other constraints are needed to resolve the RCS into its individual components. Sometimes, existing knowledge of an object (perhaps from optical light curves or previous radar experiments) can be applied to the new radar data to constrain each component of RCS.

It is the task of the investigator to isolate the individual factors, considering a priori knowledge or the results of other experimental data. This complex task is difficult enough with good signal-to-noise ratios and becomes correspondingly more difficult as the signals are weakened by travel.

III.2.5.2 Directivity

The *directivity* of a target surface is a measure of the complex geometry of the planetary surface and possibly the subsurface; it is the ratio of signal power scattered in a particular direction (per unit solid angle) to the power scattered in all directions (per unit solid angle). The directivity of a surface area depends on its angle of orientation relative to the line of sight to the radar; the radar wave reflects from the surface in the way a billiard ball bounces from the rim of the table, that is, the angle of incidence equals the angle of reflection. (The angle of incidence is zero at the subradar point and 90 deg at the planet limb.) When the surface is perpendicular to the line of sight, maximum energy is returned. This principle of orientation rises in complexity with the complexity of the surface: from the simplest smooth plain through one strewn with boulders, solidified lava flows, or craters.

Net directivity varies with the overall shape of the target. To a first approximation, planets are spherical; this is not a bad assumption for Venus, since it is only slightly oblate. The directivity for a sphere or a near sphere with gentle slopes (about 3 deg or less) is 1. For a uniformly rough (Lambert) sphere, directivity is 8/3. The directivity is larger for the rough sphere, because more energy is returned from the area near the limbs, where the rough areas scatter energy about in many directions. Rough areas are radar bright at larger angles of incidence since these areas scatter energy in many directions, including the direction back to the radar antenna. (Near the subradar point or at small angles of incidence, rough areas are radar dark.) Smooth surface patches reflect energy mostly in one direction and so look dark unless they are oriented to the radar's line of sight. The frequency spectrum of a smooth, spherical target looks like the side view of a thumbtack, with most of the energy returned from the subradar point. The radar signature from a rough target shows more power away from the central peak; that is, the skirts are thicker.

Different kinds of surfaces can be quantified, on an average, through use of a *mean surface slope*. Mathematical models have been developed to describe the mean slope of a planet's entire visible hemisphere. These models make assumptions about the overall statistics of surface slopes, such as whether the distributions are exponential or Gaussian. The models are checked against the radar data for best fit. An area with large mean or rms surface slope is rough on the average, possibly with jagged mountains, craters, boulders, or strewn with rocks, while an area with small mean surface slope is smoother. A type of analytical technique using mean surface slopes, the angle of incidence, and the backscatter function (Subsection III.2.5.3) has been applied to radar data sets from Venus (Muhleman, 1964).

Describing a planetary surface, even if it were as well known to us as that of Earth, is obviously a complicated geometric problem; directivity can be different at every point. Polarization ratios, which quantify the relative proportion of rough and smooth areas, can

help constrain the determination of surface slopes. Considering a sphere oriented with its spin axis vertical, there will be an average slope caused by curvature as the point of observation moves from the subradar point to the east or west towards a limb. Superimposed on this average slope is the smaller scale geometry—that caused by local surface features. Thus, directivity is influenced by the overall shape of the target as well as local surface features. An approximate relative brightness at a point on the surface could be predicted, given the basic shape of the target. Large departures from this prediction might mean a rougher or smoother surface than expected, or that the shape deviates from the expected shape.

Asteroids vary greatly in their surface smoothness, and many asteroids have been found to be extremely rough. A model using a Gaussian scattering law has predicted at least a 20-deg surface slope for the asteroid Pallas (Ostro, 1992).

III.2.5.3 Backscatter Function

The *backscatter function* describes the average power reflected from the surface as a function of the angle of incidence. An example of this developed by Hagfors (Evans and Hagfors, 1968) is

$$\sigma(\phi) \propto \frac{\rho_0 C}{2} [\cos^4 \phi + C \sin^2 \phi] - 3/2 \quad (9)$$

where

- σ = radar cross section, m²
- ϕ = angle of incidence, radians
- ρ_0 = reflectivity
- C = Hagfors' parameter for slopes

Large-scale geometry and gross shape are especially described by any one of several backscatter functions. A smooth sphere, for example, has a characteristic backscatter function. The simplest model of a planet usually used is that of a uniformly rough sphere, the Lambert scatterer. The Lambert scattering law for a such a sphere is a cosine-squared function. Lommel-Seeliger scattering is another type of model that is used; it is a cosine function. Backscatter functions have been developed by Beckmann, Hagfors, Hughes, and Muhleman (Carpenter and the UCLA Department of Astronomy, 1966). The Hagfors model gives a good fit to measured data for angles of incidence of 50 deg and is most accurate for the region near the subradar point (Evans and Hagfors, 1968).

III.2.5.4 Reflectivity and the Dielectric Constant

Even if directivity and backscatter were optimal for echo return to the antenna, the amount of energy reflected can still vary with the nature of the surface material. Metals, gases, ices, water, rock, and soils in various stages of compaction each have different radar *reflectivities*. Reflectivity is the efficiency of reflection, that is, energy output divided

by energy input, regardless of the reflection angle. Metallic concentrations make good reflectors and appear radar bright.

Reflectivity of solar system objects varies over a wide range. For example, on Mars, there is an area called Stealth because it returns no echo (Muhleman et al., 1991); Stealth has very low reflectivity and has been studied at normal incidence angles (Jurgens et al., 1991). Jupiter and Saturn are examples where the sizes are large enough that a good echo should be received, but this is not the case, because their atmospheric absorption of the radar signal makes them targets with low reflectivity. Even though signatures from the moons of Jupiter are obtainable (Callisto, Europa, and Ganymede have high reflectivity), Jupiter itself has not returned unmistakable echoes.

When a radar wave passes from one medium to another, it is reflected in a predictable way. This occurs, for example, when a wave passes from the vacuum of space or the atmosphere of a planet to the planet's solid surface. The reflection occurs at the interface between the two materials, and depends on the *dielectric constants* of the two media. The dielectric constant is an important mathematical link between radar reflectivity (from radar cross section measurements) and near-surface material properties, because it can constrain the bulk density (Subsection III.3.3). The following equation applies (Carpenter and the UCLA Department of Astronomy, 1966):

$$\epsilon = \left| \frac{1 + \sqrt{\rho}}{1 - \sqrt{\rho}} \right|^2 \quad (10)$$

If the reflectivity of a surface type is known, the average dielectric constant can be estimated. Although this is a constraint on the material, it may not be possible to uniquely determine the material from the dielectric constant. Materials of the same chemical composition may have different dielectric constants, because they have different physical states: solid, liquid, or various degrees of pulverization. Furthermore, different substances may have the same dielectric constant. It is possible to constrain the material, however, if accessory information is available: the polarization ratio can sometimes be used to constrain the average dielectric constant, for example. Dry or sandy soil on Earth is known to have a dielectric constant of 3.75. Using the Goldstone Solar System Radar during the 1960s, JPL experimenters determined the average dielectric constant of an observed area on Venus to be 3.75.

III.3 Applications of the Measured Data

III.3.1 Ephemerides

Because the orbits of planets and asteroids essentially follow mathematical laws (first discovered by Kepler), future apparitions of the object can be predicted. To predict orbits, the velocity of the planet and its distance from Earth must be determined from three viewing locations; planetary radar does this very well. The predictions, called ephemerides, are needed for the navigation of interplanetary space probes and for such scientific experiments as tests of the theory of general relativity.

Occasionally and over time, some orbits change in a way that is not entirely predictable. The mass of asteroids in the main asteroid belt, for example, may be sufficient to perturb the orbit of Mars; since the mass distribution in the asteroid belt is not known precisely, the effect cannot be predicted. Also, Mercury is affected by solar oblateness and relativity effects, and Earth is part of a complicated Earth-Moon system and exhibits polar drift.

Orbits are described by a set of numbers called Keplerian elements. Once the Keplerian element set of any planet has degraded to the point that accurate ephemerides cannot be generated from it, a new set of orbital elements must be obtained. Doppler spectroscopy and radar ranging provide the needed data; the new orbital elements are computed, and the ephemerides are once again precise. The required update rate of the orbital elements to maintain a given accuracy depends on the specific object. Newly discovered objects, in particular, require a period of monitoring to establish a robust set of orbital elements.

The refinement of planetary ephemerides can be performed by measurements of orbiting spacecraft; however, these spacecraft are not always available. At such times, it is essential to perform Earth-based radar ranging to the terrestrial planets Mercury, Venus, and Mars. During the Viking Lander missions, the ephemerides of the Earth-Mars relative orbits were determined to the unprecedented precision of ± 7 m (Reid, 1988). But even these very accurate elements deteriorated rapidly mainly due to the uncertainties of the masses of the asteroids. Extrapolation of these elements for only one decade past the last of the Landers' transmissions yielded several km of uncertainty in Mars' orbit. Earth-based radar ranging to Mars can reduce these uncertainties by nearly an order of magnitude. Goldstone radar ranging is sufficiently accurate to require consideration of the altitude variations on Venus and Mercury when doing the measurement; these topographic uncertainties approach one km. Continued radar ranging of these three planets is necessary to maintain the integrity of their orbital predictions.

The first task in determining the ephemerides of a newly discovered asteroid is an initial estimation of its orbit in the hope that recurrent close apparitions can be predicted; a correct prediction is called the *recovery* of an asteroid. Optical telescopes can be used for this purpose, but the accuracy of the measurements is limited because predictions must be made from very small arcs. A prediction based upon only a few optical measurements of limited accuracy will not be robust; in such cases, the object may not even be recovered.

When tracking a new target with radar, antenna pointing may not be perfect because of limited angular position information, and this may cause some loss in signal strength, according to the pattern of the antenna. Assuming the coordinates are good enough to at least track the object, radar experiments will initially be performed using dual-polarization Doppler spectroscopy (continuous-wave measurements), which determines the gross velocity to an accuracy of about 1 part in 10^5 . These data are fed back to the tracking system and used to refine the receiver tuning. Next, ranging measurements will be made. Depending on signal strength and the amount of data, the spin vector, shape, and surface properties may be determined at this point. When very long baseline interferometry (VLBI) techniques are also used, either with multistatic operation within

the Goldstone site or with reception only by the Very Large Array, an improvement in the angular position measurements to roughly the angular extent of the object in the sky is possible. Ideally, several VLBI stations would observe simultaneously and conventional Mark II or III VLBI video recorders would be used. An automated system similar to this ideal could perform the entire sequence of observations, i.e., continuous-wave mode detection, ranging, and VLBI recording, in about an hour. It is clear that a very powerful observational tool can be formed by combining the three techniques of continuous wave spectroscopy, ranging, and VLBI measurements (Reid, 1988).

Astrometric radar data were first used to refine the orbit of an asteroid in 1968 when Icarus was probed by the ground-based radar facilities of JPL at Goldstone and MIT at Haystack. Asteroids are very difficult objects to observe optically because of their small size and because the illumination is not under the control of the observer. At present, at least 37 main belt asteroids (MBAs) and 30 near-Earth asteroids (NEAs) have been observed by radar, and many of them were first detected within the last ten years (Ostro, 1992). (MBAs remain in orbit in the asteroid belt between Earth and Mars, while NEAs have orbits that cross the orbit of Earth.) Using available optical and radar data, JPL (Yeomans, 1991) presented orbits for a dozen NEAs considered to be extinct comets (Weissman et al., 1989). For at least one of these objects, Icarus, the orbital path as observed by radar could not be explained by gravitational forces alone. One plausible explanation is a rocket-like thrust that acts on and originates from the comet's nucleus as a result of ice vaporization (sublimation). Thus an "asteroid" may actually be an older, but not yet extinct, comet. For Icarus, this was unexpected because the coma usually seen with optical telescopes near comets was not present.

Some asteroids have an orbital period of 1000 years, so the opportunity to study one at its closest approach may be rare. The population of comets is less than that of asteroids and near-Earth observations are uncommon. The first comet observed with Earth-based radar was Encke (Kamoun et al., 1982).

Time-delay (distance) and Doppler-shift (velocity) data from the Goldstone planetary radar station provide orbit information complementary to that of optical measurements, which are typically celestial angular coordinates. Radar coordinates are orthogonal to the optical coordinates; thus both are normally needed. Typical uncertainties for recent time-delay measurements are on the order of a microsecond, corresponding to position uncertainties of only a few hundred meters. The additional use of data gathered with only a few radar observations greatly improves future orbital predictions, especially for objects with a small number of optical measurements. The best data are gained from radar during the object's closest approach to Earth, because then the echoes are strong and clear.

Recently, it was realized that a large population of NEAs are on Earth approach and may even intersect the orbit of Earth. There is a critical need to accurately monitor possible "megaton impactors." For the majority of Earth-approaching asteroids, there is not a long history of accurate optical-telescope orbital predictions. In the future, precise extrapolations of asteroid motions can be accomplished most readily by using radar data obtained during close approaches.

III.3.2 Surface Characteristics, Topography, and Radar Maps

Topographic data are obtained from delay-Doppler maps and interferometry. A radar-derived map of a planet is similar to a terrestrial topographic relief map in that it shows mountains, craters, plains, hills, ice caps, crevices, and generally smooth or rough areas. Surface features can be positively identified when the radar observations are performed over time and from different viewing geometries, and then compared with observations from other data types. Other useful data sets are generated from spacecraft photographic reconnaissance, Earth-based optical and infrared studies, and radio emission studies. The best altitude resolution is obtained where the area surveyed is in the subradar region; there the achievable accuracy is about 1 or 2 μs .

In measurements for studies in celestial mechanics, including astronomical unit determination, or for scientific experiments such as relativity tests, topography must be considered, and the distance to the center of mass (the position of the planet in space) is a required measurement. That is, one must account for local height variations from the modelled mean radius. (The radius of a body can be estimated from the ranging information if data spanning a period of time are used.)

In the collection of altimetry data, the target affects the observation strategy. On Mars, a 15-km peak-to-peak topography variation has been measured by mapping the longitude of interest as it transits the subradar point. This may be a slow process and require many hours of measurement. In the case of Venus, radar imaging has to be performed over a period of many days or longer, because the rotation rate is only 0.85 deg of longitude per day. Asteroid and comet shapes have been determined by analysis of their radar signatures. A good example of this type of analysis has been presented for the asteroid Eros (Ostro et al., 1990).

Monostatic observations experience a north-south ambiguity: two areas on the surface at nearly the same longitude but in opposite hemispheres produce echoes that fall in the same delay/Doppler cell. Interferometer measurements, which use several receiving antennas, can remove the ambiguity. A second method to resolve this ambiguity uses the fact that, as the planet rotates, the newly imaged points are independent of the previously imaged points; a series of such maps provides data for a large set of simultaneous equations. This is a difficult method because of the large number of equations that must be solved. A third method to determine true position follows a surface feature over a period of time, say several months. Each point on the surface will trace a unique delay-Doppler signature. A fourth method averages the reflectivity from many different directions.

III.3.3 Bulk Density and Porosity

Radar can be used to investigate the *composition* of the surface and subsurface of a solar system object. *Bulk density* is a useful measure of surface material composition and porosity in units of g/cm^3 . The combined percent and specific gravity of each constituent in the surface material specifies the bulk density of the material as a whole. Porosity affects bulk density and porosity depends on grain shape, size distributions, and grain arrangement. Rock, water ice, soils with various packing factors, or metals—each

has a characteristic bulk density: bulk densities range from 0.5 g/cm^3 for ash or dust, to 3.6 g/cm^3 for the material of an ordinary meteorite, to 4.9 gm/cm^3 for dense, stony iron.

Although it may not be possible to determine bulk density directly from radar, it can be constrained either by the dielectric constant (Subsection III.2.5.4) from ground-based radar data sets, or by the combination of radar data with other types of data. Thermal inertia maps of Mars made from infrared measurements taken with the Viking Orbiter and other missions showed that regions with high thermal inertia generally are more dense than those with low thermal inertia: ash, fluff, dust, and other unconsolidated material have low thermal inertia. The measure of microwave emissivity of the area also provides an additional constraint on the dielectric constant.

Measure of the dielectric constants of many materials with many different packing factors made evident the problem that different packing factors can cause a different dielectric constant in the same material.

From studies of the dielectric constant and density of typical basaltic soil, it was learned that reflectivity and hence radar brightness of ice is depressed significantly with the addition of even small concentrations of this soil. In this regard, Caltech and JPL investigators using the Goldstone Radar/Very Large Array as an interferometer have analyzed reflections from the Martian south pole (Muhleman et al., 1991). It is known from optical observations that the region exhibits whitening that waxes and wanes with the Martian seasons but never vanishes; a residual ice cap remains in the Martian summer. The radar data showed that the south polar region is a nearly perfect reflector and it is theorized that the polar cap is carbon dioxide ice or water ice free from soils, that is, "clean ice."

One study of the Mars Goldstone radar data sets was a search for both high Hagfors' C factor (smooth surface) and a high dielectric constant (characteristic of liquid water) at the same region. A further constraint was to search for a change in reflectivity with a change in season. The combination of these factors in the same area might mean the presence of surface or subsurface water; such a region was found on Mars at Solis Lacus (Zisk and Mouginis-Mark, 1980).

Analysis of Mars data taken from the Goldstone Radar/Very Large Array interferometer led to the conclusion that the Stealth region near the Tharsis volcano system has a surface bulk density of less than 0.5 gm/cm^3 . This underdense material may be dust or ash transported and distributed by winds.

III.3.4 Spin Vectors

Another goal of the solar system radar investigations at JPL has been to determine the *spin vector* of a planet. The magnitude of the spin vector is the period of planet rotation (angular velocity), while the direction of the spin axis (tilt) is given in right ascension and declination. Also, the magnitude can be positive or negative, indicating retrograde or direct rotation. Direct (or prograde) means that rotation is in the same direction as the planet's orbit about the Sun. (This is the same direction of the Earth's rotation, which

is counterclockwise as seen looking down at the North Pole.) Retrograde means rotation is opposite to the direction of the orbit. Typically, the spin vector of a planet is, to first approximation, the rotation of a near sphere about an axis; the direction of this axis is roughly aligned with the orbital axis of the planet. The spin vector of some asteroids is considerably more complex, because their shapes are typically irregular.

Several methods have been used to determine the spin characteristics of a solar system object from the radar signature. The method used in a particular case depends on the nature of the data. Sometimes, when evaluating the spectra of echoes from consecutive continuous-wave runs, a prominence or feature can be identified as it moves along the frequency axis. This kind of signature corresponds to a surface feature moving as the planet rotates. The spin period can be determined by measuring the time it takes the feature to completely traverse the target frequency spectrum. Figure 8 is a series of three radar snapshots that shows the progression of a prominence that moves from left to right as the planet rotates; in the last view it vanishes as it moves to the back side of the planet. Another method compares spectra from different viewing geometries and notes the limb-to-limb bandwidth observed during one particular experiment. The technique plots the bandwidth from data gathered from many experiments performed over a long period of time; the resultant plot looks like a sinusoidal curve. From this curve, the spin period can be determined. Measuring bandwidth exactly can be difficult because echo strength from the limbs is minimal, although there is a greater return for rough surfaces than for smooth. In other words, the edge may not be well defined because the signal is buried in the noise at the limbs. Limb-to-limb bandwidth is maximum when the line of sight to the radar is aligned with the equatorial plane of the planet; this is because the radial velocity is greatest at that plane. Figure 7 shows the extreme aspect angle cases of polar and equatorial spectra; the polar geometry produces zero Doppler, while the equatorial aspect produces maximum Doppler.

If it were possible for the radar to look directly along a pole, there would be no component of velocity toward or away from the observer, and therefore no Doppler shift. In reality, Equation (5) (Subsection III.2.2) shows that the Doppler bandwidth of the spin vector for a given wavelength depends on the angle of observation (aspect angle). Any one measurement of the bandwidth looks at the projection of velocities, not the true spin period. It is noted that the total angular motion is the sum of angular motions of the target plus the apparent angular motion due to the orbit. Using these facts, the direction of the spin vector can be determined.

Another technique of spin period determination uses measurements of delay-Doppler features. Finally, interferometry can be used to track features over time and thus determine the spin period and direction.

Determination of the spin vector of Earth's sister planet Venus was the first application of the Goldstone radar. (The dense cloud cover makes optical observations of the planet's surface impossible.) Applying radar techniques, JPL investigators in the early 1960s determined the spin vector of Venus (Subsection II.5.4). The direction of the spin axis was found to be nearly aligned with the orbital axis, but the surprising discovery was that Venus rotates in the retrograde direction, unlike Earth, with a spin period of -243 days. At first, it was thought possible that the measured spin period was the

same as a "synodic resonance period" of 243.16 days (Carpenter, 1970). This would mean that the spin of Venus is synchronous with its inferior conjunctions, making exactly four revolutions around its axis between successive conjunctions and always presenting the same side to the Earth. However, upon refining the data with subsequent measurements, the spin period was determined to be close, but not exactly equal to, the synodic resonance.

The first proper radar measurement of 59 days for Mercury's spin period was performed using the Arecibo radio telescope (Pettengill, 1965). Radar was used to advantage here, since the proximity of Mercury to the Sun makes it a difficult target for optical studies.

As of this writing, the GSSR is being used to measure the spin vectors of many asteroids during their closest approaches to Earth.

III.3.5 Observations of Multiparticle Systems

The rings of Saturn and comet tails are multiparticle systems. The size and spatial distributions of the particles in both systems have been investigated using planetary radar apparatus. The Goldstone experiments showed the Saturn ring system, which classically consists of the concentric rings A, B, C, and D, to be a good reflector at 3.5 cm. Before the first radar detection of these rings by Dr. Goldstein of JPL, it was thought that the rings consisted of much smaller particles, possibly small ice crystals, 0.1 to 1.0 mm in size. After the experiments, it was certain the particles had to be greater than 1 cm in length; that is, on the order of a radar wavelength or larger. Also, the particles' good reflectivity says something about their composition. It was also found that the rings which are the brightest optically (the A and B rings) also reflect most of the radar signal. The rings of Saturn are investigated differently than other solar system targets because they are greatly overspread; this means the product of the time dispersion and the frequency dispersion is greater than one. Therefore, the continuous-wave mode with random binary phase coding or pulsed radar cannot be satisfactorily used. Instead, a continuous-wave, frequency-stepping scheme is used. The Doppler dispersion of the ring system is about 600 kHz at 12.6-cm wavelength, and the delay dispersion is 1600 msec (Ostro, 1992).

Comets are another engaging target for planetary radar exploration, in that the long tail of the comet contains gases and myriad particles. Detection is difficult when they are far from Earth, as they are small in size. The radio telescope is very useful for the unambiguous identification (unlike optical or infrared methods) of the comet's nucleus.

In late 1985, scientists observed Halley's comet and measured a large broad-band component in the echo, presumed to be from a large particle swarm, but no narrow-band component. The absence of a central peak in the echo may be the result of the low dielectric constant that results from the theorized very low bulk density of the nucleus.

The comet IRAS-Araki-Alcock was observed in May 1983 by Goldstone at 3.5-cm wavelength and 12.9-cm wavelength with a high signal-to-noise ratio; it was at its closest approach to Earth of 0.03 AU. It was found that the echo from the comet had a narrow-

band component and a relatively weaker broad-band component. The broad-band component corresponded to echoes from particles that probably had been ejected from, and are not gravitationally bound to, the active 7-km-diameter nucleus. The spin period was measured at perhaps 2 or 3 days. During this experiment, the receiver ephemeris tuning had to be done manually since orbital predictions were not well refined. For the same reason, 12.9-cm signals were used at first because the antenna beamwidth is large relative to the 3.5-cm beamwidth, even though the 3.5-cm-wavelength sensitivity is greater (Jurgens, 1985). The comet was radar imaged and showed a sunward fan-shaped coma (Sekanina, 1988).

IV. GSSR Present Capabilities and Performance

IV.1 General

A planetary radar operates on the same principle as radars for aircraft navigation or measurement of automobile speeds. However, planetary radars must detect echoes from targets at interplanetary distances and are therefore the most powerful radar systems in existence.

The center of Goldstone Solar System Radar activity is the Mars Station, site of the 70-m antenna, high-power transmitters, and signal processing equipment. The GSSR system consists of four main subsystems: Microwave, Transmitter, Receiver, and Data Acquisition. These subsystems transmit and receive signals; demodulate, process, and record data; and perform system validation. To accomplish these tasks, the GSSR system interfaces with five Deep Space Network subsystems and facilities: Antenna Mechanical Subsystem, Frequency and Timing Subsystem, Technical Facilities, Monitor and Control Subsystem, and Ground Communications Facility. Figure 13 shows the functions and interfaces of the GSSR.

The design and engineering of the GSSR are directed by the need to meet scientific objectives and by the economic constraint that requires maximum commonality of large, expensive items such as the 70-m antenna. Some equipment and technology developments are shared with the DSN, resulting in scientific and economic benefits to both the DSN and the GSSR.

Most of the radar's electronic equipment is located in the radar control room in the pedestal of the antenna; some equipment is mounted within the antenna dish itself. Three conically shaped structures (feedcones) inside the antenna dish are located atop a cylindrical equipment module that houses the 12.9-cm-wavelength high-power transmitters. Two of these feedcones are used by the GSSR. One of the cones (the XKR cone) houses the 3.5-cm-wavelength high-power transmitters, receiver low-noise amplifiers, and electronic stages (the front end) that perform initial processing of the ultraweak echoes; the other cone (the SPD cone) encloses the 12.9-cm low-noise receiving equipment and the front end. The remainder of the receiving and data processing equipment is in the radar control room. The radar transmitter's power supply and cooling equipment are large, heavy units located adjacent to the antenna on concrete pads. The frequency and time reference signals sent to the pedestal originate from the Signal Processing Center located in an adjacent building.

For transmission, a modulation waveform that depends on the radar's mode of operation is generated in the Data Acquisition Subsystem. This signal is then sent to the exciter in the Transmitter Subsystem to modulate a radio frequency carrier at either 2320 MHz or 8510 MHz. Next, the modulated carrier signal is amplified to produce an output of 400 to 470 kW. The radar signal then travels through water-cooled waveguides to either the 12.9-cm transmit/receive feedhorn (located within the SPD cone) or the 3.5-cm transmit-only feedhorn (located within the XKR cone). The signal radiated from either feedhorn impinges on the subreflector, which then directs the energy

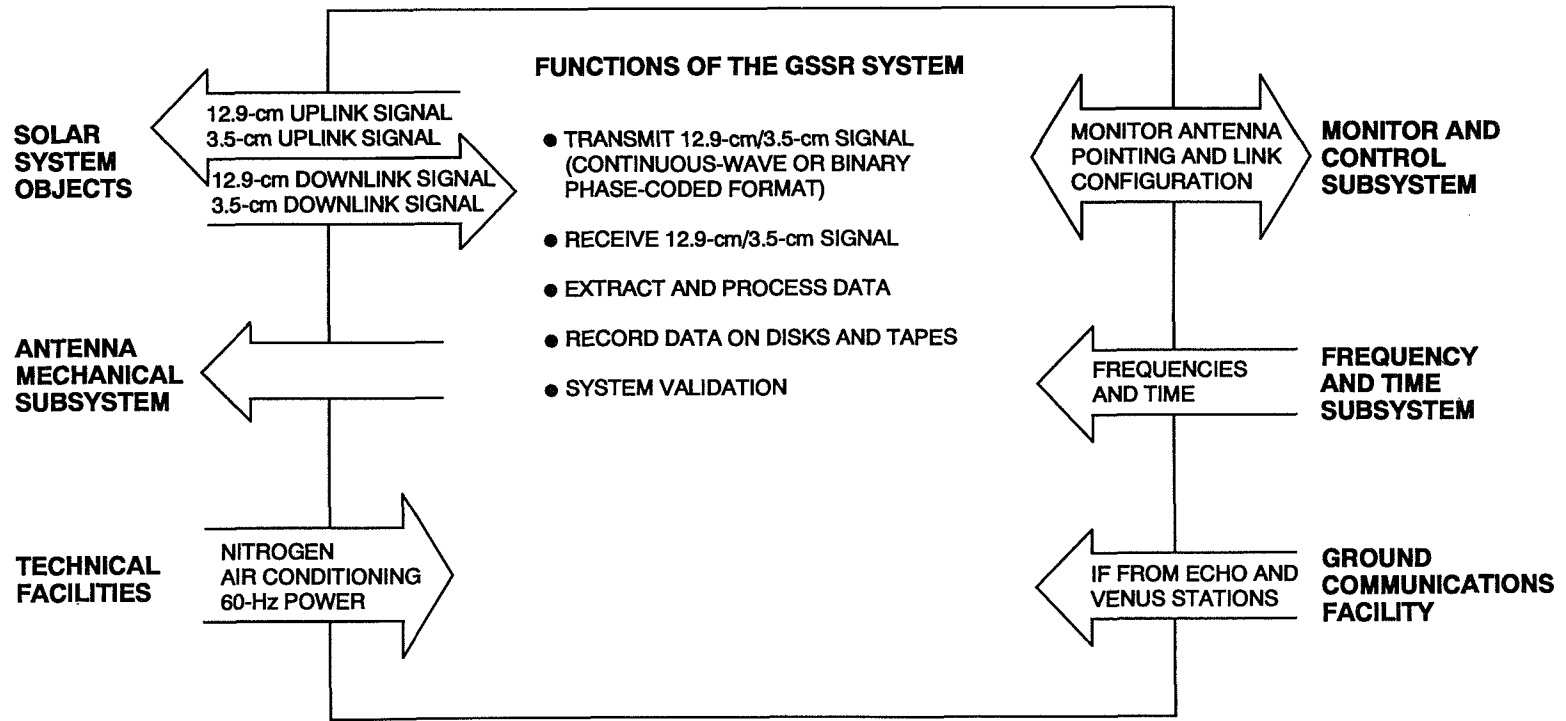


Figure 13. GSSR System Functions and Interfaces

toward the main reflector; after this second reflection, the radio signal travels toward a solar system target.

The reverse process occurs during reception of the echo, which is received through the antenna's 12.9-cm horn or the 3.5-cm receive-only horn. The signal then travels through the waveguides to the low-noise amplifier, which consists of masers for both wavelengths (Subsection IV.5.2). After strengthening by the masers, the signal is converted to a lower frequency and sent to the Receiver Subsystem in the pedestal, where further amplification and frequency conversion to a 7.5-MHz intermediate frequency take place. This output is passed to the Data Acquisition Subsystem to be processed, displayed, and recorded.

IV.2 Modes of Operation

Because there is a wide divergence in the radar observables of targets and the certainties of the target's ephemerides, GSSR modes of operation must be tailored to the specifics of the target and the investigation; one radar mode would not be suitable for the goals of all experimenters.

A mode for radar operation can be categorized according to the subsystem interconnections, the signal flow, and the specific values of several variable parameters. Among these parameters are the selected transmit waveform (Subsection IV.6.5.1) and the receiver bandwidth (Subsection IV.5.4), and configuration of the Data Acquisition Subsystem (Subsection IV.6) required to demodulate this selected waveform. The major modes of operation are *continuous wave*, *binary phase-coded*, and *multistatic*.

IV.2.1 Continuous Wave

A *continuous-wave (CW)* mode transmits a constant radio frequency signal that has no time modulation, although it is usually frequency hopped (Subsection IV.6.6). The amplitude and phase of the returned signal in this mode are used to determine such target characteristics as radar cross section, rotation rate, and surface structure.

Doppler shift and frequency spread of the received CW echo will vary greatly according to the radar scattering function of the target, and this function is related to the radius and rotation rate of the target. The radio frequency energy of an echo from a planet of relatively large radius or rapid rotation will spread over a proportionately greater range of frequencies (bandwidth) than that from a planet of lesser radius or slower rotation. Three different radar receiver bandwidths provide selectable frequency resolutions and allow optimum tailoring of the Receiving and Data Acquisition Subsystem functions to the target's radar bandwidth. A matched filter implementation, wherein the receiver's frequency response matches that of the echo, is the goal.

Frequency hopping can be used in CW mode to reduce the effects of noise. CW signals are transmitted at two different carrier frequencies near the selected radar frequency. For example, the CW signals might be 5 kHz less than the selected frequency for the first period of time and then hop to 5 kHz more than the selected frequency during the second time period. The radar echoes at the two hop frequencies are Fourier-transformed (a

mathematical process) into the frequency domain and integrated to provide power spectral densities, i.e., a spectrograph is produced. The power spectral densities corresponding to the different frequency carriers are then subtracted to cancel some noise while leaving the signals.

Occasionally, CW mode is used without frequency hopping or other modulation in order to verify antenna pointing and ephemerides. Here, the radar echo is converted to the frequency domain, and the power spectral density is displayed in real time. This display verifies location of the radar return spike at the expected frequency.

IV.2.1.1 Continuous Wave, Narrow Bandwidth

Narrow-bandwidth targets have relatively small radii and/or small rotation rates. The main targets of this mode include Mercury, asteroids, comets, Saturn's moon Titan, and Jupiter's Galilean satellites. Orbital predictions (ephemerides) of the observed object must be accurately known to successfully use this mode. If the Doppler correction (Subsection IV.5.5) applied to the receiver (or the exciter) is not exact, the radar echo will not appear in the narrow receiver bandwidth, and no signal will be detected.

The continuous-wave echo is limited to roughly 40 kHz at the receiver in the narrow-bandwidth mode. The bandwidth of the signal is divided into a number of frequency bins. Each bin can be made narrower by reducing the total receive bandwidth while keeping the number of samples constant, or alternatively taking a larger number of samples (Subsection IV.6.7.2). A narrower bin gives high resolution in frequency.

CW narrow-band data are processed by the Data Acquisition Subsystem and sent to the VAX computer for recording. Voltage samples can be recorded for processing at a later time; power spectra can be displayed and recorded in real time. The information available using this mode of operation includes radar cross sections, surface roughness, and rotation rates. CW narrow band may also be used to check antenna pointing accuracy and Doppler tracking during ranging experiments.

A recent addition to the radar Data Acquisition Subsystem is the Orbital Debris Radar Processor, which is based on a personal computer and array processor; it has up to 150-kHz bandwidth. Good scientific data from asteroids have been collected when using this unit.

IV.2.1.2 Continuous Wave, Medium Bandwidth

This radar mode supports signals with wider bandwidths than the first mode, and operates at up to 8 MHz. The CW medium band is used for radar measurements of Saturn's rings. This is a low resolution mode—less than or equal to 56 frequency (spectrograph) bins with two (left and right circular) polarization channels and cross power spectra. Autocorrelation functions (a mathematical process described in Subsection IV.6.5) of the data are recorded for processing at a later time. Frequency spectra are processed in real time and displayed.

IV.2.1.3 Continuous Wave, Wide Bandwidth

The CW wide-band mode is used to observe near-Earth asteroids, comets with poorly known ephemerides, and Mars, which has a wide frequency spectrum due to its size and high spin rate. If the target's ephemerides are not highly accurate, the Doppler shift cannot be predicted and removed to insure that the signal is within the receiver's passband. Therefore, a sufficiently wide range of frequencies is processed.

This mode is in transition to an upgraded configuration. The CW wide band has supported a maximum bandwidth of 20 MHz. A 65,536-channel spectrum analyzer has been used to process the wide-band signal and provide high resolution. This instrument was developed for SETI (Search for Extra-Terrestrial Intelligence) and used for microwave surveillance at the Goldstone complex. In the future, a multimillion-channel spectrum analyzer may be used.

IV.2.2 Binary Phase Coded

The *binary phase-coded (BPC)* mode is used for ranging measurements. A *pseudo-noise (PN) code* (Subsection IV.6.5) is modulated onto the carrier. The code is made long enough to prevent ambiguities in calculating the range to the target. These ambiguities can also be reduced by transmitting pairs of codes with slightly different baud (subpulse time duration, Subsection IV.6.5) periods. This mode is used to produce delay-Doppler maps of such targets as Venus, Mercury, the Moon, and asteroids.

Binary phase coding can be used in any of several configurations: monostatic single or dual polarization, bistatic single or dual polarization, or tristatic single polarization.

IV.2.3 Monostatic

Monostatic operation means the transmit and receive antennas are collocated (i.e., there is only one receive antenna); it is the most basic type of radar operation. Monostatic planetary radar experiments are done at the 70-m antenna (the Mars Station) since the radar control room and high-power transmitters are located there.

IV.2.4 Bistatic and Multistatic Operation

IV.2.4.1 General

Bistatic operation means that more than one antenna is used to receive the radar signal. Continuous wave, usually narrow band, or binary phase-coded waveforms can be used in multistatic operation. Bistatic and tristatic configurations are used to resolve the hemisphere ambiguity associated with monostatic delay-Doppler maps, provide high resolution, and perform altimetry of targets, at or away from the subradar region.

Although signals are always transmitted from the Mars antenna site, either the 26-m or the 34-m antenna at the Venus site or the 34-m antenna at the Echo site can be used as a receiver along with the 70-m antenna in bistatic or tristatic mode. The combined signals from two or more antennas can then be used as interferometer measurements,

whereby a *fringe (or interferometric) pattern* is produced. The pattern consists of *multiple* lobes that span much smaller angles than the *single* main lobe of a monostatic antenna pattern (Hagfors and Campbell, 1973). The number of fringes spanned by the planet depends on the distance between the antennas relative to the size of the wavelength. Figure 14 shows an interferometer configuration. Other radio observatories such as the Owens Valley, California, Observatory; the Arecibo Observatory at Arecibo, Puerto Rico; or the Very Large Array at Socorro, New Mexico, can be used in conjunction with Goldstone's high-power radar station to form a bistatic radar.

Because the Goldstone system can handle up to four channels of signal processing, several modes with bistatic or tristatic configurations are possible, including bistatic single or dual polarization, or tristatic single polarization. The 26-m Venus antenna can simultaneously receive both right and left polarizations at 12.9-cm wavelength or one polarization (either right or left) at 3.5-cm wavelength. The new 34-m beam waveguide antenna at the Venus site will be capable of simultaneous dual-polarization reception on

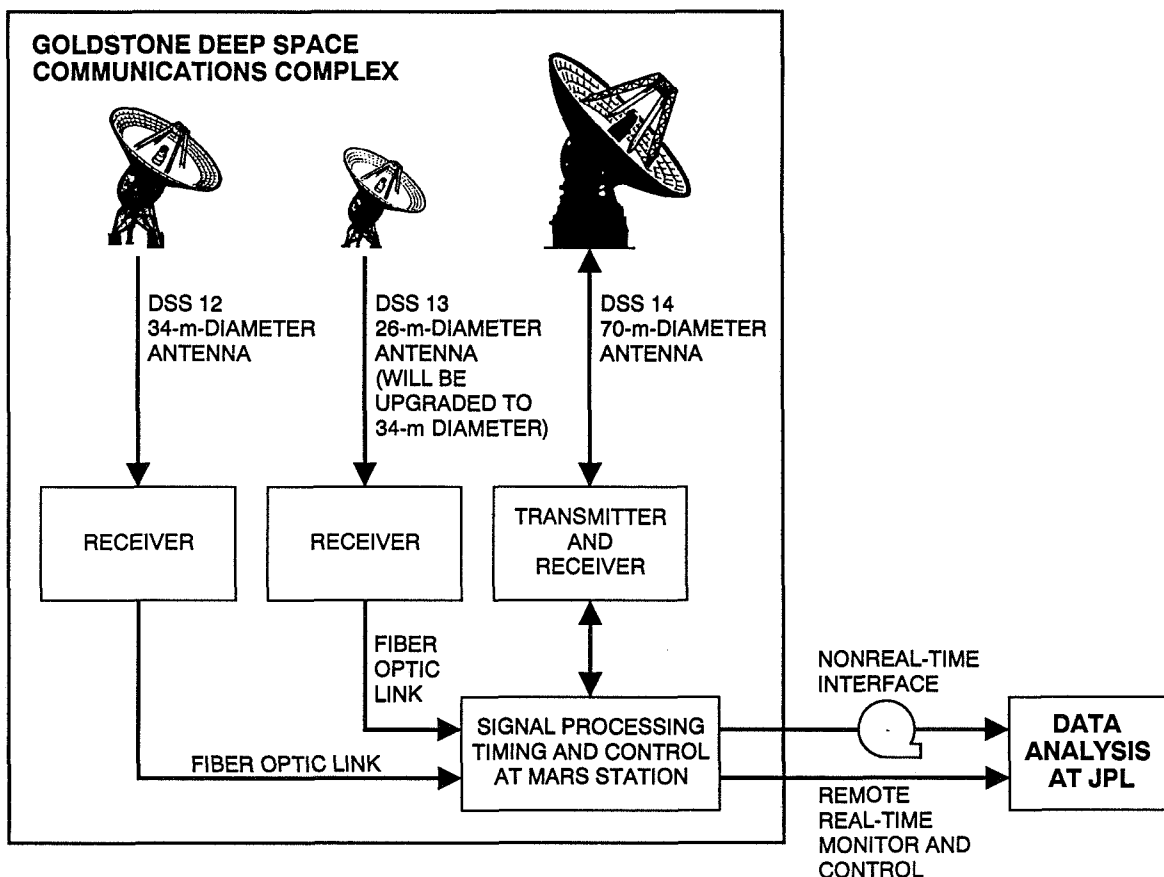


Figure 14. Interferometry

either 3.5-cm or 12.9-cm wavelengths. The station at the Echo site can receive either polarization on either wavelength. (A station operates on one wavelength at any one time.)

IV.2.4.2 Echo Station

The signal from the Echo Station may be either downconverted to 7.5 MHz for transmission to the Mars Station via a microwave link or converted to 50 MHz for transmission to the Mars Station via a fiber-optic link. The performance parameters of the station are listed in Table 4.

IV.2.4.3 Venus Station

The signal from the Venus Station (the station normally reserved for research and development) is downconverted to a 50-MHz intermediate frequency and can be transmitted to the Mars Station via a fiber-optic link. The performance parameters of the Venus Station are listed in Table 5.

IV.2.5 Goldstone/Very Large Array Collaboration

The combination of the GSSR and the National Radio Astronomy Observatory's Very Large Array (VLA) at Socorro, New Mexico (Figure 15), forms the world's most powerful

Table 4. *Echo Station Performance (34-m Antenna)*

Parameter	Wavelength, cm	
	12.9	3.5
Polarization ^a	RC or LC	RC or LC
Frequency range, ^b MHz	2320 ±10	8510 ±10
Antenna gain, dBi	56.1	66.2
Beamwidth, two-sided, deg	0.27	0.075
Ellipticity, dB	0.6	0.8
Low-noise amplifier	Block III maser	Block IIA maser
Center frequency, ^b MHz	2320	8510
Bandwidth, MHz	30	> 100
Gain, dB	45	44.5
Noise temperature, K	8	4
Receiver bandwidth, ^b MHz	20	20
Dynamic range, ^b dB	≥ 60	≥ 60
System noise temperature, ^b K	< 20	25

^aRC is right circular; LC is left circular.
^bGSSR requirement, not actual.

Table 5. Venus Station Performance (26-m Antenna)

Parameter	Wavelength, cm	
	12.9	3.5
Polarization ^a	RC	RC and LC
Frequency range, MHz	2192 to 2332	8510 ±10 ^b
Antenna gain, dBi	52.2	
Beamwidth, deg	0.36	0.030 ^b
Ellipticity, dB	0.7	
Low-noise amplifier		
Center frequency, MHz	2320 ^b	8510 ^b
Bandwidth, MHz	12	20 ^b
Gain, dB	37.6	50 ^b
Receiver bandwidth, MHz	14	20
Dynamic range, ^b dB	≥ 60	≥ 60
System noise temperature, K	30	30

^aRC is right circular; LC is left circular.
^bGSSR requirement, not actual.

3.5-cm transmitter with the largest 3.5-cm receiving aperture to produce the world's most sensitive imaging radar telescope. The VLA uses as many as 27 steerable, 25-m-diameter antennas configured in a Y-shape to form a real-time interferometer; the VLA telescopes permit spatial resolution across the plane of the sky. The GSSR-VLA configuration can observe the terrestrial planets, Earth's moon, Jupiter's Galilean satellites, Saturn's ring system and satellites, and a number of asteroids and comets.

IV.3 Transmitter

IV.3.1 Exciter

The exciter uses the ultrastable Frequency and Time Subsystem Reference along with modulation information from the VAX computer to generate the radar waveform to be transmitted. The exciter is common to the transmitted 12.9-cm- and 3.5-cm-wavelength signals. Pseudonoise codes (modulation) are used in the binary phase-coded (ranging) mode, and either frequency hopping or no modulation is used in the continuous-wave mode to generate a low-level transmit waveform. This signal is then sent to the transmitter where it is amplified to a very high power. The Transmitter Subsystem (including exciter) interfaces to the Data Acquisition Subsystem for monitor and control (Figure 16). Performance specifications are given in Table 6.

ORIGINAL PAGE
BLACK AND WHITE PHOTOGRAPH

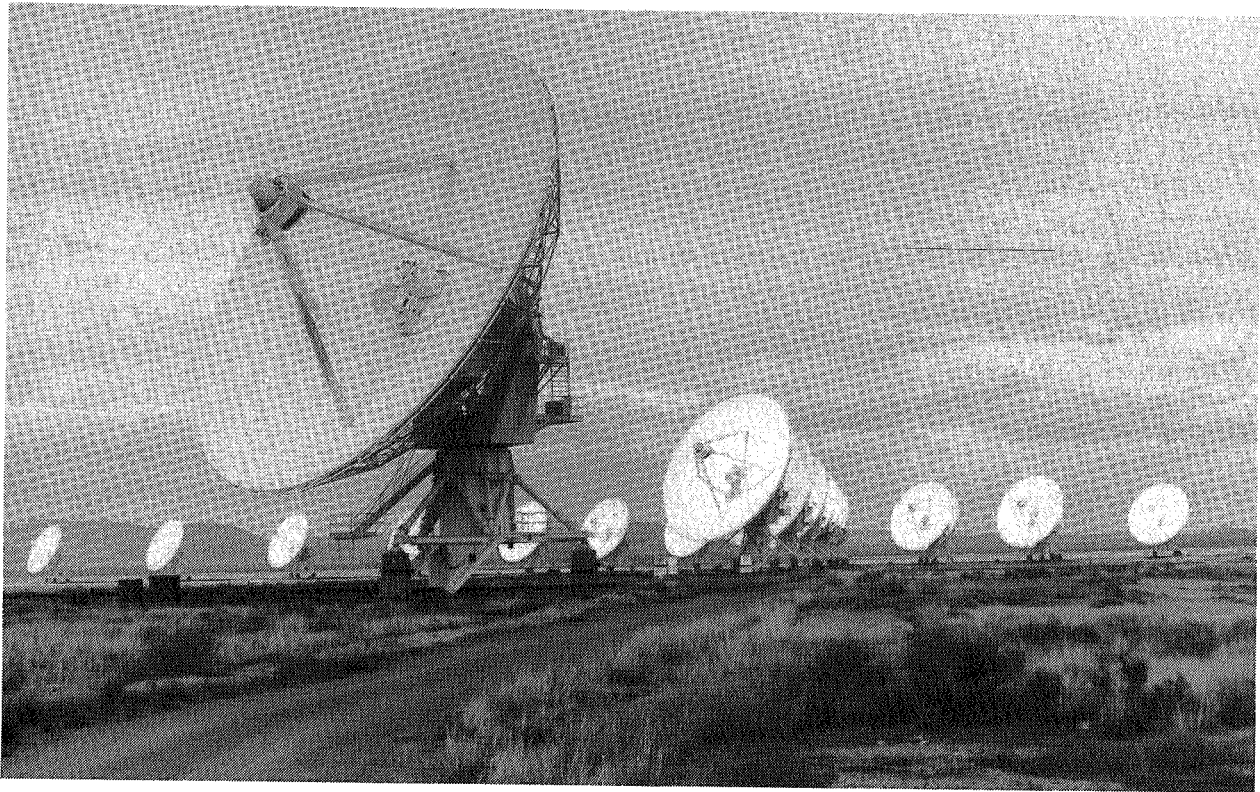
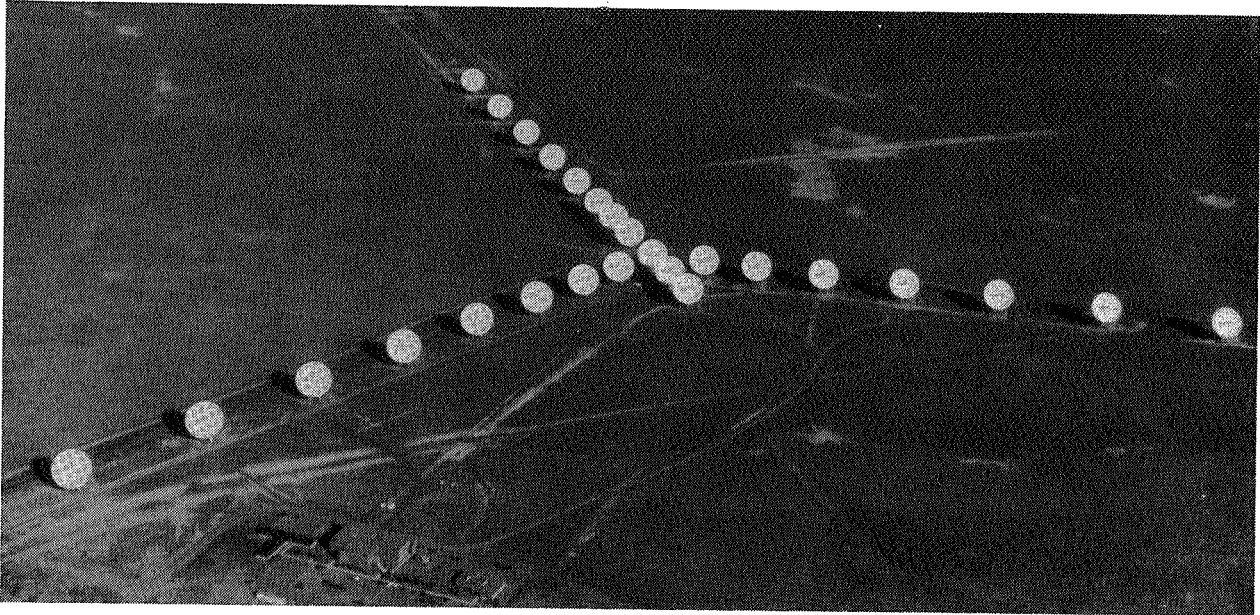


Figure 15. *Very Large Array*

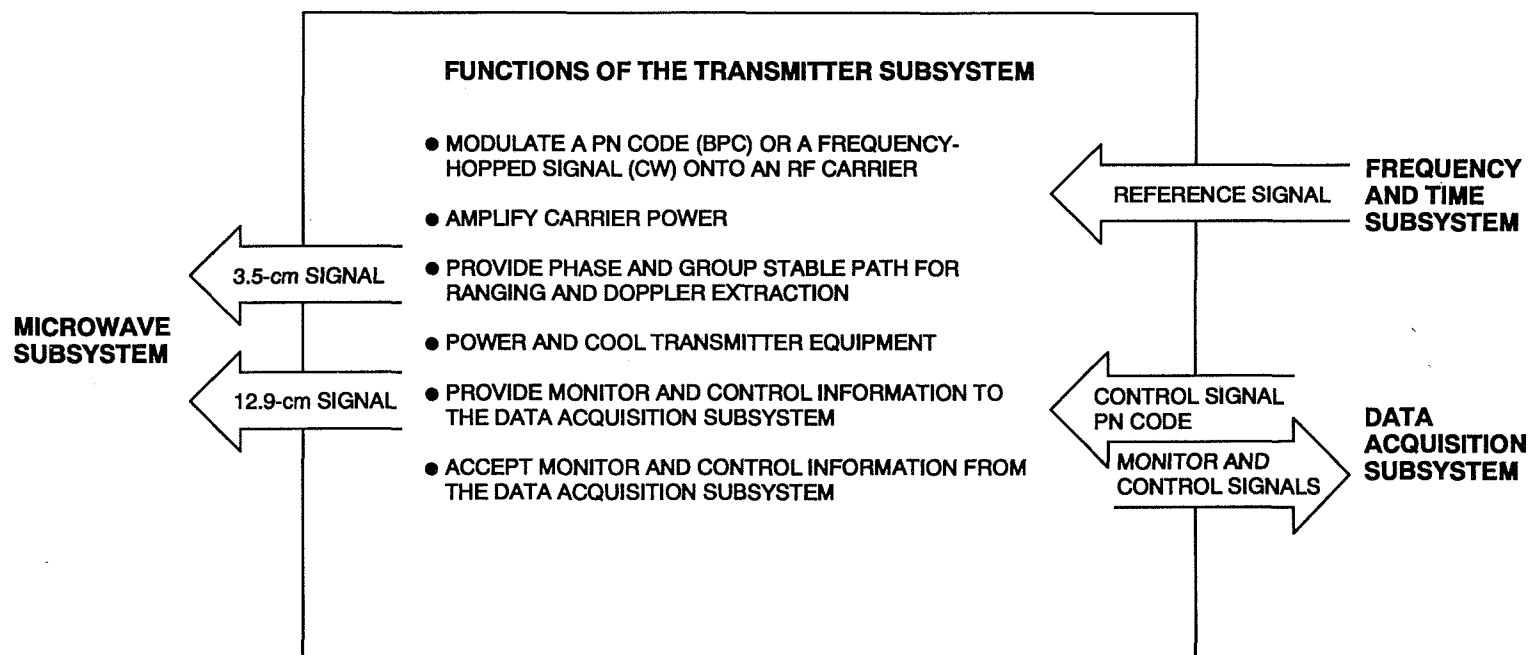


Figure 16. *Transmitter Subsystem Functions and Interfaces*

Table 6. Transmitter Performance

Parameter	Wavelength, cm	
	12.9	3.5
Transmitter power, kW	400	465
Frequency, MHz	2320	8510
Antenna gain, dB	62.4	74.0
Antenna beamwidth, deg	0.119	0.030
Polarization ^a	RC, LC	RC, LC
Frequency accuracy	$\pm 3 \times 10^{-13}$	$\pm 3 \times 10^{-13}$
Modulation	Biphase	Biphase
Cross polarization, dB	<-25	<-25
Frequency hopping	≤ 2 MHz apart	≤ 2 MHz apart
Max Doppler shift, MHz	0.5	1.7

^aRC is right circular; LC is left circular.

IV.3.2 Final Amplifier

Very high transmitter power levels are used to overcome the large signal losses caused by the extreme distances to solar system targets. The 3.5-cm-wavelength final amplifiers are water-cooled *klystrons* (Figure 17). Two klystrons are connected in parallel, and their power output is added. They are located in the 3.5-cm feedcone to place them as close as possible to the radar-dedicated transmit feedhorn. This location minimizes energy loss in the thick-walled waveguide, a loss that can be as much as 1 kW/ft. The klystrons amplify the signal from the exciter for a combined output power at the feedhorn of 465 kW. Klystrons can amplify carriers with either binary phase-coded or continuous-wave modulation, with or without frequency hopping. In these tubes, electromagnets focus electrons falling through a potential drop of some 51 kV (for the 12.9-cm-wavelength tube, 60 kV are used). The electron beam's velocity is modulated by the excitation signal, and this in turn modulates the electron density and energy flux at radio frequencies. Internal resonant cavities enhance this modulation and about one-half of the nearly 1 MW of input direct-current power is converted to radio frequency power, which is sent out through a waveguide to the antenna feedhorn and radiated toward the target. The other half of the input power is waste heat, which, in addition to heat from waveguide losses, is transported away from the klystrons and feedlines by cooling water to the Heat Exchanger Assembly. Radio frequency power measurement, an important quantity in radar experiments, is via temperature sensing of this cooling water flow; water loads are used during test and adjustment.

The high-velocity impact of the electrons on the collector anode of the 12.9-cm-wavelength klystron generates dangerous X rays that must be contained by heavy metal

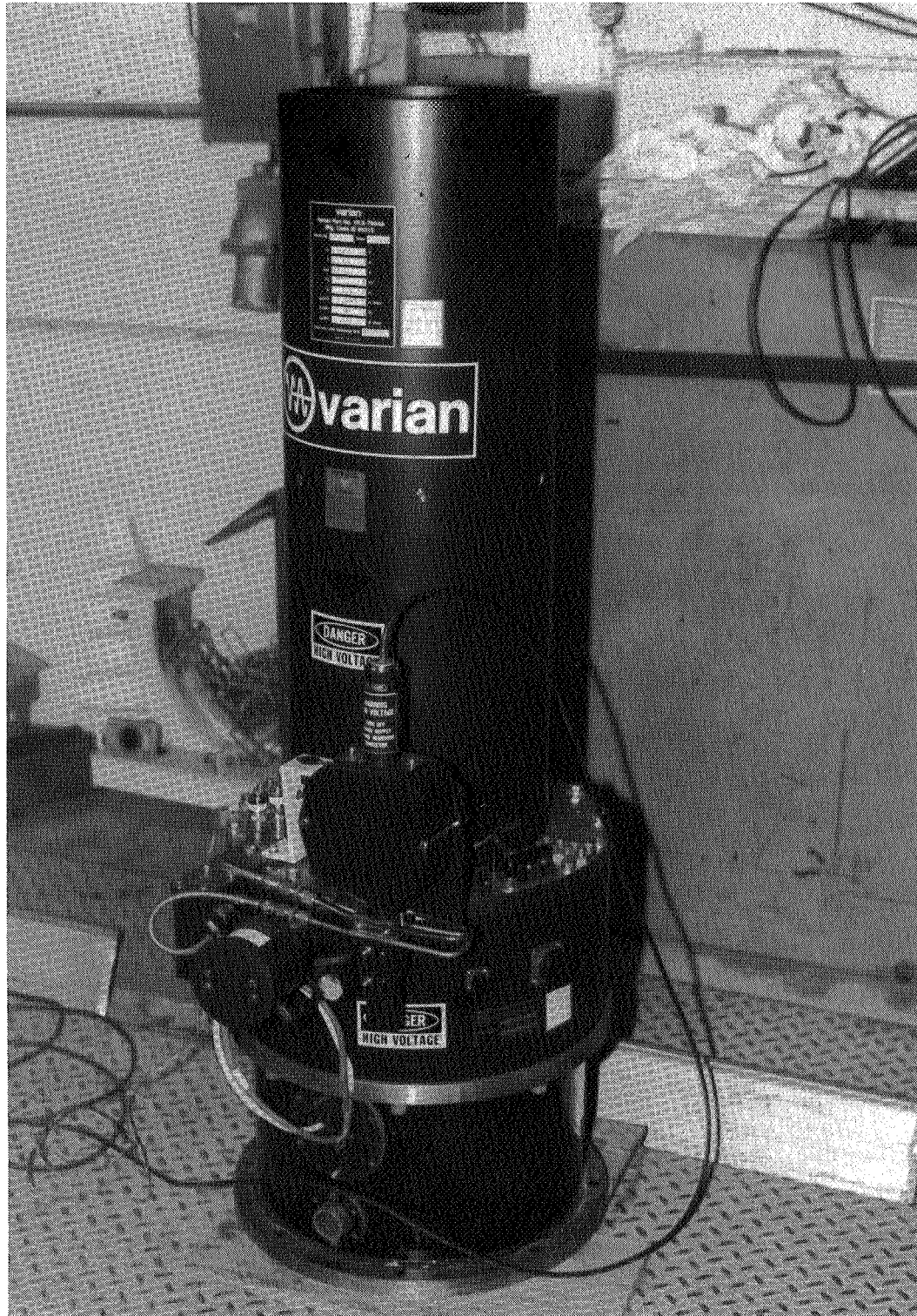


Figure 17. *The 3.5-cm-Wavelength Klystron*

shielding surrounding the tube, a requirement that further boosts the weight, complexity, and cost of the klystrons.

Any klystron amplifies over a relatively narrow band of frequencies, and so a tube other than the 3.5-cm klystrons must be used for 12.9-cm work. The tube required is a single water-cooled klystron that amplifies the 2320-MHz exciter signal for a radio frequency power output of 400 kW; this output is sent to the 12.9-cm (S-band) transmit/receive feedhorn in the SPD feedcone. The 2320-MHz klystron is located within the antenna dish in the equipment module that supports the feedcones.

On either frequency band, one selected polarization is transmitted, either right circular or left circular. The control panel for the klystrons is shown in Figure 18.

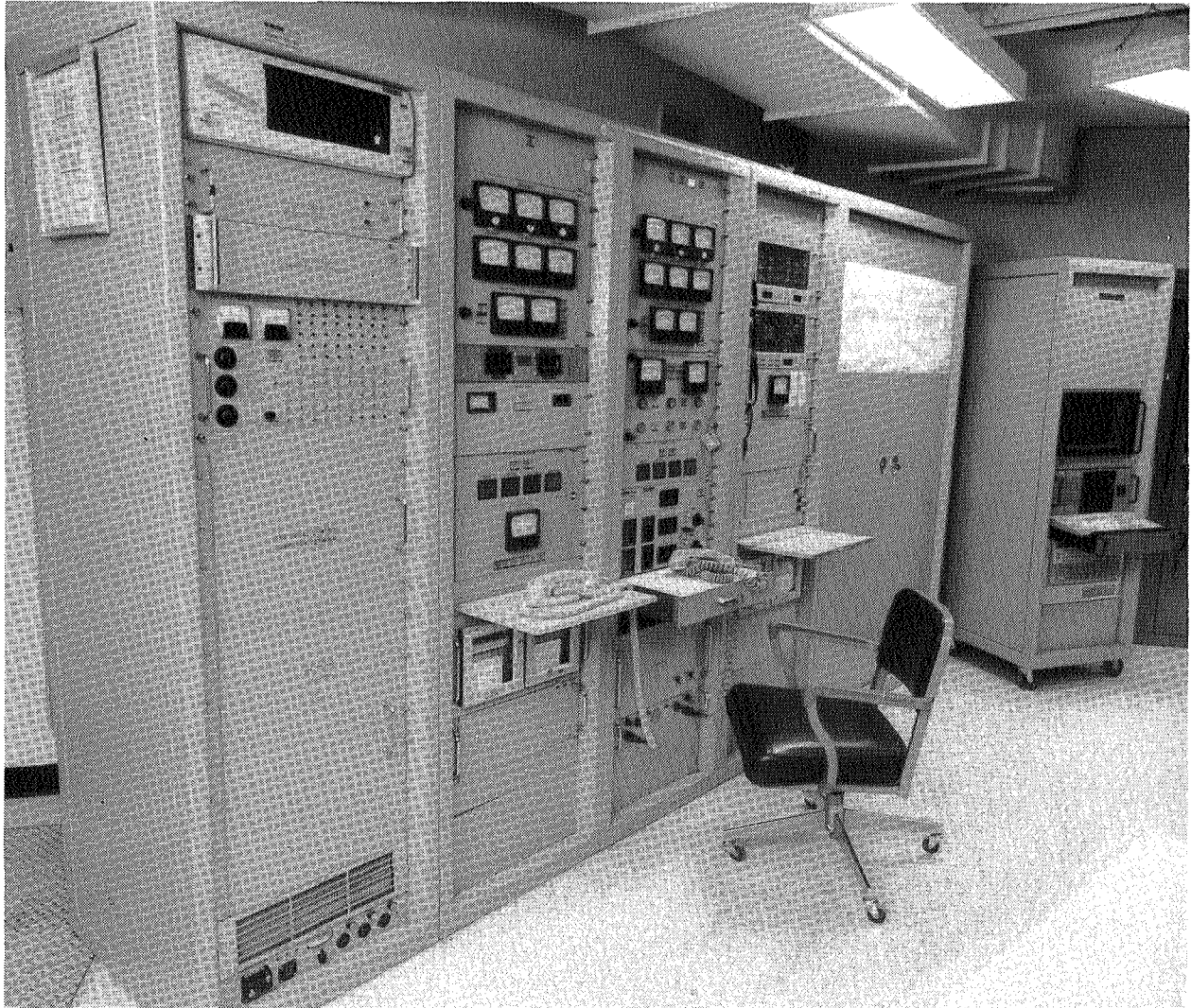


Figure 18. *Final Amplifier Control Panel*

IV.3.3 Power Supply

The high-voltage power supply equipment is located both inside and outside the antenna. The power supply provides high voltage to the klystron power amplifiers.

IV.3.3.1 Motor Generator

The motor generator provides voltage regulation (it maintains a constant voltage on its output), isolates the power supply from the mains during crowbar operation (Subsection IV.3.3.4), and changes the frequency of the available 2400-V, 60-Hz alternating current mains to 400-Hz electrical power. Three-phase power at 60 Hz is supplied either commercially or by diesel generators located at the Mars Station. The frequency is changed to facilitate filtering the high-voltage direct-current power.

IV.3.3.2 Transformer/Rectifier

The electrical power output of the motor generator is not suitable for use by the klystron final amplifiers. The 2400-V, three-phase, 400-Hz electrical current must first be increased to between -50,000 and -70,000 V direct current. This function is performed by the step-up transformer/rectifier.

IV.3.3.3 Filter

The output of the transformer/rectifier is high-voltage direct current, but not pure and smooth enough for use by the high-power amplifier. The direct current still contains alternating-current ripple components that must be removed; if not filtered out, these components would impart undesired modulation to the signal. Pure direct current is obtained by passing the current through a pi-network filter.

IV.3.3.4 Crowbar

The klystrons are expensive and difficult to replace. Their protection during fault conditions is a crucial system-reliability consideration: the klystron could be damaged or destroyed by a system fault, and the result would be expensive downtime. To protect the klystron, the high-voltage power supply is short-circuited whenever monitoring circuits detect trouble, such as an electric arc within a tube. A fast sensor in the monitoring circuits detects the fault and triggers an ignitron tube that short-circuits (crowbars) the power supply in about 10 μ s; following this, the generators's field current is set to zero and then three vacuum switches disconnect the generator's output.

IV.3.4 Heat Exchanger

The klystrons generate roughly 500 kW of waste heat and the waveguide about 40 kW of heat; these energy losses are great enough to require major provision for cooling. The heat is transferred to a circulating coolant that is pumped to a water-to-water heat exchanger mounted on the alidade. The cooling water from the second loop circulates through a water-to-air heat exchanger near the base of the antenna.

IV.4 Antennas

IV.4.1 General

The primary GSSR Antenna Subsystem consists of the 70-m-diameter main reflector, the subreflector and its supporting quadrapod, the pointing system, and the concrete pedestal building upon which it rests. The pedestal is partitioned into the offices of the Radio Astronomy and Radar Group, equipment rooms, and the radar control room. The total weight of the antenna including the pedestal is about 7258 metric tons. Its overall height is 71 m (234 ft), making it the largest Goldstone antenna. The weight of the rotating structure is about 2700 metric tons. The pedestal is over 10 m high and contains 4400 metric tons of reinforced concrete. For an antenna of this size, an azimuth-elevation mount is more economical than an equatorial or X-Y mount.

The giant dish and its azimuth-elevation mount atop the pedestal rotate in azimuth on three flat bearing surfaces that float on a thin film of oil over a flat circular runner or track several feet wide. The counterweighted dish assembly is supported in elevation by two horizontal stub shafts, each of which rests on two roller-bearing assemblies.

Construction as a 64-m antenna was completed in 1966. The antenna began operation as part of the Deep Space Network in 1966 by communicating with the 1964 Mariner Mars spacecraft, which was then 328 million km (205 million mi) away. The upgrade to the present 70-m diameter was complete in June 1988. Performance specifications for the present antenna are listed in Table 7.

Table 7. Antenna Performance

Parameter	Wavelength, cm	
	12.9	3.5
Sky Coverage		
Azimuth, deg	0 to 360 (full)	
Elevation, deg	0 to 88	
Slew rate, each axis, deg/s	0.2	
Pointing accuracy, each axis, single track rms, deg	< 0.002	< 0.002
Effective collecting area, m ²	2.77×10^3	2.5×10^3
Transmit-to-receive switch time, s	10	30

IV.4.2 Main Reflector

The 70-m Goldstone antenna is a fully steerable, beam-shaped reflector with horn feeds. The configuration is Cassegrain, as shown in Figure 19, and the wavelengths of operation are 3.5-cm and 12.9-cm. Greater sensitivity is achieved with the shorter wavelength. The benefit of a very large aperture can be seen from the radar equation (Equation (2)); the received signal power varies as the square of the antenna gain.

The Cassegrain configuration was originally used in 17th-century optical telescopes. The double reflector design offers advantageous positioning of the microwave feed structure, which can be inside the dish at the bottom or behind the reflector. The alternative requires feed-structure mounting at the main reflector focal point (relatively far above the surface of the reflector). If the receiving and transmitting equipment is mounted at the focal point, an unacceptable blockage of the signal occurs. On the other hand, if cabling and waveguides connect a feed (small in size relative to the equipment) mounted at the focal point to the transmitter and receiver located outside the antenna, long, lossy feedlines and complicated plumbing and cabling are required. The Cassegrain design positions the feed so the loss in gain associated with waveguide length is minimized. (Waveguide losses also become more significant as the frequency is increased.) The large size of the main reflector makes it possible to mount the feedhorns, low-noise maser amplifiers, and high-power final amplifiers right within the antenna dish.

Antenna surface accuracy is critical to signal gain. The main reflector surface consists of about 1200 precision-shaped aluminum trapezoidal panels individually adjusted for optimum performance by means of screws. The panels are secured to an open, welded steel framework. Optical techniques and radio frequency holography are used for alignment. While the panels near the center of the dish are solid, the panels near the rim are perforated to reduce weight and the effects of wind. Regardless of where the antenna is pointed in azimuth or elevation, the reflecting surface must remain accurate to a fraction of the signal wavelength, meaning that the measured surface across the 3850 m² surface has to be within one cm of the calculated surface. Usually, the accuracy required is 1/16 of a wavelength for near-perfect performance. In use, there is some small distortion of the antenna shape as a function of elevation

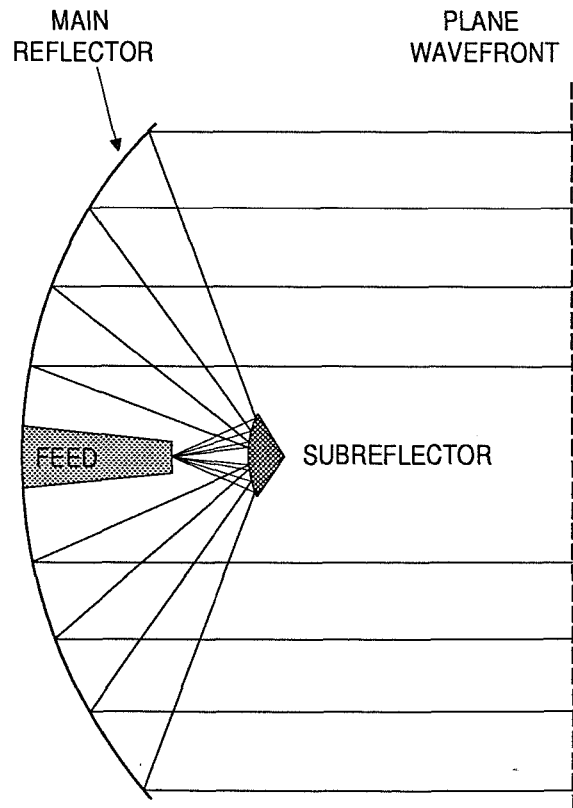


Figure 19. Cassegrain Configuration

pointing angle because of the varying stresses from gravity on the structure; wind loading and thermal stress as well can cause the structure to deviate slightly from the preferred theoretical shape. These distortions result in a small loss in gain. The effect of mechanical surface deviations on antenna gain is greatest at smaller wavelengths and is roughly 0.5 dB at 8510 MHz and less than this at 2310 MHz. During the upgrade from 64-m to 70-m diameter, the surface was reshaped to improve efficiency.

The signal efficiency of the overall Antenna Subsystem is affected by several factors, including feed- and transmission-line losses, blockage loss from the subreflector and its quadrapod support structure, surface mechanical imperfections, and spillover and aperture loss (Evans and Hagfors, 1968). It is noted that atmospheric attenuation increases at low elevation angles where there is more of the atmosphere to look through; also, because the atmosphere radiates, the noise temperature is higher.

IV.4.3 Subreflector

The subreflector is mounted on a quadrapod support structure inside the main antenna dish, and its shape is nearly hyperbolic. During radar operation at 3.5-cm, the subreflector physically moves to switch the radar system from transmit to receive (i.e., the focal point of the subreflector is moved from the transmit to the receive feedhorn). Because this motion requires about 30 s, the target of a 3.5-cm observation must be at least 4,500,000 km from Earth. The same technique is used to switch from 3.5-cm- to 12.9-cm-wavelength operation because the single 12.9-cm transmit/receive horn is in a separate feedcone.

IV.4.4 Antenna Pointing Subsystem

The Antenna Pointing Subsystem is installed in the rotatable Instrument Tower that rises through the center of the pedestal but is completely separate from it to provide a stable, vibration-free platform. High pointing accuracies are maintained to avoid losses in signal power and to permit the use of signal integration techniques. Pointing control of the antenna is done remotely from the Signal Processing Center, which is housed in an adjacent building. The antenna has access to the entire sky north of declination -50 deg and can track a target at declinations near 35 deg for nearly 11 hours. Coordinates are given in right ascension and declination form. Pointing accuracy is maintained even during windy conditions, but deflections on the order of millidegrees occur with winds of 45 mph.

Master equatorial pointing is the primary high-accuracy pointing method; the necessary hardware is contained in the Instrument Tower. The tower first rotates in response to a pointing command sent from the computer in the Signal Processing Center. A light source mounted on the rotating antenna structure aims a beam at a mirror mounted on the rotating tower; after several reflections, the beam is ultimately detected by a precise autocollimation light sensor also mounted on the movable antenna structure. This feedback signal controls hydraulic motors that continue moving the antenna until the commanded coordinates are reached.

Computer-controlled pointing of the antenna is also available; azimuth and elevation position encoders provide the feedback information. While this method is not as precise as that of master equatorial pointing, it can function as a backup.

IV.5 Receiver

IV.5.1 Receiver Subsystem

The Receiver Subsystem amplifies the extremely weak echoes received by the antenna. The receiver must perform this function while adding little noise of its own to the signal. The Goldstone system achieves this goal primarily through the use of special ultralow-noise maser front-end amplifiers and locating the crucial first receiver stages within the antenna at a minimum distance from the feedhorns. The amplified signals from the liquid-helium-cooled masers are then sent to the remainder of the receiving equipment at the base of the antenna. This arrangement minimizes losses caused by long runs of waveguide. The Receiver Subsystem outputs the amplified signal to the Data Acquisition Subsystem, where analog and digital signal processing is performed.

The nominal frequencies at which the Receiver Subsystem can operate are 2320 MHz (12.9-cm wavelength) and 8510 MHz (3.5-cm wavelength). At any given time, one of the two frequency ranges is selected. The Goldstone receivers can process two orthogonal circular polarizations (left and right circular), while a single circularly polarized signal is transmitted. For signals of either wavelength, there are in effect two identical receiver channels, one for each polarization. By operating two channels, investigators can observe the two polarizations simultaneously. This yields additional information about the radar scattering properties of the target.

The Receiver Subsystem is *superheterodyne*. This design converts, in steps, the maser-amplified microwave radio signal to lower frequencies called intermediate frequencies (IF). The subsystem downconverts this radar echo to a final IF of 7.5 MHz. This is achieved by a process of mixing, or heterodyning, the echoes with frequency-stable, pure sine waves called local oscillators. The advantages of this design are small transmission line losses and high-gain electronic amplification, which is more readily optimized at IF rather than higher microwave frequencies.

In the radar control room, either the 3.5-cm or the 12.9-cm wavelength signals are selected for further processing; this is achieved through the Receiver Select Module. All signal processing performed after the Receiver Select Module is common to both the 3.5-cm- and the 12.9-cm-wavelength signals. The selected signal is then passed to the Receive-Transmit Switch Module, which prevents the transmitted signal from leaking into the receiver. This module is followed by several IF modules that provide signal gain, mixing, and filtering. The performance parameters of the receiver are listed in Table 8.

IV.5.2 Microwave Subsystem (Receive)

The Microwave Subsystem hardware for reception is located in both the 3.5-cm and 12.9-cm feedcones within the antenna (Figure 20). Two separate feedhorns are used at 8510 MHz—one for receive and one for transmit. The 3.5-cm receive horn collects energy

Table 8. Receiver Performance

Parameter	Wavelength, cm	
	12.9	3.5
Frequency range, MHz	2200 to 2325	8510 \pm 10
Antenna gain, dB	63.1	74.0
Antenna beamwidth, deg	0.108	0.031
Aperture efficiency, %	70	65
Sensitivity, K/Jansky	1.00	0.90
Feed polarization ^a	RC, LC	RC, LC
Pointing loss, dB, 3 σ (master equatorial pointing)	0.020	0.020
Low-noise amplifier	Maser	Maser
System temperature, K (listen only)	15 \pm 3	22
Intermediate frequency, MHz	30, 50, 75	325, 75, 50, 7.5

^aRC is right circular; LC is left circular.

from the subreflector and passes it to the orthomode transducer, which resolves the signal into right- and left-circular polarization components. From this stage forward to the output of the receiver, there are two identical channels. Because the critical first stages of a receiver have a greater effect on the final signal-to-noise ratio than subsequent stages, the 3.5-cm orthomode transducer and the masers are cryogenically cooled to a temperature of 4 K to reduce the amount of thermal noise added to the signal; a liquid-helium closed-cycle refrigeration system is used. The 3.5-cm dual maser (Figure 21) is a traveling wave maser with superconducting magnets and klystron (amplifier tube) pumps. The pump frequencies are 19 GHz and 24 GHz. The maser is followed by a post-amplifier stage that uses field-effect transistors as the active elements. This Microwave Subsystem output is fed to the 3.5-cm Front-End Module (also in the feedcone) for mixing, amplification, and filtering.

The 12.9-cm transmit and receive horn, when in receive mode, passes the echo signal to the 2320-MHz orthomode transducer for resolution into left- and right-circular polarization components. The two 12.9-cm masers, which are the first active 12.9-cm stage, follow the filters and provide the required low-noise amplification. The masers may be bypassed via waveguide switches. The amplified, but still weak, output signal from the masers is then fed to the 12.9-cm Front-End Module (also in the feedcone) for further processing.

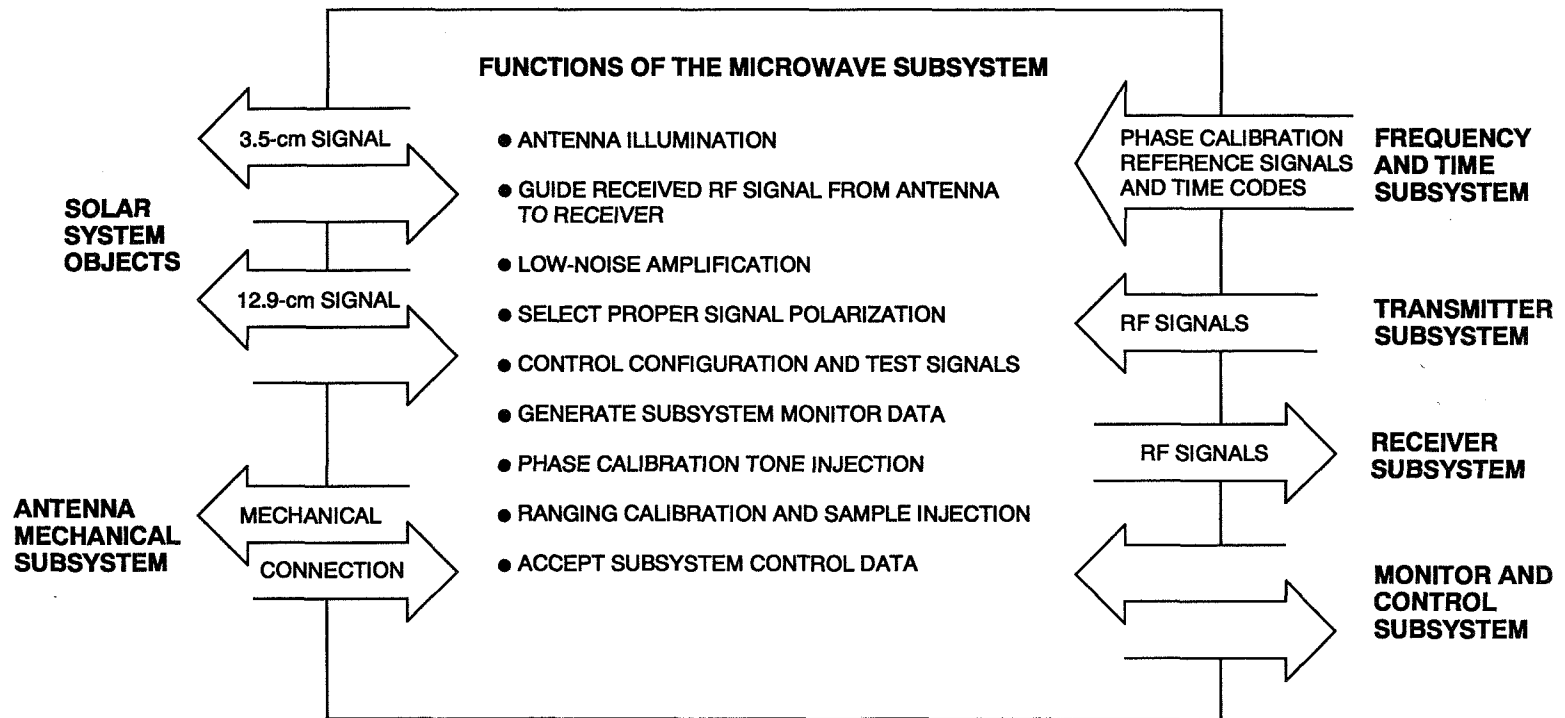


Figure 20. Microwave Subsystem Functions and Interfaces

ORIGINAL PAGE
BLACK AND WHITE PHOTOGRAPH

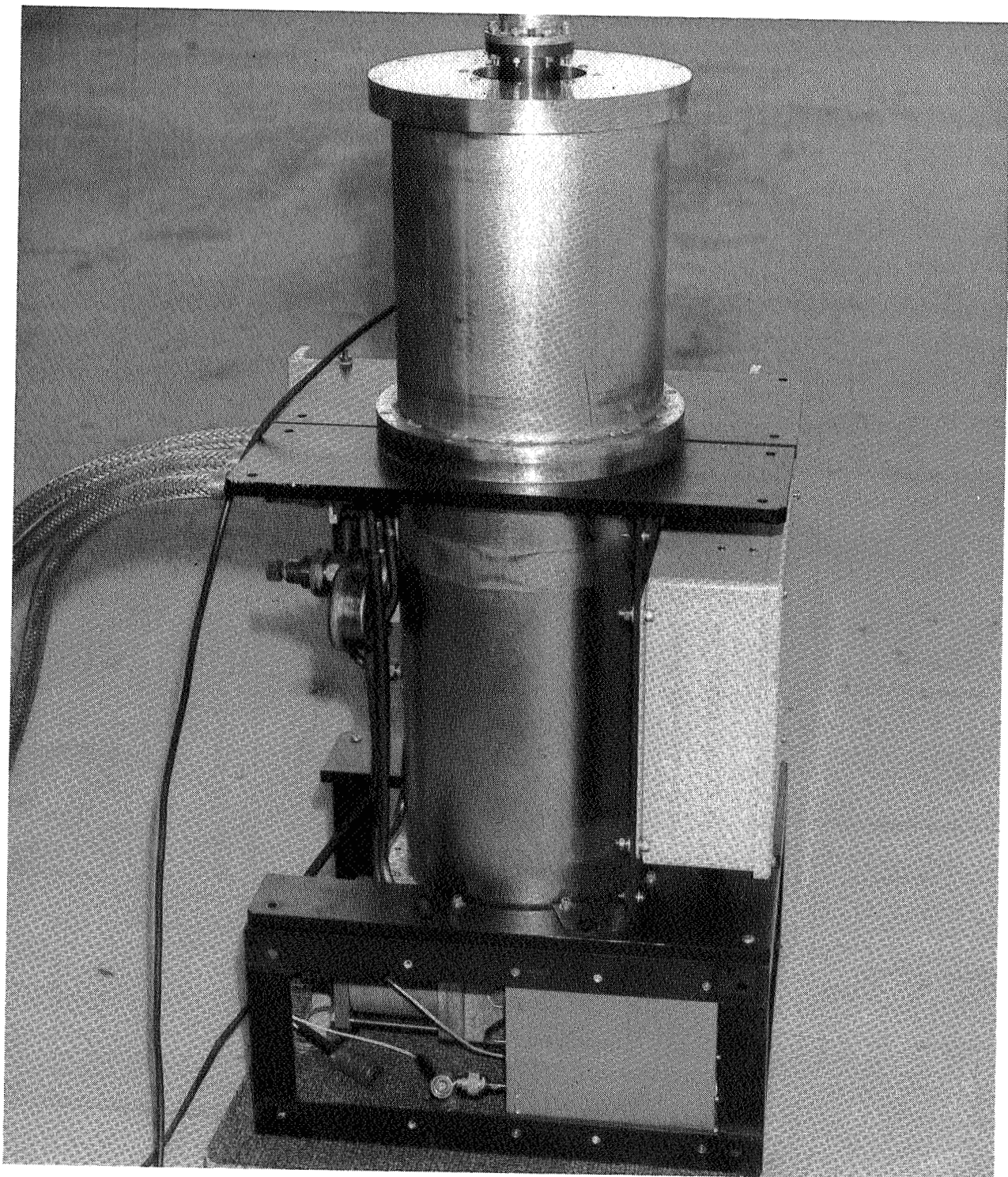


Figure 21. *The 3.5-cm-Wavelength Maser Under Test*

IV.5.3 Front-End Modules

The received radar signals, even though greatly amplified by the maser low-noise amplifiers of the Microwave Subsystem, are still extremely weak. Much more amplification is required to increase the signal strength to useful levels. The Front-End Modules located in the feedcones provide the additional needed signal gain.

The 3.5-cm Front-End Module accomplishes this task by using mixers to convert the signal to lower frequencies, amplifiers to boost signal strength, and filters to reject unwanted (spurious) signals. These functions are applied to both polarizations.

The signal from the Microwave Subsystem is first applied to a front-end mixer that downconverts the 3.5-cm radio signal to an IF of 325 MHz. The local oscillator required by the mixer to do this is located in the pedestal and referenced to the stable Deep Space Network hydrogen-maser frequency standard.

Typically, an IF amplifier requires a fixed frequency of operation to facilitate the extensive filtering and amplification of the signal. However, the frequency of the echo will vary from the frequency of the transmitted carrier because of the Doppler effect. Since the mixer outputs the *difference in frequency* between the echo and the local oscillator, one mixer input (the local oscillator) must be adjustable if the other mixer input (echo) varies and the output (IF) must remain fixed. This "ephemeris tuning" (Subsection IV.5.5) requirement is implemented by a computer-controlled Programmable Local Oscillator. (The tuning can also be done at the transmitter's exciter, rather than at the receiver.)

The local oscillator signal used with 3.5-cm signals begins with a frequency of about 25.5 MHz at the pedestal. The signal is sent over coaxial cable to the Front-End Module in the feedcone, where it is multiplied by an amount necessary to produce 325 MHz when mixed with the 8510-MHz echo. The downconverted signal is now amplified and filtered. The 325-MHz signal is then mixed with a fixed-frequency 400-MHz signal sent from the pedestal over coax; the 400-MHz signal is derived from the Frequency and Time Subsystem 100-MHz reference (the hydrogen-maser frequency standard). The resulting frequency difference of 75 MHz is filtered and amplified, then output to the pedestal for further processing.

The 12.9-cm Front-End Module, located in the 12.9-cm feedcone, provides additional gain and filtering to the radar return signals, which have been boosted by the maser, and downconverts them to a 30-MHz IF. The nominal radio frequency input to this module is about 2320 MHz. The 12.9-cm front-end mixer uses the Programmable Local Oscillator's ultrastable signal from the pedestal and multiplies the frequency the proper amount to produce the IF of 30 MHz when mixed with the 2320-MHz echo. The still weak signal is boosted by 30-MHz IF amplifiers, and filtering is applied to reject spurious signals and limit noise power. This signal is now fed to the receiver equipment in the pedestal for further processing.

IV.5.4 Intermediate Frequency Stages

The IF stages (75 MHz for the 3.5-cm wavelength and 30 MHz for 12.9-cm wavelength) in the pedestal provide additional signal gain and filtering to the downconverted radar return signal. Because there is only one pair of IF amplifier stages (one for each of the two polarizations), provision is made for selection of either the 12.9-cm or 3.5-cm wavelength signal. Finally, test signals are injected and monitored with test instrumentation to verify subsystem performance and perform troubleshooting.

In the pedestal room at the base of the antenna, the receive signal path begins with the Receiver Select Module. When a switch selects the IF used by 3.5-cm signals, a 50-MHz *difference* frequency output is produced by mixing the 75-MHz IF with a 125-MHz local oscillator signal. When the IF used by the 12.9-cm wavelength signal is selected, a 50-MHz *sum* frequency output is produced by mixing the 30-MHz IF signal with a 20-MHz local oscillator signal. Both local oscillator signals are derived from the stable Frequency and Time Subsystem reference frequencies.

After the Receiver Select Module, signal processing in the pedestal is the same for either wavelength signal. The signal is carried to the Receive-Transmit Switch Module, which contains attenuators and switches that prevent the transmitted signal from leaking into the receive path and connection points to allow test inputs such as noise to be injected into the receive signal path.

The next stage, the First IF Module, is a 50-MHz intermediate frequency amplifier that provides filtering to approximately a 10-MHz bandwidth and a large signal gain. The amplified 50-MHz signal is next split into three paths within this module. One path is output to the Final IF Amplifier; the second is connected to a filter with a 10-MHz bandwidth. This filter's output can be monitored with a spectrum analyzer, noise measurement instrument, or other test instrumentation. The third 50-MHz signal is applied to a mixer to produce a 10-MHz output that is split into three paths. Two of these paths produce outputs of 10-MHz and are filtered to about 2-MHz bandwidth; the third 10-MHz path is output to the 10-MHz IF Module.

Bandwidth is important because it controls the amount of noise power in the final receiver stage:

$$P_n = kTB \quad (11)$$

where

- k = Boltzmann's constant, 1.38×10^{-23} W•s/K
- T = absolute temperature, K
- B = bandwidth, Hz
- P = maximum power in the load, W

It can be seen from this thermal noise equation that noise power varies directly with receiver bandwidth. The bandwidth must be wide enough to pass the signal, but not so wide as to allow excessive noise to degrade the signal.

Continuing with signal flow through the receiver, one of the 10-MHz outputs with 2-MHz bandwidth from the first intermediate frequency amplifier is connected to the 10-MHz IF Module. This module splits the 10-MHz input signal into two branches, each of which is filtered. One branch becomes an output of 10 MHz with a reduced bandwidth of 150 kHz, and the other branch is divided into two other 10-MHz outputs, each of which has a narrow 10.8-kHz bandwidth. One 10.8-kHz bandwidth output can be monitored by instrumentation such as an oscilloscope or root-mean-square (RMS) voltmeter. The two other outputs (the 10.8-kHz bandwidth output and the 150-kHz bandwidth output) connect to a matrix switch that allows various equipment connections.

The last stage of the receiver is the Final IF Amplifier, which contains a mixer that downconverts the 50-MHz input to 7.5 MHz. It also provides signal gain and filtering. The 7.5-MHz echo signal output from this last receiver module has been amplified many times since entering the feedhorn; it is now sent to the Data Acquisition Subsystem for analog-to-digital conversion and digital signal processing.

IV.5.5 Ephemeris Tuning and Local Oscillators

The Deep Space Network Frequency and Time Subsystem (Section IV.7) maintains an extremely stable hydrogen maser time and frequency standard. These reference frequencies are used by the radar system for fixed and variable local oscillators and for the Data Acquisition Subsystem. The fixed and variable frequencies required by the mixers in the receivers are generated from the reference frequencies by the local oscillators in the radar control room. A Programmable Local Oscillator is used at both 12.9-cm and 3.5-cm wavelengths as the local oscillator input to the first mixer.

In planetary radar, the Doppler shift of the echo is typically not negligible, and in fact, provides important information about the target. If a radar echo changes in frequency because of Doppler shift (Subsection III.2.2), the local oscillator must be adjusted in real time to compensate for this change; alternatively, the transmitter's exciter frequency must be adjusted. (Goldstone applies most of the correction to the exciter, and a smaller amount of correction to the receiver.)

The design goal is to keep the received radar signal centered within the narrow IF passband of the receiver even as the input signal varies in frequency. This generally requires advance knowledge of the object's motion. The orbit of the Earth and its rotational motion are well known. For planets and some other solar system objects, knowledge of the orbital motions (perhaps from optical or previous radar observations) is sufficient to provide a good prediction of the required Doppler compensation. If an object's ephemerides are not well refined, there is uncertainty in the required Doppler compensation. If the magnitude of the uncertainty is small compared with the bandwidth of the receiver, the Doppler shift can be used to refine the ephemerides.

In part, Doppler shift is affected by the motional characteristics of the planet, asteroid, or comet. Rotation, for instance, may be complex; one observed asteroid appears as an irregular shape rotating about several axes. Mars has a relatively rapid rotation rate on the order of one Earth day and a characteristically large frequency bandwidth. Venus, on the other hand, has a slow rotation of several hundred days per one revolution. Most of the information of interest from Venus is contained in a frequency band only 30 to 80 Hz wide. Therefore, one would choose a narrow-bandwidth receiver to process the signal; but if the Doppler correction is not accurately known, the signal will not appear in the later stages of the receiver although it is present at the front end, where the bandwidth is wider. Thus a process of refinement of Doppler correction and receiver bandwidth may be required over several target tracks.

The procedure uses a wider than optimum receiver bandwidth for first observations and accepts greater than optimum receiver noise power. (Some marginal objects may not even be detectable because of this noise degradation.) The actual Doppler shift of the signal can then be measured; from this measurement, future, more accurate ephemerides are calculated. During the next track, the refined local oscillator (or exciter) settings are used along with a narrower receiver bandwidth. Corrections occur throughout a radar track. Recording the actual measured Programmable Local Oscillator frequency at the start of a radar track is standard operating procedure to verify proper Doppler compensation. The result of this process is a better signal because of the reduced noise power from a narrower receiver bandwidth and a more accurate knowledge of the ephemerides of the object. Only extremely stable transmitter and receiver local oscillator frequencies allow the Doppler shift to be measured precisely enough to improve knowledge of the rotation rate or the ephemerides or both.

The Programmable Local Oscillator, located in the Goldstone radar control room, is a commercial instrument under digital control via a data bus (IEEE interface) linking the VAX to a MAC-16 dedicated computer. The computer performs Doppler calculations based on ephemerides (from JPL) that have been downloaded to it from the VAX 11/780 general-purpose computer.

IV.5.6 Instrumentation

Receiver Subsystem performance is verified by measurements and tests. An important measure is the system noise temperature, which is taken at the receiver/transmitter switch. At this test input, an IF amplifier stage provides a 50-MHz signal output with a 10-MHz bandwidth for connection to a frequency spectrum analyzer and noise-adding radiometer. Further, there is provision for connection of an RMS voltmeter and oscilloscope at the output of a 10-MHz IF amplifier. The frequency of the Programmable Local Oscillator (about 25 MHz) is measured by a frequency counter.

IV.6 Data Acquisition Subsystem

IV.6.1 General

This primarily digital subsystem is located in the Goldstone radar control room (Figure 22) and performs overall monitoring and control of the GSSR. The Data

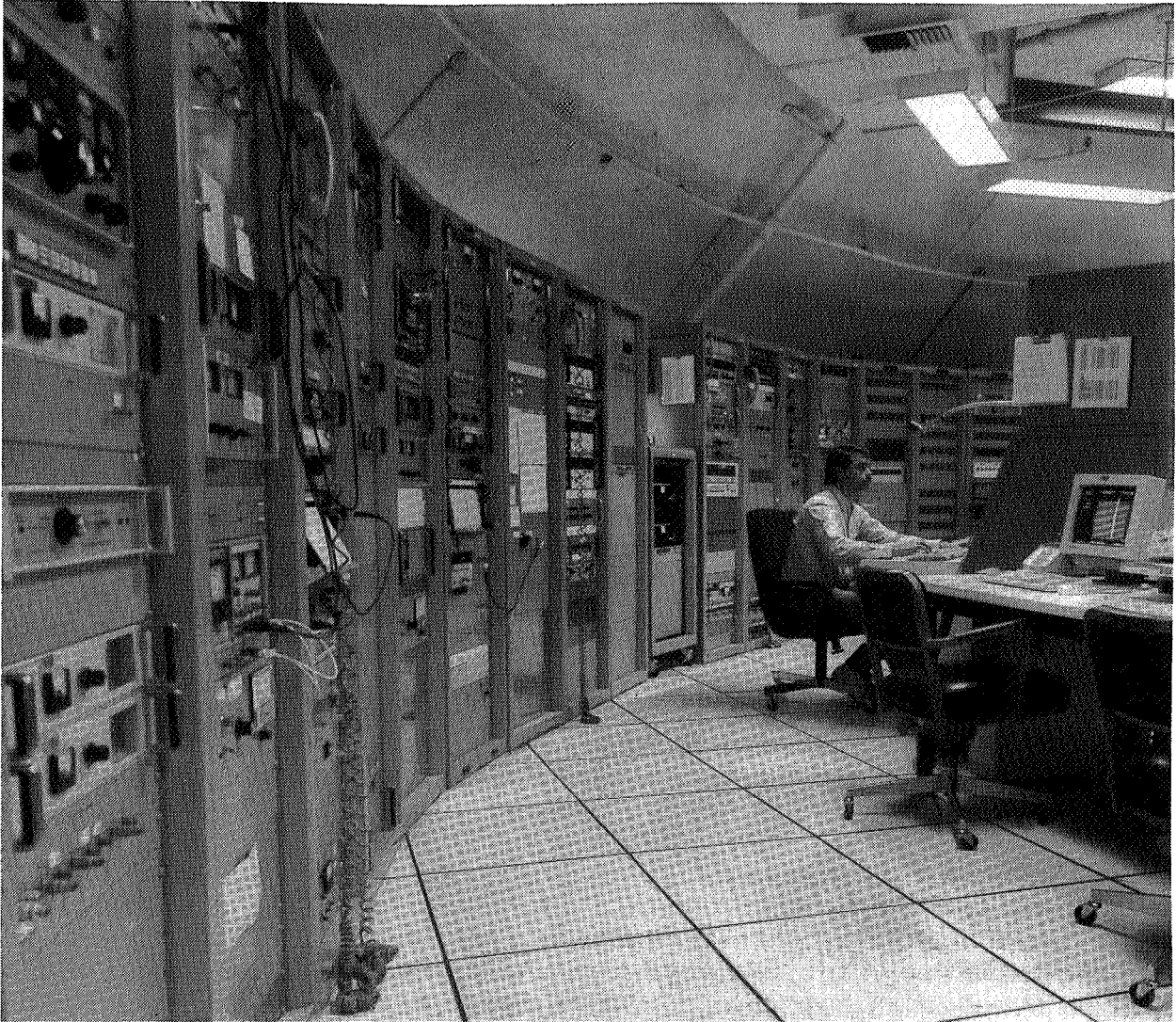


Figure 22. *Radar Control Room*

Acquisition Subsystem (DAS), dedicated exclusively to radar and radio astronomy, consists of computer hardware and software and may be the most rapidly evolving part of the radar system. The DAS is the beginning and the end of the radar signal. It monitors and configures transmitter and receiver; generates the radar waveforms to be transmitted; digitally processes, displays, and records the scientific data from the Mars Station receivers or other Goldstone antenna sites; and handles remote communications with JPL. The major components of the DAS include a DEC VAX 11/780 digital computer with disk and tape drives, a DEC LPA-11 analog-to-digital converter, several IBM-PC compatible computers, a Sun Workstation, an array processor, correlators, and other equipment to process and record the received signal and generate transmitted waveforms.

The DAS receives the two channels of 7.5-MHz IF signals from the GSSR Receiver Subsystem outputs (Subsection IV.5.4). One channel contains left-circular polarization

information and the other channel contains right-circular information; the two channels are processed simultaneously. For single-polarization experiments, only one channel is used.

Signals sent over the Goldstone Ground Communications Facility during multistatic operation are received at the Mars 70-m antenna site as 50-MHz IF and downconverted to 7.5-MHz IF. As many as four 7.5-MHz channels are input to the DAS during multistatic operation.

IV.6.2 Monitor and Control

A VAX 11/780 computer at the 70-m antenna pedestal performs overall monitor and control functions for the GSSR. The parameters of the computer and digital signal processing hardware are described in Table 9.

Specifically, the computer monitors and controls functions for the Receiver Subsystem and the Transmitter Subsystem, and interfaces with the remainder of the DAS. The VAX downloads commands for pseudonoise code generation and transmitter frequency hopping; it also sends information to the computer that is dedicated to the Programmable Local Oscillator, which generates compensation for Doppler frequency drift. The VAX handles remote communications with JPL; it enables an operator at JPL to control the configurations of many test modes by remotely activating the computer controlled matrix switches in the pedestal radar room; it can send scientific data to JPL. Finally, the VAX can record and display the several forms of scientific data that have been processed by the DAS. The VAX is synchronized by a clock slaved to the 5-MHz Frequency and Time Subsystem stable frequency reference.

IV.6.3 Complex Mixers

The complex mixers in the DAS acquire signals from the Receiver Subsystem and downconvert them into baseband or low-frequency signals suitable for digital signal processing. The processing that is later performed requires two forms of a baseband signal that differ in phase by 90 degrees. These two forms are called I and Q, for in-phase and quadrature. They are necessary for the complex mathematics (involving both real and imaginary components) used to form the frequency spectrum of the signal. The I form of the signal is designated the reference phase because, by convention, it is a phase of 0 deg. The Q form of the signal differs in phase from the reference by 90 deg. There are two separate mixers per channel, one for I and one for Q (Figure 23). After mixing, the I and Q signals are passed to the analog-to-digital converters for further digital signal processing.

IV.6.4 Programmable Local Oscillator Frequency Setting

A means is provided at the radar receiver to compensate for the Doppler effect. Information including target ephemerides (from JPL) is input to the VAX in the radar control room. This information is downloaded to the dedicated MAC-16 local oscillator computer before the beginning of the radar track. This computer performs the detailed calculations for Doppler compensation and sends them over a digital data bus to a commercial

Table 9. Data Acquisition Subsystem Performance

Parameter	Value
Range gates	8 × 256 complex
Bandwidth	
CW narrow band, kHz	40/(no. of channels)
CW medium band, ^a MHz	8 complex
CW wide band, ^a MHz	20
BPC, ^a MHz	10
Sampling Rate, MHz	Four channels at 40 ^b
CW narrow band, kHz	40 complex/(no. of channels)
CW medium band, ^a MHz	8 complex
CW wide band, MHz	20
BPC, MHz	40
Transmitter phase encoder	
Baud, μs	0.125
Resolution, ns	12.5
Array processing rate, Mflops	18
1-k FFT computation rate, ms	2.6
Computer	
Central processing unit, data bus, bits	32
Bus speed, Mbytes/s	13
Memory, Mbytes	8
Disk storage, Mbytes	600
Data transfer rate, Mbytes/s	1.2
Tape drives	2
Data rate, kbit/s	650
Density, bits/in.	6250
Speed, in./s	125
^a Two channels.	
^b Usually only three channels are available.	

frequency synthesizer. This process of "ephemeris tuning" continues during the radar track.

IV.6.5 Binary Phase-Coded Modulation and Demodulation

IV.6.5.1 Generation and Use of Binary Phase-Coded Signals

Binary phase-coded signals are used only when making ranging measurements. To obtain the distance to the target, the radar system measures the round-trip travel time of the radar signal, from which the distance can be calculated (Subsection III.2.3). If continuous wave were used, ranging information from points other than the subradar point would not be discernable.

Generally, to make ranging measurements, a time modulation has to be applied to the transmitted waveform. A simple system would switch the high-power transmitter carrier on and then off during some short time interval t_{on} , creating a pulse; after a wait of some time t_{off} during which the transmitter is shut off and the receiver listens for the echo, the process is repeated. The delay time from transmission to reception of the radar echo is then measured to give range to the target. The important parameters of the transmitted periodic waveform are the repetition frequency and time duration (pulsewidth) of the pulse. Transmitting repetitive pulses allows the energy of many received pulses to be added, thus improving the signal strength over noise.

In practice, this simple scheme is not the best choice for extremely distant objects that have weak radar returns or when high resolution ranging is required to observe finer features. Increased range resolution depends in part on shortening the transmitted pulse width. There are disadvantages to this. The amount of energy returned from the target decreases with shorter transmitted pulse widths, since energy is the time integral of power; the signals are already ultraweak from traveling such extreme distances, and they must compete with noise power in the receiver. Furthermore, the bandwidth of the receiver has to be increased to accommodate the shorter pulse width and, since Fourier analysis shows that a short pulse is richer in high-frequency harmonic content than a longer pulse, the wider receiver bandwidth required for a short pulse allows more noise into the system, mutilating the signal. Also, switching difficulties are created and reduced klystron life is caused by modulating the high-power amplifier of the transmitter with short pulses.

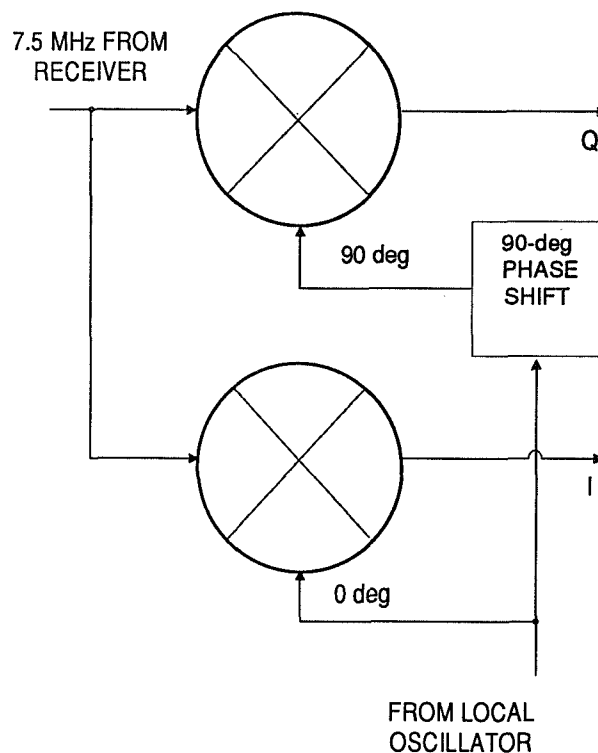


Figure 23. Complex Mixer

An improved ranging technique that simultaneously achieves high resolution and higher signal-to-noise ratios than those of a single short pulse uses a *biphase pulse compression* transmit waveform, which is a long pulse divided into some number N of subpulses, each of equal time duration. During the time for each subpulse (one baud), the phase of the transmitted waveform is one of two discrete states, either 0-deg phase or 180-deg phase; this process is biphase modulation. The phase of each subpulse is selected in accordance with a specific phase code. The resultant signal is a *binary phase coded* signal. Each of the many possible phase codes produces particular performance characteristics.

The range resolution depends on the time duration of one baud, not the overall pulse. A subpulse is made short to give high range resolution, while keeping the overall transmitted pulse longer, resulting in high average transmitted power. Because power is transmitted continuously during the subpulses rather than being gated (i.e., the transmitter is shut off), there are fewer klystron switching problems, longer klystron life, and greater echo energy. The number of subpulses per long pulse is called the compression ratio or code length. A code zero (or +) corresponds to 0-deg phase of the transmitter carrier, and a one (or -) corresponds to a 180-deg phase change, or phase reversal. Figure 24 shows a simple example of a binary phase-coded transmit modulation, with five subpulses (Skolnick, 1970).

IV.6.5.2 Demodulation (Ranging)

In the received signal, when using binary phase codes, energy is present away from the central peak of the range profile; these unwanted *range sidelobes* are small with a well-designed code. One set of codes with good characteristics is Barker codes, where the magnitude of the range sidelobes is very small (either 0 or 1; 0 is ideal), while the magnitude of the central peak is equal to the code length. Known Barker codes have a maximum length of 13 subpulses. Codes with length greater than this are typically used; they are called *pseudonoise codes* because their frequency spectrum is similar to that of noise. Codes selected by the experimenter can be programmed into the VAX, allowing flexibility in performance trade-offs; typically, the same code is used for both transmit and receive.

Demodulation of the received signal is performed through *autocorrelation*, where the correlation process is based on Equation (12):

$$\phi_i(\tau) = \int_{\tau}^{(i+1)\tau} dt \chi(t)BPC(t+\tau) \quad (12)$$

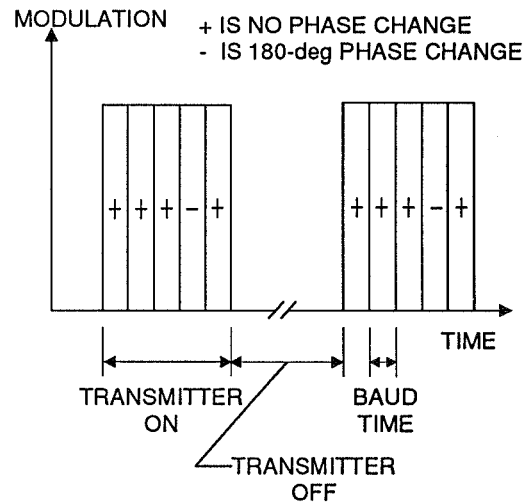


Figure 24. Transmitter Modulation

where

- $\phi_i(\tau)$ = correlated output
- BPC* = transmitted binary phase code
- $x(t)$ = echo signal

In this process, one sample of the incoming code is multiplied by one subpulse or element of the transmitted or reference code and then accumulated; this is done for each element in the code (N multiplications). The calculation is repeated with the received signal advancing one subpulse with each sample time. When the incoming signal ($x(t)$) matches the transmitted code (*BPC*) at each of N sample times, the correlator output ($\phi_i(\tau)$) reaches a maximum. An example of the correlation process is shown in Table 10, and this is shown in graphical format in Figure 25 (the code shown is not actually used; the real codes are much longer).

At the maximum, a signal voltage gain equal to the code length N has been produced. The signal power gain is N^2 and the noise gain is about $N \times \{\text{noise power}\}$, so an improvement in signal-to-noise ratio (a figure of merit of the receiving system) equal to the code length occurs, as in Equation (13):

$$SNR = \frac{N^2 \times \text{signal voltage}}{N \times \text{noise power}} = N \tag{13}$$

where

- SNR = signal-to-noise ratio of received signal
- N = pseudonoise code length

Table 10. Pseudonoise Code Example

Sample time	Transmitted code					Correlator out
	+	+	+	-	+	
t_0	0	0	0	0	0	0
$t_0 + t_r$	+	0	0	0	0	+1
$t_0 + 2t_r$	-	+	0	0	0	0
$t_0 + 3t_r$	+	-	+	0	0	+1
$t_0 + 4t_r$	+	+	-	+	0	0
$t_0 + 5t_r$	+	+	+	-	+	+5
$t_0 + 6t_r$	0	+	+	+	-	0
$t_0 + 7t_r$	0	0	+	+	+	+1
$t_0 + 8t_r$	0	0	0	+	+	0
$t_0 + 9t_r$	0	0	0	0	+	+1
$t_0 + 10t_r$	0	0	0	0	0	0

By repeating this entire correlation process at incrementally greater time delays, data from a range of radar depths (the difference between limb and subradar point) can be gathered to provide information on the entire surface of the object.

In the early 1960s at the beginning of radar investigations, baud times of 60 or 70 μs were used. As technology improved, the times grew shorter, increasing ranging resolution. In the 1970s, 6 μs were used for baud length, and in 1986 1 or 2 μs were used. The resolution obtainable from a 1- μs range gate size is 150 m.

In the Goldstone radar, the VAX downloads the code to the pseudonoise generator of the DAS. The pseudonoise generator also uses the Frequency and Time Subsystem's 5-MHz and 40-MHz stable frequency references to generate the low-level transmit waveform, which is then sent to the Transmitter Subsystem for amplification. The code is also sent digitally to the Correlator/Accumulator for range correlation of the received signal. The baud that sets the minimum range gate size is selectable and can be as short as 125 ns. The pseudonoise code and code length are also selectable.

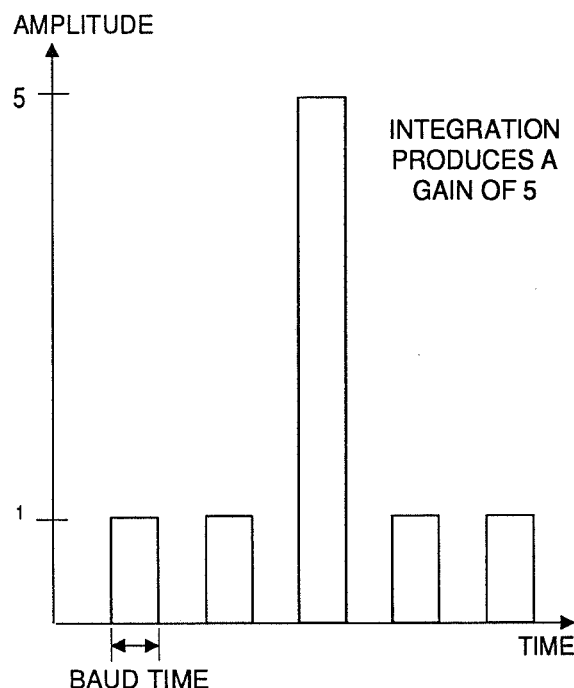


Figure 25. Autocorrelation

IV.6.6 Frequency Hopping

The technique of transmitter frequency hopping (see also Subsection IV.2.1) is used to reduce the effects of noise; the frequency hopping signal is generated in the DAS. Upon reception, the power spectra of the echoes are Fourier transformed as usual, but the returns corresponding to the different transmitted frequencies are subtracted. A two-hop, or a four-hop sequence can be used.

The selected frequency hopping sequence is programmed into the VAX 11/780. A stable clock from the Frequency and Time Subsystem along with hopping profiles sent from the VAX are used by the DAS Frequency Hopper Module to generate the frequency hopping signals. The resultant low-level transmit waveform is output by the Frequency Hopper Module to the Exciter/Transmitter.

IV.6.7 Signal Processing

IV.6.7.1 Low-Pass and Band-Pass Filtering

The signal voltages from the complex mixers (Subsection IV.6.3) must be limited in bandwidth before passing to the analog-to-digital converters. If this is not done, high-

frequency components in the signal could cause unwanted responses, called aliases, in the data. Also, noise and any spurious signals are reduced by low-pass or band-pass filtering. In the binary phase-coded and continuous-wave medium-bandwidth modes, low-pass filtering is performed, while in the continuous-wave narrow-band mode, low-pass or band-pass filtering can be used.

IV.6.7.2 Analog-to-Digital Conversion

The baseband signal output of the complex mixers is analog voltages. To take advantage of high-speed digital processing capability, these signals must be converted to a form suitable for use with digital hardware. The analog-to-digital converters perform this interfacing function. The analog-to-digital converters accept as input the complex mixer outputs; there is one analog-to-digital converter for I form and one for Q.

An important parameter for the converters is the sample rate or time between successive conversions. The sample rate and number of available channels for analog-to-digital conversion vary with the mode of operation and are shown in Table 9. The sampling time must be at least fast enough to match the transmitter baud time in binary phase-coded (ranging) mode. Generally, the sample rate must be at least twice the desired bandwidth to avoid false signals (aliasing) in the data. If the sample rate exceeds this minimum, the signal is oversampled. Since this is an I-Q system, the sampling rate has to be made just equal to the bandwidth.

The number of available channels for analog-to-digital conversion varies depending on the system configuration. In the continuous-wave narrow-band mode, the analog-to-digital converter used is the DEC LPA-11; up to three channels (I-Q pairs) of filtering/analog-to-digital conversion are simultaneously available. Tristatic operation uses three channels. In the continuous-wave medium-bandwidth mode, two channels of analog-to-digital conversion are available; in the binary phase-coded mode, up to four channels of analog-to-digital conversion can operate simultaneously.

An alternative signal path from the complex mixers to personal-computer-based analog-to-digital converter units is available. The flexibility for such connections is built into the Receiving and Data Acquisition Subsystems.

IV.6.7.3 Range Gate Processing

A *range gate* passes a signal from one range, or time delay, and rejects all others. Range gates provide discrimination in distance by virtue of the fact that different areas on the planet have different round-trip time delays. Range gate processing is done only in the binary phase-coded mode of operation. This is the only mode that has the proper transmitter modulation to obtain accurate range information. The sampling rate of this mode is 40 MHz. The subpulse width can be relatively short and this modulation requires a wide bandwidth. There can be up to 256 range gates. The groups of 256 range gates can be chained together.

IV.6.7.4 Doppler Processing

The digitized data from the analog-to-digital converters are voltage samples in the time domain. Mathematical computation must be done on the time samples to transform them into the frequency domain; the calculation (Equation (14)) is based on the Continuous Fourier Transform:

$$X(f) = \int_{-\infty}^{\infty} e^{-j2\pi ft} x(t) dt \quad (14)$$

where

$$\begin{aligned} X(f) &= \text{transform value at frequency } f \\ x(t) &= \text{time domain signal} \end{aligned}$$

From this, the Discrete Fourier Transform (DFT) is derived:

$$X(k) = \sum_{n=0}^{N-1} x(n) e^{-j2\pi \frac{nk}{N}} \quad (15)$$

where

$$\begin{aligned} X(k) &= k\text{th filter coefficient, } k \text{ varies from } 0 \text{ to } N-1 \\ N &= \text{number of time samples and number of frequency bins} \\ x(n) &= \text{discretely sampled time domain signal} \\ n &= \text{discrete sample number} \end{aligned}$$

For each filter k , the magnitude of Equation (15) can be calculated to give the frequency distribution of the radar echo. For a 1000-filter DFT, 1000 time samples are required and $N = 1000$.

Calculating the DTF is a matter of considerable practical significance: the calculations are so numerous that those required for some solar system targets cannot be performed in real time, even with relatively fast computational hardware. Algorithms that reduce the amount of calculation have been developed and are known as the Fast Fourier Transform (FFT). Transforms are usually specified in terms of the number of sample points N taken to form one frequency spectrum. The number of calculations needed to do this is $(N - 1)^2$ complex multiplications and $N \times (N - 1)$ additions. This is on the order of N^2 multiplications and additions. Using the FFT, only $N \log_2 N$ are required. The FFT divides the overall calculation into elemental units known as butterflies (Figure 26), which are implemented in the array processor.

The result of the computation is a set of numbers or filters that contains the amount of energy present at that particular frequency. The interpretation of these results is complicated in that this information is used with the ranging and polarization data to form a more complete view of the radar scattering function of the object.

A dedicated array processor is used because of the large number of calculations that must be done in real time. The continuous-wave narrow-band mode uses the LPA-11 analog-to-digital converters for sampling; the data then can be sent to the VAX for recording or to the array processor for spectral analysis. In the continuous-wave medium-bandwidth mode, the right- and left-circular polarization components are correlated in the complex digital correlators. These data are passed to the array processor for FFT computations.

In the binary phase-coded mode after analog-to-digital conversion, the signals are autocorrelated in the correlators using the pseudonoise ranging codes and then sent to the array processor for floating-point spectral computations. Floating-point processors can handle a wide range of magnitudes. The results are sent to the VAX for recording and display. If the amount of throughput required exceeds the processing rate of the system, the digitized voltage samples may be stored for later processing.

IV.6.8 Data Display

Scientific data can be displayed in real time in the pedestal by patching intermediate frequencies of the receiver to a spectrum analyzer, which measures distribution of signal energy in the frequency domain. Real-time display of the digitally processed frequency spectrum of the signal is also available on a computer screen at the pedestal. Very weak signals may require extensive computer processing before they are visible at all.

IV.6.9 Data Recording

IV.6.9.1 VAX

In the continuous-wave narrow-band mode, the VAX 11/780 monitor and control computer receives digitized scientific data from the LPA-11 computer or processed frequency spectra data from the array processor and records them on hard disk or tape for later study. CW medium-band spectral data that have been processed by the array processor are sent to the VAX for recording. When performing ranging measurements in binary phase-coded mode, the array processor outputs delay-Doppler data to the VAX for recording. During bistatic or tristatic operation using the Venus and/or Mars Stations, the signal is sent as a 50-MHz IF to the centralized equipment in the 70-m antenna pedestal. After analog-to-digital conversion at the radar control room, the digital data are passed to array processors and then to the VAX for recording. The VAX records on 6250-bit-per-inch magnetic computer tape or a 600-Mbyte hard disk drive. Analysis of the data can take place either at JPL or at the home institution of the principal investigator (Figure 27).

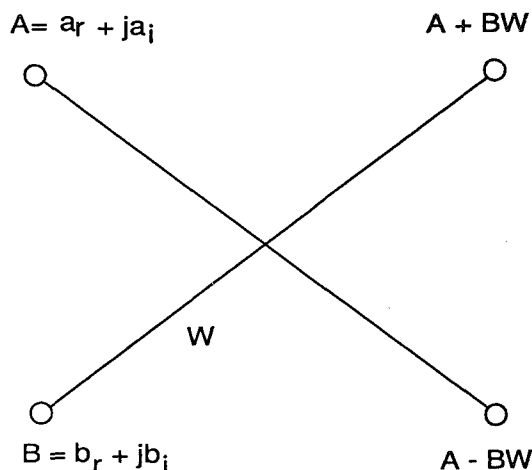


Figure 26. Butterfly



Figure 27. *Data Reduction and Analysis at JPL*

IV.6.9.2 Personal Computer

An alternative signal processing path to the LPA-11 and VAX is possible. Signals may be patched into a personal computer (PC) or custom signal processing hardware. This allows flexibility in the digital signal processing hardware and software and provides compatibility with the IBM PC format. This also enables data to be recorded on a 3.5-in. or 5.25-in. disk in a file format compatible with either MS-DOS or Macintosh personal computers. As of this writing, the PC-supported configuration is similar to the VAX CW narrow-bandwidth mode, with a bandwidth of about 150 kHz.

IV.7 Frequency and Time References

The Deep Space Network requires stable frequency and time references for spacecraft navigation and communication and so supplies these same essential references to the GSSR through the DSN Frequency and Time Subsystem. The references are hydrogen masers and have a time stability of several parts in 10^{15} ; they depend for their accuracy on the stability of the hydrogen-atom resonance.

The Frequency and Time Subsystem is located at an environmentally controlled area of the DSN Signal Processing Center. Coaxial cable is used to carry the references in the form of 5-MHz and 100-MHz signals to the GSSR Reference Generator Module in the pedestal; this module creates additional frequencies of 10 MHz, 20 MHz, 50 MHz,

100 MHz, and 125 MHz. The signals are then connected to the Reference Distribution Module from which they are distributed to radar subsystems, including the Exciter, Receiver, and Data Acquisition Subsystems.

Another reference output of the Deep Space Network Frequency and Time Subsystem is the time of day. The time of day in 24-hour Coordinated Universal Time format is fed to the Data Acquisition Subsystem and VAX 11/780 configuration control computer in the pedestal.

The frequency and time references of a planetary radar instrument have much more stringent accuracy requirements than those for most ground-based or airborne radars because of the need for precise measurement of the Doppler frequency shift, from which relative motion of the target can be determined. Knowledge of this relative motion permits refinements to the orbit determination of solar system objects.

Each subsystem of a planetary radar has its unique requirements for frequency or time stability, beginning with the transmitter, which requires stable frequency of the transmitted signal. The radar receiver requires stable frequencies as well, for the fixed and variable local oscillators. These two requirements are the most demanding. Timing of the pseudonoise code generation on transmit and timing of the analog-to-digital converters that sample the received signal are critical in the digital Data Acquisition Subsystem. Because the Earth and the targets are in relative motion and the beam of the antenna is very narrow, the antenna pointing must be continually adjusted to keep the antenna precisely aimed at the target. Thus the antenna pointing system requires a reasonably accurate time-of-day reference.

High stability of the transmitter frequency over the time of one radar transmit-receive cycle is essential. This round-trip at the speed of light varies directly with distance to the object. When at closest approach, targets vary in range from several minutes to 3 hours of round-trip light time.

One parameter that can be successfully measured by the radar system is relative motion as indicated by Doppler shift of the radar echo. In an ideal system with perfectly stable transmitter and receiver local oscillator frequencies, any change in frequency of the reflected signal could be caused only by relative motions. In an actual radar system, transmitter frequency drift during transmission might be misinterpreted as target motion. Similar problems are caused by any drift of the receiver local oscillators. While it is difficult to resolve the ambiguity between short-term transmitter frequency drift and target motion, a stable reference minimizes these problems.

The degree of stability required also relates to the occupied frequency range, or bandwidth, of the reflected signal. Consider as an example an echo received from Venus. The single-frequency transmitted signal upon reflection occupies a range of frequencies; for Venus, the echo bandwidth covers roughly 30 to 80 Hz. If the transmitter frequency changes while all else is stable, the scientific data would be degraded because the returned signal would move to incorrect frequency bins, "smearing" the data. To prevent this, the transmitted frequency should change by less than several parts in 10^{12} during the transmit time. Accuracy of this order requires extraordinary care.

Generally, stability in transmitter frequency is either long-term or short-term. Long-term stability is considered to be days, weeks or months; short-term stability is on the order of less than a second to several hours. The stringent long-term frequency stability requirement can be eased by using the same frequency reference for both the transmitted signal and the receiver local oscillators: if the transmitter carrier drifts up or down in frequency, the local oscillator will drift up or down by the same amount. Where the receiver's mixer outputs the difference between the received signal and the local oscillator, the frequency drifts tend to cancel, reducing the error. However, short-term drifts in the reference frequency (and, therefore, the receiver local oscillator) *after* the radar signal has been transmitted cannot be compensated by this arrangement. Thus, long-term variations can be made to cancel, but short-term variations cannot be compensated, and excellent short-term stability is needed.

In the Data Acquisition Subsystem, several functions sensitive to instabilities or changes in timing require stable clocks. To convert the voltages output by the Receiver Subsystem to a form suitable for use with computers, analog-to-digital converters within the DAS are used. If the clock pulse to the converters does not occur at exactly the right instant (timing *jitter*), the signal will be distorted, and the correlator output for ranging measurements will not reach its potential maximum. Also, range gate size is determined by the clock frequency, and a range error could occur as a result of clock variations; these errors are most noticeable for rapidly varying signals and small range gates.

V. The Arecibo Observatory: Performance and Comparison with the GSSR

V.1 General

There are two active planetary radar facilities: Arecibo Observatory in Puerto Rico, operated by the National Astronomy and Ionosphere Center, and the Jet Propulsion Laboratory's Goldstone Solar System Radar in California. The Arecibo Observatory is a visitor-oriented, scientific research center operated by Cornell University of Ithaca, New York, under a cooperative agreement with the National Science Foundation and with support from NASA. The observatory is the primary research facility of the National Astronomy and Ionosphere Center, and its research activities include radio astronomy, radar astronomy, and ionospheric/atmospheric science. The antenna of the radiotelescope at Arecibo is the largest filled-aperture antenna in the world. Arecibo on-site support includes a scientific staff, electronic and mechanical maintenance and development groups, a computing center, a technical library, photographic and drafting services, and living quarters for visiting scientists. At Ithaca, there are scientific and electronics support groups. The instrument was inaugurated in 1963, and since that time it has contributed much scientific knowledge of stellar radio sources, objects within the solar system, and atmospheric physics.

V.2 Location

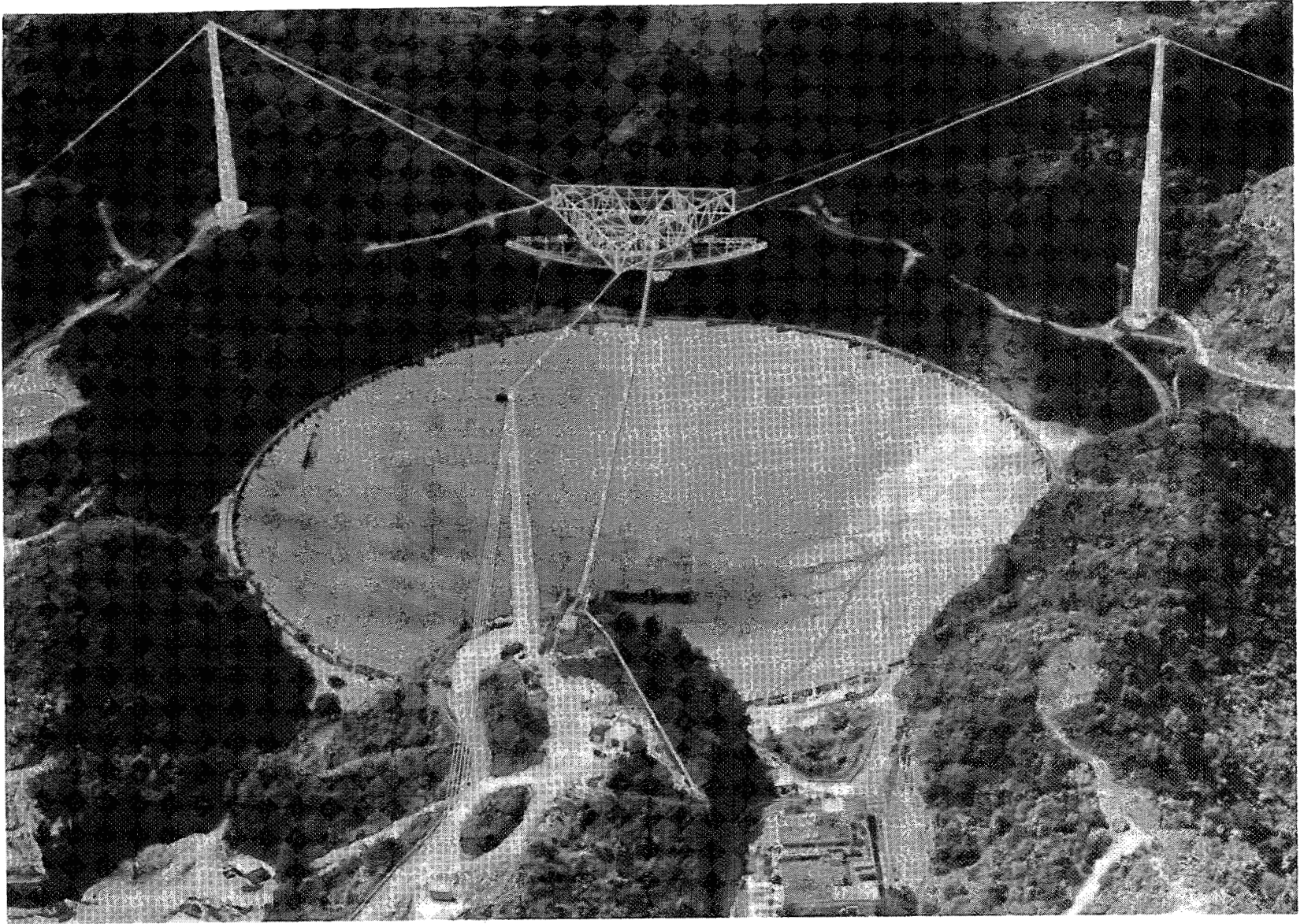
Observed from tropical latitudes, the planets pass nearly overhead, because the declination windows of their trajectories span approximately ± 23 deg. For this reason, the ideal observatory site must be located on or near the equator to maximize planetary observation time.

Puerto Rico offered the advantages of roughly the right latitude and a cooperative government. These, together with numerous natural limestone sinkholes (karst topography) that looked promising as natural bowl-shaped antenna sites, were the deciding factors in locating the radar telescope (Gordon, 1964). The chosen site is about 12 km south of Arecibo, a town on the north coast of Puerto Rico, 80 km west of San Juan (Taylor and Davis, 1987) (Figure 28).

V.3 Main Antenna

The size of a planetary radar system antenna is of great importance because the echo power that can be received from distant solar system targets depends on the square of the antenna gain. The Arecibo antenna is a fixed, 305-m spherical reflector whose surface is a section of a 265-m radius sphere (Renzetti, et al., 1988). When operated as a planetary radar instrument, an aperture of this size greatly extends the reach of the instrument into the solar system.

The main reflector is illuminated with line feeds for various frequencies from 318 to 2695 MHz plus Yagi feeds for frequencies as low as 25 MHz and, since 1990, a mini-Gregorian feed for frequencies up to 5000 MHz. The line feeds are designed to correct for spherical aberration from the main reflector. The feeds are suspended from a triangular platform about 130 m above the reflector and can be aimed at areas on the reflector such



ORIGINAL PAGE
BLACK AND WHITE PHOTOGRAPH

Figure 28. *The Arecibo Observatory*

that any feed can point anywhere within a 40-deg cone centered at the zenith. That is, beam deviation is limited to about 20 deg from zenith. The feeds are connected to structures that provide motion in elevation and azimuth and can track targets continuously for slightly less than 3 hours at declinations near 18 deg, for 2 hours at declinations of 3 deg or 33 deg, and 1 hour at declinations of 0 deg or 36 deg. The feeds can illuminate the full 305-m aperture using the 70-cm-wavelength feeds or an area as small as 137 m in diameter. At the 12.6-cm wavelength used for planetary radar, the feed is dual polarized and illuminates a 213-m-diameter area.

A signal with circular polarization is transmitted and there are two receivers for the simultaneous reception of the right- and left-circular polarization components; this capability is used in determining the surface properties of planets and asteroids.

Since the radio telescope began operation, improvements in antenna gain, transmitter power, frequency coverage, receiver noise figure, and data acquisition system capabilities have increased overall performance by a very large factor. There are plans to install in 1993 a Gregorian feed as a replacement for most of the high-frequency line feeds now used. The proposed Gregorian feed will yield higher and more uniform gains, reduced background noise, and frequency coverage from 300 MHz to 8000 MHz. A mini-Gregorian feed has been successfully installed and has proven the concept (Arecibo Observatory, 1989). This scaled-down prototype illuminates a 107-m-diameter aperture—only a portion of the entire reflector—and its pointing capability is 17 deg from zenith in any azimuth. Furthermore, a ground screen similar to an inclined fence is under construction at the perimeter of the main reflector. This screen will prevent thermal noise from the relatively warm Earth from spilling into the feed, and it will increase overall system sensitivity. Finally, the main reflector surface was recently readjusted to a root-mean-square accuracy of about 2 mm, a significant accomplishment since the total collecting area is $7 \times 10^4 \text{ m}^2$ (18 acres); an accurate surface contour maximizes antenna performance.

V.4 Transmitter and Receiver

Arecibo planetary radar operates at either of two wavelengths, 12.6 cm or 70 cm. There is a separate transmitter for each wavelength. The 12.6-cm transmitter yields a radio frequency power output of 450 kW, and the assigned frequency is 2380 MHz. There are plans for an upgrade to 1000 kW on the 12.6-cm wavelength. The continuous-wave mode is used for Doppler measurements; for ranging, the binary phase-coded continuous-wave mode is used. The 70-cm radar transmitter operates at 430.00 MHz and transmits with 2000-kW peak power and 150-kW average power.

Technology advances brought receiver performance near the level of theoretical maximum performance, and system performance can be further enhanced only by improving the antenna and the transmitter. Arecibo uses a maser as the low-noise, 2380-MHz receiver. For the other receivers, either gallium-arsenide field-effect transistors (GaAs FET) or high-electron-mobility transistor (HEMT) amplifiers are used.

V.5 Data Acquisition System

At Arecibo, the energy of the radar echo is collected by the antenna, passed to low-noise amplifiers, and downconverted to video. The samples are then passed through analog-to-digital converters. The voltage samples are usually recorded on tape, and decoding and spectral analysis are done later on, although real-time spectral analysis is also available and used routinely in radar and radio astronomy. Real-time decoding has been done at Arecibo for radar ranging experiments, and an upgraded data acquisition system now being installed will be fully capable of simultaneous acquisition of power and voltage samples, and the display of power arrays. The station at Arecibo is capable of receiver ephemeris tuning in Doppler and range, and binary phase-code generation.

For antenna pointing, real-time data taking, and on-line monitoring, a Harris H800 machine is used. For image processing, a VAX 11/750 computer has been used in the past, but this work is increasingly being done on Sun Workstations. For data analysis, a Harris H1000 computer has been used, but now the trend is towards the use of a Sun 4 file server with Sun 3 Workstations running UNIX. The workstations, H1000, and VAX are linked on an Ethernet connection, and Macintosh and IBM-compatible PC machines are available. Data are recorded on 6250 bits-per-inch tape and 6-gigabyte disks. Radar data acquisition programs permit the user to select the number of bits in recorded data, down to 1 (hard clipping) (Ostro, 1992). When the instrument is operated in the bistatic mode using the accessory antenna (Section V.6), Mark II videotape recorders are available for very long baseline interferometry (VLBI).

Various kinds of digital signal processing hardware are available to process the echo, including a configurable 2048-lag autocorrelator running at 40 MHz, a floating point array processor, a 4-channel fast sampler, and dual 32-channel filter banks with selectable filters.

V.6 Interferometry

A 30.5-m-diameter parabolic reflector to be used for bistatic operation was constructed about 11 km north of the main antenna at Higuialles. It operates at 430, 1420, and 2380 MHz and is connected to the main observatory site by a wide-band data link. The pointing coverage of this secondary antenna is comparable to that of the main antenna.

V.7 Comparison with GSSR

The GSSR shares with the Deep Space Network such major hardware as the 70-m antenna. The primary purpose of the Deep Space Network is to communicate with interplanetary spacecraft. As a consequence, the Goldstone radar can be operated as a radio and radar science instrument *only* when its capabilities are not used for spacecraft communication. The Arecibo Observatory is a scientific instrument, and, like the GSSR instrument, it is not dedicated *exclusively* to planetary radar astronomy.

Experimental procedures used in asteroid and planetary radar observations at Arecibo and Goldstone are fundamentally similar. The main differences are in the antennas and the wavelengths of the transmitted signals.

Both radars have accessory antennas on site to perform interferometry or bistatic measurements, but Goldstone can perform tristatic measurements or use the Very Large Array for interferometry. The GSSR has an azimuth–elevation mount 70-m reflector that is steerable at elevations greater than roughly 15 deg; Arecibo is a fixed, 305-m spherical reflector with steerable feeds that track at elevations greater than about 70 deg. For planetary radar operation at 12.6 cm, Arecibo’s illuminated diameter is about 213 m. Off-zenith pointing changes the gain of both antennas in a specific way. The declination of the targets that can be observed at Goldstone ranges from –35 deg to +90 deg; with Arecibo, the declination range is –1 deg 39 min to +38 deg 21 min. Goldstone has an advantage in this regard, because it can track objects in the southern declinations, and its northern declination range is much greater; also, it can track targets in Arecibo’s declination range longer than Arecibo can track them. The minimum elevation limit at Goldstone is 12 deg as determined by the Federal Aviation Administration radiation safety considerations and depends on declination; 20 deg is the usual limit. Both radars have transmitter outputs near 450 kW and transmit signals of single circular polarization and are able to simultaneously receive signals with two orthogonal polarizations. Wavelengths used are 12.6 and 70 cm for Arecibo and 3.5 and 12.9 cm for Goldstone; greater sensitivity is achieved at both sites with the shorter wavelength. Arecibo is twice as sensitive at 13 cm as Goldstone is at 3.5 cm. Since the sensitivity of the shorter wavelengths is an order of magnitude larger at both stations, these will be considered for purposes of comparison in Table 11.

Another important difference between Arecibo and Goldstone is the maximum observation time, or hour-angle span. Arecibo can observe a target for a maximum of just under 3 hours at best, while Goldstone tracking time for ecliptic objects varies from 6 to 12 hours (*Arecibo Observatory Users’ Manual*). The signal-to-noise ratio can be affected by maximum observation times because this ratio improves as the square root

Table 11. *Radar Parameters: Arecibo and Goldstone*

Radar parameter	Arecibo		Goldstone
Year	1992	1994	1992
Transmitter power, kW	450	1000	450
Peak antenna gain, dB	71.3	73.7	73.9
Nominal receiver temperature, K	34	20	22
Wavelength, cm	12.6		3.5
Antenna diameter, m	305		70
North latitude, deg (approx.)	18		35
West longitude, deg (approx.)	67		117

of the observation time. Goldstone can fill in observational gaps, or blind spots in the rotational and orbital phase, that occur when an object is out of Arecibo's view. Saturn, for example, is in southern declinations from 1988 to 1996 and thus out of Arecibo's view for approximately 8 years.

The capabilities of both instruments are important. For example, Goldstone could perform an experiment at 3.5-cm wavelength and Arecibo the same experiment at 12.6-cm or even 70-cm wavelength. Radar data from the same observed point taken at two or more wavelengths, when compared, may yield insights into the scale of surface features. Multiwavelength radar experiments are also important when studying the properties of Saturn's rings or when studying detectable surface layers (regoliths) of other planets and asteroids.

Observations at the 3.5-cm wavelength used by Goldstone are useful in absorption studies of the atmosphere of Venus. Because the higher frequency waves are absorbed more in an atmosphere than lower frequency waves, 3.5-cm-wavelength experiments may give an indication of transmission loss and therefore physical properties of the Venusian atmosphere.

VI. Future Capabilities

VI.1 Planned and Possible Upgrades to the Existing Radar Instrument

VI.1.1 General

The GSSR and the DSN share research and development and advanced technology. This synergistic arrangement avoids duplicate development efforts and simplifies maintenance and operation. In the first section of this chapter, changes of an evolutionary nature are discussed. These incremental improvements have been occurring since the beginning of planetary radar experiments in 1961 and are driven by advancing technology. The major components such as the pedestal and the antenna are assumed to be fixed.

VI.1.2 Single-Horn Switch

At the Mars Station, in monostatic mode, the 70-m antenna is used for both transmit and receive. Two feedhorns (located within the XKR cone in the antenna dish) are used at 3.5-cm wavelength—one for transmit and one for receive. The switch from transmit to receive is accomplished by physically moving (rotating) the subreflector such that its focal point aligns with the transmit or receive feedhorn. A limitation of this design is that the switching is relatively slow, requiring about 30 s. As a consequence of this delay, radar targets must be at least 4,500,000 km from Earth before they can be observed with the GSSR at 3.5-cm wavelength. However, comets and a class of objects known as near-Earth asteroids fall within this range at their closest approach to Earth, and have great importance in studies of the solar system, and perhaps to the future of human civilization (Subsection III.3.1).

An upgrade to the existing two-horn system is the single-horn switch (Figure 29), which greatly reduces the switching time; it will be implemented in 1992. The single-horn switch will not require any movement of the subreflector and will reduce the switching delay from the present 30 s to less than 1 s. This will enable objects much nearer the Earth to be observed by the radar at 3.5 cm. The single-horn switch is a complementary capability—the two-feedhorn system will remain.

The current 3.5-cm transmit path horn will be modified with a novel waveguide switch that allows the ultrahigh transmitter power and the weak echo to alternately pass through the same feedhorn. This is accomplished within the switch through two separate waveguide parts—one for the transmitter and one for the receiver. These parts are mounted in the rotor assembly of the switch, which has precision bearings to maintain mechanical integrity. The high-power transmitter arm of the switch is cooled by the same water flow that cools the rest of the transmitter. In one position, the switch directs the transmitter power to the horn, from which it radiates to the antenna; in the other position, the echo power focused on the feedhorn is separated in polarization, and the left- and right-hand circular polarization signals pass to the input of a dual-channel low-noise cryogenically cooled HEMT (high-electron-mobility transistor) amplifier. The switch moves between the two positions by a motor drive.

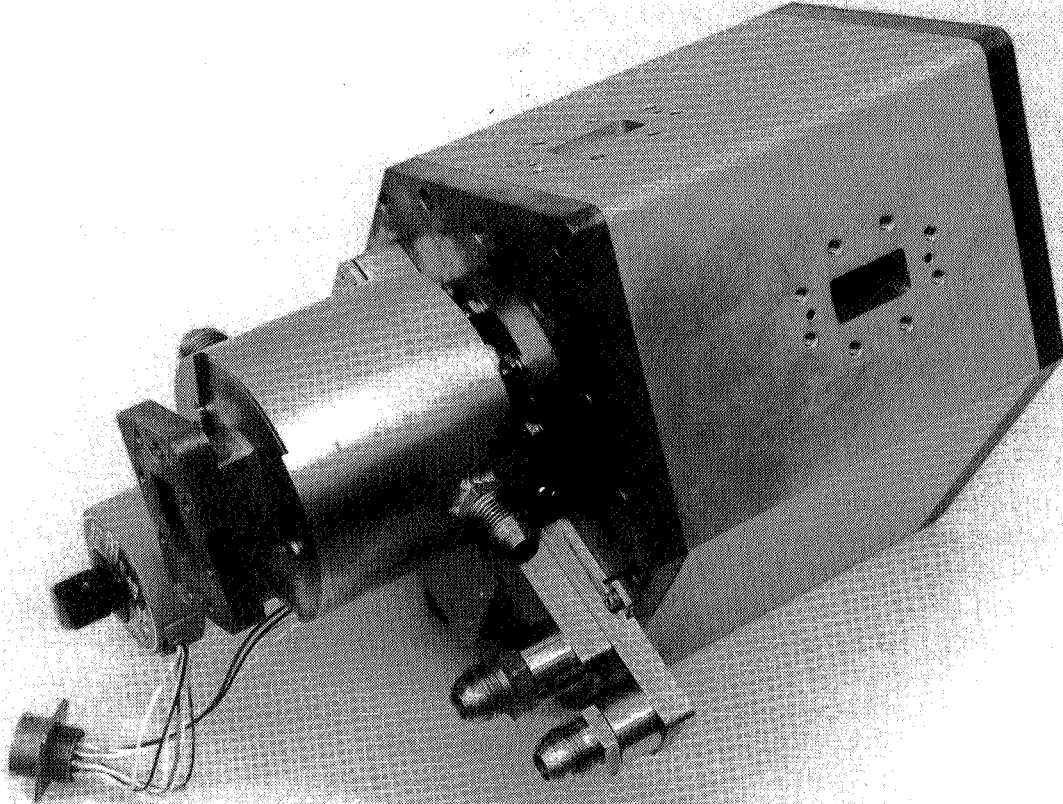


Figure 29. *Single-Horn Switch*

When using the single-horn switch, the ultrasensitive masers will not be used as the low-noise amplifier, because they are attached to the receive feedhorn. In their place will be the slightly less sensitive dual-HEMT receivers connected to the receiver side of the switch. This is a good trade-off, because the single-horn switch will be used to observe near-Earth objects, from which much stronger echoes are received.

To test the high-power switch and other transmitter components, a special test fixture called the dual-klystron test bed has been constructed at the Venus site. (The Venus site is reserved for communications technology research and development.) The test bed combines the output power of two klystrons. This combined power simulates the power levels from the Mars Station transmitter.

There is a very significant astronomical event in December 1992. The asteroid Toutatis will approach within 23.6 million km (about 10 lunar orbit radii) of the Earth, which, in astronomical terms, is a close passage. If all goes well, the single-horn switch will be fully operational, and GSSR will observe the asteroid.

VI.1.3 Megawatt Transmitter at 3.5-cm Wavelength

An upgrade that would enable the 3.5-cm radar system to transmit a 1000-kW signal has been proposed; however, funding has not been allocated to the project (Freily et al., 1992).

VI.1.4 Data Acquisition System Upgrade

A goal of the GSSR Data Acquisition Subsystem upgrade is compatibility with the Arecibo Observatory data processing system. A comparison of data from both observatories, from the same target at the same or different wavelengths, is a useful cross-check. Compatibility will expedite the evaluation of scientific data from solar system radar experiments. In particular, the intent is compatibility of user interfaces and final data interfaces.

At the Arecibo Observatory, the data processing system is being redesigned, and the continuous-wave system is now being implemented. The GSSR DAS will produce data output formats and have a user interface compatible with that of Arecibo.

The DAS at Goldstone will be upgraded so that current technology can improve system reliability and system performance. The DAS consists of both computer software and electronic hardware subsystems and is to be replaced in two stages. In the first stage, the existing continuous-wave mode DAS will be completely rebuilt. In the second stage, much of the binary phase-coded DAS used in the ranging modes will be replaced. After the two new systems have been accepted, the current systems will be removed. Also, the central processor, a VAX 11/780 computer with data storage peripherals, will be replaced.

VI.1.5 GSSR Receiver Upgrade

The DSN has developed an improved receiver, the Block-V Receiver, and will convert existing facilities to use of this unit in 1994. Because the Block-V Receivers meet all of the performance requirements imposed by GSSR, including stability and bandwidth, it will be advantageous for the GSSR to adopt this receiver.

Modifications required in the GSSR for use of the new receivers would ensure compatibility between the Block-V Receiver and the GSSR Data Acquisition Subsystem. The primary change is the addition of signal paths between the GSSR and the DSN equipment, because the Block-V Receivers will be in the Signal Processing Center. Signal paths including microwave switches are required from the GSSR 3.5-cm-wavelength dual maser and dual HEMT to the 3.5-cm-wavelength VLBI RF/IF downconverter. (All of these units are in the feedcone.) The second modification is a signal path from the Block-V Receiver output to the DAS in the pedestal.

Two modifications to the Block-V Receiver are required for GSSR use. The passband of the 12.9-cm VLBI RF/IF Downconverter would have to be increased to accommodate the radar frequency of 2320 MHz; the other modification adapts the Radio Science Processor to provide inphase and quadrature output signals at 40 Msamples/s.

The DAS would also have to be modified to accommodate digital signals at both 40 Msamples/s and 40 kwords/s. The final modification is the addition of a 50-MHz to 350-MHz upconverter at the Signal Processing Center, to allow the Block-V Receiver to receive signals from the Venus and Echo Stations during bistatic and tristatic measurements (Priest, 1992).

A preferable design that would increase flexibility of the system for investigating scientists and lessen the load on the DSN Block-V Receiver channels would include two channels of the Block-V Receiver dedicated solely to GSSR use.

If no changes are made to the GSSR receivers, the conversion to the Block-V Receiver by the DSN will not interfere with GSSR operation or any of the DSN equipment that GSSR uses.

VI.1.6 Programmable Local Oscillator

The new Programmable Local Oscillator (PLO) system will replace the existing PLO, and will improve performance of the transmitters' exciter (Subsection IV.5.5) and of the receivers.

The new PLO was designed and built at JPL and tested at JPL's Frequency Standards Test Laboratory. Two new PLO units have been installed at Goldstone at the Mars site, and one has been installed at the Venus site.

At the Mars site, the two PLOs are undergoing closed-loop testing and system integration with the existing radar. One PLO is used as the receivers' local oscillator, and the other provides the frequencies for the transmitters' exciter. At the Venus site, a new PLO has been installed and generates the required local oscillators for the receivers there. This PLO has been used during an actual tracking of the Magellan spacecraft.

The low phase noise and low jitter of this improved PLO are important in coherent radar signal processing, especially in the accurate demodulation of binary phase-coded waveforms and during interferometry (multistatic) experiments. Even with the worst case condition for phase noise, which occurs during fast slewing, the new PLO improves performance by at least a factor of 8. Typical performance is much better than this.

The new PLO outputs a frequency from 1 to 1280 MHz, a range greater than the previous design. In the receiver, frequency conversion from the low synthesized frequency to the operating frequency is done primarily by mixing, rather than using frequency multipliers. The low-frequency synthesized signal is mixed with a pure sine wave at a 3.5-cm wavelength derived from the FTS. This is significant because it avoids any frequency or phase noise, jitter, or instabilities that occur in the process of multiplication.

Two other improvements are a faster tracking rate and better resolution in setting the frequency. The local oscillator resolution is less than 1 μ Hz at the first mixer during receiver operation at the 3.5-cm wavelength (Subsection IV.5.3).

The PLO accepts the FTS 100-MHz frequency reference and the FTS time of day (to 1-ms resolution). Frequency vs. time information, in the form of truncated Chebyshev expansions of the ephemeris, is downloaded to the PLO from the monitor and control computer (now a VAX) or via a keyboard.

The new PLO system consists of two units, one containing a number-controlled oscillator (NCO) and the other a frequency conversion unit. The unit containing the NCO is based on an 80286 microcomputer. The NCO uses digital processing and a digital-to-analog converter followed by low-pass filtering to synthesize the required variable frequency. This frequency is input to a commercial radio frequency unit (Hewlett Packard 8662A/C03) that converts its input signals to output signals in the range of 1 to 1280 MHz plus the Doppler.

For the receiver local oscillators, the Hewlett Packard output signal is sent to the feedcones, where it is mixed with a 3.5-cm sine wave derived from the FTS reference and finally applied as a variable local oscillator at 8185-MHz (plus Doppler) to the first mixer. The mixer uses the 8185-MHz signal and the 8510-MHz radar echo to produce an intermediate frequency of 325 MHz.

At the Mars site, the signal from the second PLO is sent to the exciter in the pedestal. The target Doppler can be (and usually is) compensated at the exciter.

VI.2 Stand-Alone Radar System

VI.2.1 General

In the following subsections, a summary of requirements for each subsystem of an advanced planetary radar is presented. System performance is first considered as being derived from a mathematical expression containing important system parameters.

Equation (16) is the ratio of the power received from a target to the thermal noise power; it can be used as the measure of system sensitivity.

$$\frac{P_r}{P_n} = \frac{P_t G_t A_e \sigma}{k T_s (4\pi D_p^2)^2} \quad (16)$$

where

- P_r = received power, W
- P_n = system noise power, W
- P_t = transmitted power, W
- G_t = gain of the antenna while transmitting
- A_e = effective collecting area while receiving, m^2
- σ = cross-sectional area of the target, m^2
- k = Boltzmann's constant, $1.38 \times 10^{-23} \text{ W} \cdot \text{s/K}$
- T_s = effective temperature of the receiver system, K
- D_p = the distance to the target, m

With Equation (16), variables that are not functions of the radar system parameters can be eliminated; these variables include target radar cross section and distance to the target. An expression containing the terms P_t , G_t , A_e , and T_s can be considered a figure of merit for comparison with various radar systems. Wavelength influences all four parameters.

While the proposed subsystems offer a substantial increase over the sensitivity of existing subsystems, they do not represent the limit of what can be achieved within certain theoretical limits and present technology (Jurgens, 1974). Improvements can be made in all subsystems, but receivers are already near the theoretical limit of sensitivity. A stand-alone system that could be constructed within the limits of modern technology would use a 128-m-diameter fully steerable antenna, a 1600-kW transmitter operating at the 12.9-cm wavelength, a 1000-kW transmitter operating at the 3.5-cm wavelength, and an improved receiver system operating to wavelengths as short as 3 cm. Table 12 gives comparative performance parameters of this system.

When evaluating radar receiver performance for detailed studies, sky background temperature must be considered. Generally, sky background temperature is wavelength dependent, but the range of variation over the most useful range of wavelengths is not large. Therefore, only the limits defined by the antenna system, single transmitting tubes, and system temperature are considered (Jurgens, 1974).

VI.2.2 Antenna

The largest increases in sensitivity in a radar system can be attained by designing larger and more precise antenna systems: any improvement made in the antenna increases performance both in transmission and reception. The sensitivity of the system is increased by the product $G_e A_e$. Equation (17) shows that gain is related to the effective area by

Table 12. Existing and Proposed Radar Systems Performance

Parameter	Goldstone 70-m antenna		128-m antenna	
	12.9-cm wavelength	3.5-cm wavelength	12.9-cm wavelength	3.5-cm wavelength
Effective antenna area, m ²	2.7×10^3	2.5×10^3	9.0×10^3	8.4×10^3
Antenna gain ratio	2.0×10^6	2.5×10^7	6.8×10^6	8.5×10^7
Transmitted power, W	4.0×10^5	4.65×10^5	1.6×10^6	1.0×10^6
System temperature, K	20	20	15	15
Observing time, h	10.0	10.0	10.0	10.0
Relative sensitivity, dB	0.0	+8.4	+17.7	+23.5

$$G_t = \frac{4\pi A_e}{\lambda^2} \quad (17)$$

where

- G_t = transmitting antenna gain
- A_e = effective area of the receiving antenna, m^2
- λ = wavelength of radar signal, m

Total sensitivity is dependent upon the diameter of the antenna to the fourth power. For example, an increase in the diameter of the antenna by a factor of 2 provides an increase factor of 16 in the radar's sensitivity.

The transmitted wavelength must be considered in relation to the antenna's surface accuracy, which must be maintained to within a fraction of the wavelength: the shorter the wavelength, the more stringent the demand upon the precision of the antenna surface contour. This demand is especially severe at the 3.5-cm wavelength now used for radar astronomy.

The largest antenna diameter possible within structural stress limits is about 600 m (S. von Hoerner, 1967). The construction of a 600-m antenna for operation at the 3.5-cm wavelength would be a tremendously expensive enterprise. However, a steerable spherical shell supported by a fixed spherical shell solidly implanted in the Earth might be designed to provide steerage over a far greater angle than that of the present Arecibo system (Jurgens, 1974).

Below the 3-cm wavelength, thermal limits decrease the maximum possible diameter in proportion to the wavelength. Because thermal distortion of the structure occurs during daytime, considerable improvement in sensitivity is possible with nighttime operation.

Antenna structures similar to the Arecibo system could be designed with larger diameters than the present 305 m of Arecibo, and studies indicate that large, fully steerable antennas can be constructed to operate into the millimeter range (Findlay and von Hoerner, 1972).

VI.2.3 Transmitter

Equation (2) shows that the received power increases in direct proportion to the transmitted power. As of this writing, the transmitter power levels used are 465 kW at the 3.5-cm wavelength and 400 kW at the 12.9-cm wavelength. Large amounts of power at the required frequencies are most readily generated using klystrons. There are only a few types of high-power klystrons available. Therefore, unless a project is undertaken to develop completely new types of high-power tubes, higher output powers are possible only by connecting in parallel the presently available tubes.

Evans and Hagfors show that 300 kW is the maximum power output of these transmitting tubes, which operate at wavelengths as short as approximately 5 cm. Klystron amplifiers operating at wavelengths shorter than this cannot generate as much power because the tubes are smaller in size; consequently, they cannot dissipate the large amounts of waste heat. The amount of power that can be generated by the present type of klystron varies approximately inversely with the square of the frequency for wavelengths shorter than 5 cm. However, this scaling law does not apply to the *gyroklystron* type of tube. A single gyroklystron can theoretically generate up to 1 MW at 3.5-cm wavelength and 400 kW at wavelengths as short as 1 cm.

There is no technological reason why a 1600-kW transmitter could not be built for the 12.9-cm wavelength by paralleling four of the present klystrons (Jurgens, 1974). A 1000-kW transmitter could be built for the 3.5-cm wavelength by paralleling four of the available 3.5-cm klystrons. There are several design considerations in doing this:

- (1) A system of radio frequency amplitude and phase control is required to maintain the power balance among the four klystrons.
- (2) A fault protection system must be designed to disconnect the high-voltage power supply, if an electric arc or other fault occurs.
- (3) Provision must be made for cooling since the klystrons for the 12.9-cm transmitter generate more than 1600 kW of waste heat.
- (4) The weight of the transmitter should be kept to a minimum, since it would have to be placed at the back of the parabolic reflector—the antenna structure must support the amplifier's weight.
- (5) If a 1000-kW-power output level is planned for the 3.5-cm wavelength, a special waveguide would have to be designed, because this power level is beyond the power-handling capability of the present waveguide.
- (6) Several unique components would have to be designed and tested.

VI.2.4 Receiver

VI.2.4.1 Sensitivity

Modern receivers are nearly at the ideal level of performance. Little further progress can be expected in the important characteristic of receiver sensitivity, but improvements in long-term stability and increased bandwidth can be expected. It may be possible to improve sensitivity by a factor of 2 by cooling the input feed system. This would be accomplished with liquid-helium cryogenic cooling and would reduce the input feed temperature from the present 20 K to about 10 K.

VI.2.4.2 Bandwidth

The bandwidth of the received signal varies with the particular binary phase-coded modulation applied to the transmitter and with the Doppler shift from the particular target. The targets that require the greatest bandwidth are the rings of Saturn and the planet Mars. The full bandwidth of the rings of Saturn at the 3.5-cm wavelength is about 3.0 MHz. In general, to pass the rectangular figure of the binary phase-coded waveform without degradation, as much as 60 MHz of receiver bandwidth is required.

Experiments with marginally detectable targets require long integration times to establish detection. It is necessary to keep the shape of the receiver passband to 0.01% during the observation time.

VI.2.5 Data Acquisition System

The quantity of data that must be processed varies with the characteristics of the particular target, and the most difficult targets are the overspread targets Mars and the rings of Saturn. Also, as time or frequency resolution is increased, the demands upon the precision of system timing are greatly increased.

VI.2.5.1 Continuous Wave

For this mode, the rings of Saturn present the maximum data processing load. The DAS parameters discussed in this section were chosen to handle this load. If these parameters are implemented, then other targets will be easily handled by the DAS.

The proposed system operates at a 3.5-cm wavelength, and, by virtue of its greater Doppler dispersion, requires greater sampling rates than a 12.9-cm wavelength system. A large number of frequency bins are preferred for high-resolution studies, but higher resolution requires additional digital signal processing (a larger number of samples). The proposed system could resolve the echoes from the rings into as many as 1000 cells (3 kHz per cell) with a reasonable detectability in each cell. The data rate could be handled in real time using a 1-bit autocorrelator (Subsection IV.6.5.2).

A sampling rate approximately 25% above the Nyquist rate (Subsection IV.6.7.2) is preferable (Jurgens, 1974). To obtain the required resolution, at least 2000 lags—a lag is the output of a single autocorrelation calculation—would have to be computed. The accumulated correlation count at each lag would be transferred to a general-purpose digital computer at a rate fast enough to prevent overflow of the accumulator and stored on magnetic tape for further processing. Fourier transforms of autocorrelation functions would give the power spectral density (Subsection IV.6.7.4). The bandwidth and frequency resolution of this system would be more than adequate for continuous-wave observations of other targets (Jurgens, 1974). An exception is Mars, where the signal-to-noise ratio is large enough to obtain higher resolutions, thereby increasing the amount of data; however, the major goal of future Martian CW experiments would be to obtain the backscattering function (Subsection III.2.5.3) at a large angle of incidence. For this experiment, 1000 resolution elements would be adequate; very high resolution is not essential.

VI.2.5.2 Delay-Doppler Mapping

The planets Venus and Mars present the largest demand on the data processing requirements of experiments directed at surface mapping. The Martian experiment requires rapid data processing to handle the broad bandwidth of the spectra, while the Venus experiment requires a very large number of map elements. Also, in the case of Venus, the use of the interferometer roughly doubles the quantity of data that must be handled (Jurgens, 1974). When observing either Mars or Venus, another doubling of the

data acquisition rate is required since optimum acquisition principles demand that dual-polarization observations be made. Fortunately, dual-polarization mapping would be done with lower resolution, which results in a greatly reduced number of map elements.

The system requirements for delay-Doppler mapping of Venus are considered for 12.9-cm operation only. Because of atmospheric attenuation by the atmosphere of Venus, changing from 12.9-cm wavelength to 3.5-cm wavelength results in no improvement in capability. Therefore, the next stage of significant improvement depends upon the construction of a larger antenna system that can track the target for periods as long as 10 hours (Jurgens, 1974). A highly useful system configuration might employ both the 70- and 128-m antennas as a two-element interferometer. A sizeable portion of the surface of Venus can be mapped with resolution of 1 km². Near inferior conjunction, the angular coverage extends to nearly 40 deg away from the subradar point. To obtain this level of resolution, only one spectrum per range gate could be obtained in a single round-trip period. In a 10-hour observing period, only 60 spectra sets could be acquired (Jurgens, 1974).

VI.2.6 Time Stability

To satisfy time stability requirements, any short-term variations over two round-trip periods must be less than about 10% of the needed time resolution. The requirements for bistatic operation are more stringent than those for monostatic because the two receiving stations must be time synchronized to avoid drift during the reception of the echo. The highest time resolution considered here is 100 ns. The round-trip time for an experiment using such resolution is 5 to 10 minutes; therefore, a clock stability of about three parts in 10¹³ is needed. The hydrogen masers of the FTS at Goldstone achieve a time stability of several parts in 10¹⁵, which is considerably better than required.

Clock synchronization between two sites operated as an interferometer would require about the same accuracy; however, it is unlikely that the time resolution would be finer than 1 μs (Jurgens, 1974). Clock synchronization between two widely separated sites has been demonstrated using the correlation of noise signals received from quasars. The local stations at Goldstone use the FTS reference; a travelling clock can be used to synchronize other local sites. Experiments with long baselines indicated that 100-ns accuracy can now be achieved and that 10-ns synchronization should be possible using receiving systems with greater bandwidth (Jurgens, 1974). The 10-ns limit is required for certain high-resolution mapping experiments.

Certain experiments require much greater long-term accuracy than the short-term time stability required to perform a single radar observation (one round-trip light time). Experiments directed at ephemeris development, determination of the geocentric coordinate system, and testing general relativity theory are ultimately limited by the long-term stability of the master clock (Jurgens, 1974).

VI.2.7 Frequency Stability

The frequency stability requirements of a radar system are dependent directly upon the resolution requirements. Furthermore, in high-resolution radar mapping, the greatest demand in frequency stability is the lock of frequencies required to provide a stable phase at two or more stations operating as an interferometer. Radio frequency phase stabilities of 10 deg are required over a period of as long as 10 to 20 minutes. The most severe requirements are associated with the high-resolution mapping of Venus, where a frequency resolution of up to 0.003 Hz is needed at 12.9 cm wavelength. This represents a stability of eight parts in 10^{13} . Since the transmitter and receiver frequencies are synthesized from the master clock frequency generated at the FTS, the required stability is obtainable.

The frequency jitter associated with the PLO, which removes the Doppler drift associated with a moving target, usually establishes the limit on the frequency stability. However, the PLO used in the present system provides feedback to the control computer to provide not only frequency stability, but also phase stability to better than 5 deg rms at 12.9-cm wavelength. This system appears to be adequate for all radar experiments considered here, including bistatic experiments (Jurgens, 1974).

The present system uses frequency multiplication to generate the PLO. As a result, any phase jitter on the signal is also multiplied. A further improvement in system performance will be achieved by mixing (heterodyning) the PLO output with a phase-stable signal such that the sum of the frequencies is the required LO frequency, thus avoiding the multiplication of any phase jitter.

VI.2.8 Phase Stability

Phase stability is the most difficult requirement to satisfy. Random and systematic phase variations are introduced by all parts of the radar system. Systematic errors are associated with changes in the environment such as temperature or with aging of components in the system. Random phase errors may be caused by gusts of wind that stress the antenna structure and by electrical and mechanical noise in the electronic systems.

It appears that interferometry at 3.5 cm will require careful attention to the problem of achieving end-to-end phase drifts below 10 deg on the individual sites for periods at least as long as 10 to 20 min.

Phase-stability measurements on some parts of the system have not been made recently, and therefore the level of improvement cannot be determined easily. The phase stability of the basic antenna structure is difficult to measure by any technique, but simplified calculations indicate that the phase stability of the antenna system should be considerably better than that of the microwave cable system, which can change phase with temperature and pressure. (Experiments have been performed using pressure variation in the cables to correct the path length; a full 360 deg of phase change at 12.9-cm wavelength is possible. A servo pressure-control system reduced the variation by an order of magnitude. The severity of the problem depends on the length of the cable and

the frequencies that pass through it—the higher the frequency, the greater the phase shift.)

If very long cable runs are needed at high frequencies, variations can be removed by monitoring the phase path from the antenna system to the control room such that a servo system can correct the path length by introduction of a phase-variable device in the signal path.

VI.2.9 Optimal Wavelength of Operation

Although no quantitative results are given, this discussion outlines the technical considerations involved in changing to a wavelength of operation shorter than the present 3.53-cm wavelength, such as wavelengths in the 1.3-cm region. With advancing technology, it may be possible to improve system performance through the use of shorter wavelengths. The discussion would apply to the combination of GSSR transmitting and the VLA receiving on wavelengths shorter than are now used, for example.

The wavelength of operation affects sensitivity in several ways. The overall sensitivity for a given antenna is increased at shorter wavelengths (assuming the needed surface accuracy can be achieved), and the antenna beam becomes narrower (i.e., the beam spans a smaller angle). These gains in system sensitivity are offset by several effects: Antenna pointing is more critical because the pattern of the antenna spans a smaller angle; it becomes more difficult to generate the required amounts of power in the transmitter; increased losses occur in waveguides and in the atmosphere.

Choosing a shorter wavelength also affects what happens during the reflection of the signal at the target. One effect is an increase in the Doppler dispersion of the target (Equation (5)), which decreases the power density of the signal; this reduces sensitivity by $\lambda^{0.5}$. For example, if the wavelength of operation is decreased from 12.9 cm to 3.5 cm (a factor of 3.6), a further increase in sensitivity of roughly $3.6^{1.5}$ can be realized.

Another effect is a rougher appearance of all known planetary surfaces as the wavelength is made shorter. Therefore, additional echo power will be received from the limbs, widening the spectrum and reducing the power density. Whether this is an advantage or a disadvantage depends upon the experiment. From the standpoint of surface mapping, increased surface roughness may actually improve detectability if the normal to the surface is tilted away from the observer by more than about 10 deg (Jurgens, 1974). From the standpoint of detectability of a weak target, spreading the spectrum over a broader bandwidth *reduces* the power density and thus detectability. Also, less power will return from the subradar region.

In all planetary surfaces studied so far except that of Venus, a net *increase* in detectability results as the wavelength is made shorter. The dense atmosphere of Venus is an effective absorber of radio waves in the low-centimeter region. Radar data indicate that wavelengths shorter than 3.8 cm would not be particularly useful for Venus, except to study the absorption. (These absorption experiments appear to be very useful if carried out simultaneously at several wavelengths.) However, shorter wavelengths would be useful for Mercury and near-Earth asteroids.

VII. Conclusion

Since its inception in 1961, the GSSR has evolved with the DSN through the synergistic development of technology. Many of the scientific achievements of the GSSR have been of direct and indirect benefit to NASA's flight projects.

The GSSR has proven its value in tracking newly discovered near-Earth asteroids, in providing accurate measurements for experiments in gravitation and relativity, and in the accurate determination of orbits. The instrument is now sensitive enough to make the first 3.5-cm-wavelength observations of several solar system objects. Future GSSR efforts will include further polarization studies, the refinement of planetary spin periods and directions, the survey of planetary surfaces for spacecraft landing sites, and mapping areas of the planets that are beyond Arecibo's declination window. The GSSR/VLA combination can complete the full-disk radar mapping of the terrestrial planets to high resolution.

VIII. References

- Arecibo Observatory User's Manual*, Arecibo, Puerto Rico: National Astronomy and Ionosphere Center.
- Arecibo Observatory, Arecibo Observatory Annual Report, 1988-1989*, pp. 401-412, Arecibo, Puerto Rico: National Astronomy and Ionosphere Center, 1989.
- Bay, Z., "Reflection of Microwaves from the Moon," *Hungarica Acta Physica*, edited by K. Novobatzky, Vol. 1, no. 1, pp. 1-21, Budapest, 1947.
- Carpenter, R. L., and R. M. Goldstein, "Radar Observations of Mercury," *Science*, Vol. 142, no. 3590, pp. 381-382, October 18, 1963.
- Carpenter, R. L., and the Department of Astronomy, University of California, Los Angeles, "Study of Venus by cw Radar—1964 Results," *The Astronomical Journal*, Vol. 71, no. 2, pp. 142-152, March 1966.
- Carpenter, R. L., "A Radar Determination of the Rotation of Venus," *The Astronomical Journal*, Vol. 75, no. 1, pp. 61-66, February 1970.
- Corliss, W., *A History of the Deep Space Network*, Washington, D. C.: NASA Contractor Report CR-151915, November 1976.
- DeWitt, J. H. Jr., and E. K. Stodola, "Detection of Radio Signals Reflected from the Moon," *Proceedings of the I.R.E.*, Vol. 37, no 3., pp. 229-242, March 1949.
- Dyce, R. B., G. H. Pettengill, and I. I. Shapiro, "Radar Determination of the Rotations of Venus and Mercury," *The Astronomical Journal*, Vol. 72, no. 3, pp. 351-359, April 1967.
- Evans, J. V., and T. Hagfors, *Radar Astronomy*, New York: McGraw-Hill Book Company, 1968.
- Findlay, J. W., and S. von Hoerner, "A 64-meter Telescope for Millimeter Wavelength," *National Radio Astronomy Report*, April 1972.
- Freily, A. J., B. L. Conroy, D. J. Hoppe, and A. M. Bhanji, "Design Concepts of a 1-MW CW X-Band Transmit/Receive System for Planetary Radar," *IEEE Transactions on Microwave Theory and Techniques*, Vol. 40, no. 6, pp. 1047-1055, June 1992.
- Goldstein, R. M., and W. F. Gillmore, "Radar Observations of Mars," *Science*, Vol. 141, pp. 1171-1172, 1963.
- Goldstein, R. M., "Radar Observations of Jupiter," *Science*, Vol. 144, pp. 842-843, May 15, 1964a.

- Goldstein, R. M., "Radar Studies of the Planets," *Reviews of Geophysics*, Vol. 2, no. 4, pp. 579–592, November 1964b.
- Goldstein, R. M., "Preliminary Mars Radar Results," *Radio Science, Journal of Research*, Vol. 69D, no. 12, pp. 1625–1627, Paper 69D12–611, December 1965.
- Goldstein, R. M., and H. Rumsey, Jr., "A Radar Image of Venus," *Icarus*, Vol. 17, p. 699, 1972.
- Goldstein, R. M., and G. A. Morris, "Radar Observations of the Rings of Saturn," *Icarus*, Vol. 20, no. 3, pp. 260–262, January 1973.
- Goldstein, R. M., R. R. Green, G. H. Pettengill, and D. B. Campbell, "The Rings of Saturn: Two-Frequency Radar Observations," *Icarus*, Vol. 30, pp. 104–110, January 1977.
- Gordon, W. E., "Arecibo Ionospheric Observatory," *Science*, Vol. 146, pp. 26–30, October 2, 1964.
- Green, P. E., and G. H. Pettengill, "Exploring the Solar System by Radar," *Sky and Telescope*, Vol. 20, no. 1, pp. 9–14, July 1960.
- Hagfors, T., and D. B. Campbell, "Mapping of Planetary Surfaces by Radar," *Proceedings of the IEEE*, Vol. 61, no. 9, September 1973.
- Harmon, J. K., M. A. Slade, and R. S. Hudson, "Mars Radar Scattering: Arecibo/Goldstone Results at 12.6-cm and 3.5-cm Wavelengths," *Icarus*, Vol. 98, pp. 240–253, 1992.
- Jurgens, R. F., "A Survey of Ground-Based Radar Astronomical Capability Employing 64 and 128 Meter Diameter Antenna Systems at S and X Band," Pasadena, California: Jet Propulsion Laboratory, JPL Technical Document 890–44 (internal report), June 1974.
- Jurgens, R. F., "Seeing Comet IRAS with a Radar Eye," *Spaceflight*, Vol. 27, no. 5, pp. 221–224, May 1985.
- Jurgens, R. F., M. A. Slade, and S. H. Zisk, "Normal Incidence Radar Observations of the 'Stealth' South Tharsis Region," *Lunar and Planetary Science XXII*, pp. 673–674, Lunar and Planetary Science Institute, Houston, 1991.
- Kamoun, P. G., D. B. Campbell, S. J. Ostro, G. H. Pettengill, and I. I. Shapiro, "Comet Encke: Radar Detection of Nucleus," *Science*, Vol. 216, p. 293, 1982.
- Kerr, F. J., "On the Possibility of Obtaining Radar Echoes from the Sun and Planets," *Proceedings of the I.R.E.*, Vol. 40, pp. 660–666, June 1952.

- Muhleman, D. O., "Radar Scattering from Venus and the Moon," *The Astronomical Journal*, Vol. 69, no. 1, pp. 34–41, February 1964.
- Muhleman, D. O., B. J. Butler, A. W. Grossman, and M. A. Slade, "Radar Images of Mars," *Science*, Vol. 253, pp. 1508–1513, September 27, 1991.
- Ostro, S. J., K. D. Rosema, and R. F. Jurgens, "The Shape of Eros," *Icarus*, Vol. 84, pp. 334–351, 1990.
- Ostro, S. J., "Planetary Radar," to be published in *The Encyclopedia of the Solar System*, edited by Torrence Johnson and Paul Weissman, New York: Academic Press, 1992.
- Pettengill, G. H., R. B. Dyce, and I. I. Shapiro, "A Radar Determination of the Rotation of the Planet Mercury," *Nature*, Vol. 206, no. 4990, p. 1240, June 19, 1965.
- Pettengill, G. H., "A Review of Radar Studies of Planetary Surfaces," *Radio Science, Journal of Research*, Vol. 69D, no. 12, pp. 1617–1623, Paper 69D12–609, December 1965.
- Priest, P. "Goldstone Solar System Radar—Capabilities and Performance," Pasadena, California: Jet Propulsion Laboratory, JPL D-9949 (internal report), August 1, 1992.
- Reid, M. S., "Radar and the DSN," *39th Congress of the International Astronautical Federation*, Bangalore, India, IAF-88-417, pp. 1–6, October 8–15, 1988.
- Renzetti, N. A., "A History of the Deep Space Network, from Inception to January 1, 1969," Pasadena, California: Jet Propulsion Laboratory, JPL Technical Report 32-1533, September 1, 1971.
- Renzetti, N. A., T. W. Thompson, and M. A. Slade, "Relative Planetary Radar Sensitivities: Arecibo and Goldstone," in *TDA Progress Report 42-94, April–June 1988*, Pasadena, California: Jet Propulsion Laboratory, August 15, 1988.
- Sekanina, Z., "Nucleus of Comet IRAS–Araki–Alcock (1983 VII)," *The Astronomical Journal*, Vol. 95, no. 6, pp. 1876–1894, June 1988.
- Shapiro, I. I., "Radar Observations of the Planets," *Scientific American*, Vol. 219, no. 1, pp. 28–37, July 1968.
- Shapiro, I. I., M. E. Ash, R. P. Ingalls, W. B. Smith, D. B. Campbell, R. B. Dyce, R. F. Jurgens, and G. H. Pettengill, "Fourth Test of General Relativity: New Radar Result," *Physical Review Letters*, Vol. 26, no. 18, pp. 1132–1135, May 3, 1971.
- Skolnick, M. I., *Radar Handbook*, New York: McGraw-Hill Book Company, 1970.

- Slade, M. A., S. Zohar, and R. F. Jurgens, "Venus: Improved Spin Vector from Goldstone Radar Observations," *The Astronomical Journal*, Vol. 100, no. 4, pp. 1369–1374 (plates 1396–1401), October 1990.
- Slade, M. A., B. J. Butler, and D. O. Muhleman, "Mercury Radar Imaging: Evidence for Polar Ice," accepted for publication in *Science*, 1992.
- Taylor, J. H., and M. M. Davis, "Scientific Benefits of an Upgraded Arecibo Telescope," in *Proceedings of the Arecibo Upgrading Workshop, Cornell University, October 13–15, 1986*, Arecibo, Puerto Rico: National Astronomy and Ionosphere Center, 1987.
- von Hoerner, S., "Design of Large Steerable Antennas," *The Astronomical Journal*, Vol. 72, no. 1, pp. 35–47, February 1967.
- Weissman, P. R., M. F. A'Hearn, L. A. McFadden, and H. Rickman, in *Asteroids II*, edited by R. P. Binzel, T. Gehrels, and M. S. Matthews, Tucson: University of Arizona Press, pp. 920–990, 1989.
- Yeomans, D. K., "A Comet Among the Near-Earth Asteroids?" *The Astronomical Journal*, Vol. 101, no. 5, pp. 1920–1928, May 1991.
- Zisk, S. H., and P. J. Mouginiš–Mark, "Anomalous Region on Mars: Implications for Near-Surface Liquid Water," *Nature*, Vol. 288, no. 18, pp. 735–738, December 25, 1980.

IX. BIBLIOGRAPHY

IX.1 Mercury

Carpenter, R. L., and R. M. Goldstein, "Radar Observations of Mercury," *Science*, Vol. 142, no. 3590, pp. 381–382, October 18, 1963.

Goldstein, R. M., "Radio and Radar Studies of Venus and Mercury," *Radio Science*, Vol. 5, no. 2, pp. 391–395, February 1970.

Goldstein, R. M., "Mercury: Surface Features Observed During Radar Studies," *Science*, Vol. 168, no. 3930, pp. 467–469, April 24, 1970.

Goldstein, R. M., "Radar Observations of Mercury," *Astronomical Journal*, Vol. 76, no. 10, pp. 1152–1154, December 1971.

Goldstein, R. M., "Review of Surface and Atmosphere Studies of Venus and Mercury," *Icarus*, Vol. 17, pp. 571–575, December 1972.

Zohar, S., and R. M. Goldstein, "Surface Features on Mercury," *Astronomical Journal*, Vol. 79, no. 1, pp. 85–91, January 1974.

Clark, P. E., M. S. Leake, M. A. Slade, R. F. Jurgens, L. Robinett, and C. Franck, "Scattering and Altimetry Measurements from Goldstone Radar Observations of Mercury in 1987," *Bulletin Astronomical Society*, Vol. 19, pp. 863, 1987.

Clark, P. E., M. S. Leake, and R. F. Jurgens, "Goldstone Radar Observations of Mercury," in *Mercury*, edited by C. R. Chapman, F. Vilas, and M. S. Matthews, University of Arizona Press, 1988.

Slade, M. A., B. J. Butler, and D. O. Muhleman, "Mercury Radar Imaging: Evidence for Polar Ice," accepted for publication in *Science*.

Butler, B. J., D. O. Muhleman, and M. A. Slade, "Mercury: Full Disk Radar Images, and the Detection and Stability of Ice at the North Pole," submitted to *Journal of Geophysical Research—Planets*.

Harmon, J. K., and M. A. Slade, "Radar Mapping of Mercury: Full-Disk Images and Polar Anomalies," *Science*, in press, 1992.

IX.2 Venus

Victor, V. K., and R. Stevens, "Exploration of Venus by Radar," *Science*, Vol. 134, pp. 46–48, 1961.

- Muhleman, D. O., "Early Results of the 1961 JPL Venus Radar Experiment," *The Astronomical Journal*, Vol. 66, no. 7, p. 292, September 1961.
- Malling, L. R., and S. W. Golomb, "Radar Measurements of the Planet Venus," *Journal of the British Institution of Radio Engineers*, Vol. 22, no. 4, pp. 297-300, October 1961.
- Muhleman, D. O., D. B. Holdridge, and N. Block, "The Astronomical Unit Determined by Radar Reflections from Venus," *The Astronomical Journal*, Vol. 67, no. 4, pp. 191-203, May 1962.
- Muhleman, D. O., "Radar Results as Constraints on the Models of Venus," *The Astronomical Journal*, Vol. 67, no. 5, p. 277, June 1962.
- Victor, W. K., and R. Stevens, "The 1961 JPL Venus Radar Experiment," *IRE Transactions on Space Electronics and Telemetry*, pp. 85-97, June 1962.
- Rechtin, E., "Informal Remarks on the Venus Radar Experiment," in *Space Age Astronomy*, Proceedings of the International Symposium at California Institute of Technology, edited by Armin J. Deutsch and Wolfgang B. Klemperer, pp. 365-369, New York: Academic Press, 1962.
- Goldstein, R. M., and R. L. Carpenter, "Rotation of Venus: Period Estimated from Radar Measurements," *Science*, Vol. 139, no. 3558, pp. 910-911, March 8, 1963.
- Muhleman, D. O., "The Electrical Characteristics of the Atmosphere and Surface of Venus from Radar Observations," *Icarus*, Vol. 1, pp. 401-411, April 1963.
- Carpenter, R. L., "Study of Venus by CW Radar," *The Astronomical Journal*, Vol. 69, no. 1, pp. 2-11, February 1964.
- Goldstein, R. M., "Venus Characteristics by Earth-Based Radar," *The Astronomical Journal*, Vol. 69, no. 1, pp. 12-18, February 1964.
- Levy, G. S., and D. Schuster, "Further Venus Radar Polarization Experiments," *The Astronomical Journal*, Vol. 69, no. 1, pp. 29-33, February 1964.
- Muhleman, D. O., "Radar Scattering from Venus and the Moon," *The Astronomical Journal*, Vol. 69, no. 1, pp. 34-41, February 1964.
- Schuster, D., and G. S. Levy, "Faraday Rotation of Venus Radar Echoes," *The Astronomical Journal*, Vol. 69, no. 1, pp. 42-48, February 1964.
- Goldstein, R. M., "Preliminary Venus Radar Results," *Radio Science, Journal of Research*, Vol. 69D, no. 12, pp. 1623-1625, Paper 69D12-610, December 1965.
- Carpenter, R. L., "Study of Venus by CW Radar—1964 Results," *The Astronomical Journal*, Vol. 71, no. 2, pp. 142-152, March 1966.

- Goldstein, R. M., "Radar Studies of Venus," in *Moon and Planets: A Session of the Seventh International Space Science Symposium*, edited by A. Dollfus, Vienna, May 10–18, 1966, pp. 126–131, Amsterdam: North-Holland, 1967.
- Melbourne, W. G., D. O. Muhleman, and D. A. O'Handley, "Radar Determination of the Radius of Venus," *Science*, Vol. 160, pp. 987–989, May 31, 1968.
- Zohar, S., and R. M. Goldstein, "Venus Map: a Detailed Look at the Feature β ," *Nature*, Vol. 219, pp. 357–358, July 27, 1968.
- Goldstein, R. M., "Radar Time of Flight Measurements to Venus," *The Astronomical Journal*, Vol. 73, no. 9, p. 829, November 1968.
- Anderson, J. D., D. L. Cain, L. Efron, R. M. Goldstein, W. G. Melbourne, D. A. O'Handley, G. E. Pease, and R. C. Tausworthe, "The Radius of Venus as Determined by Planetary Radar and Mariner 5 Radio Tracking Data," *Journal of the Atmospheric Sciences*, Vol. 25, pp. 1171–1173, November 1968.
- Goldstein, R. M., "A Radar View of the Surface of Venus," *Proceedings of the American Philosophical Society*, Vol. 113, no. 3, pp. 224–228, June 1969.
- Carpenter, R. L., "A Radar Determination of the Rotation of Venus," *The Astronomical Journal*, Vol. 75, no. 1, pp. 61–66, February 1970.
- Goldstein, R. M., "Radio and Radar Studies of Venus and Mercury," *Radio Science*, Vol. 5, no. 2, pp. 391–395, February 1970.
- Goldstein, R. M., and H. Rumsey, Jr., "A Radar Snapshot of Venus," *Science*, Vol. 169, pp. 974–977, September 1970.
- Goldstein, R. M., "Review of Surface and Atmosphere Studies of Venus and Mercury," *Icarus*, Vol. 17, pp. 571–575, December 1972.
- Goldstein, R. M., and H. Rumsey, Jr., "A Radar Image of Venus," *Icarus*, Vol. 17, p. 699, 1972.
- Rumsey, H. C., G. A. Morris, R. R. Green, and R. M. Goldstein, "A Radar Brightness and Altitude Image of a Portion of Venus," *Icarus*, Vol. 23, no. 1, pp. 1–7, September 1974.
- Goldstein, R. M., R. R. Green, and H. C. Rumsey, "Venus Radar Images," *Journal of Geophysical Research*, Vol. 81, no. 26, pp. 4807–4817, September 10, 1976.
- Schaber, G. G., and J. M. Boyce, "Probable Distribution of Large Impact Basins on Venus: Comparison with Mercury and the Moon," in *Impact and Explosion Cratering*, edited by D. J. Roddy, R. O. Pepin, and R. B. Morrell, pp. 603–612, New York: Pergamon Press, 1977.

- Malin, M. C., and R. S. Saunders, "Surface of Venus: Evidence of Diverse Landforms from Radar Observations," *Science*, Vol. 196, pp. 987-990, May 27, 1977.
- Saunders, R. S., and M. C. Malin, "Geologic Interpretation of New Observations of the Surface of Venus," *Geophysical Research Letters*, Vol. 4, no. 11, pp. 547-550, November 1977.
- Saunders, R. S., and M. C. Malin, "Venus: Geologic Analysis of Radar Images," *Geologic Romana*, Vol. 15, pp. 507-515, 1977.
- Ward, W. R., and W. M. DeCampi, "Comments on the Venus Rotation Pole," *The Astrophysical Journal*, Vol. 230, pp. L117-L121, June 1, 1979.
- Jurgens, R. F., R. M. Goldstein, H. R. Rumsey, and R. R. Green, "Images of Venus by Three-Station Radar Interferometry—1977 Results," *Journal of Geophysical Research*, Vol. 85, no. A13, pp. 8282-8294, December 30, 1980.
- Thompson, T. W., R. S. Saunders, and D. E. Weissman, "Lunar and Venusian Radar Bright Rings," *Earth, Moon, and Planets*, Vol. 36, pp. 167-185, 1986.
- Slade, M. A., S. Zohar, and R. F. Jurgens, "Venus: Improved Spin Vector from Goldstone Radar Observations," *Lunar and Planetary Science XVIII*, pp. 932-933, Houston, Texas: Lunar and Planetary Sciences Institute Publications Office, 1987.
- Jurgens, R. F., R. E. Arvidson, J. J. Plaut, R. S. Saunders, and M. A. Slade, "New Ground-Based Radar Images of Venus," *Lunar and Planetary Science XIX*, pp. 575-576, Houston, Texas: Lunar and Planetary Sciences Institute Publications Office, 1988.
- Slade, M. A., S. Zohar, and R. F. Jurgens, "Venus Spin Vector: 1980-82 Goldstone Radar Additions," *Lunar and Planetary Science XIX*, pp. 1095-1096, Houston, Texas: Lunar and Planetary Sciences Institute Publications Office, 1988.
- Jurgens, R. F., M. A. Slade, and R. S. Saunders, "Evidence for Highly Reflecting Materials on the Surface and Subsurface of Venus," *Science*, Vol. 240, pp. 1021-1023, May 20, 1988.
- Jurgens, R. F., M. A. Slade, L. L. Robinett, S. Brokl, G. S. Downs, C. Franck, G. A. Morris, K. H. Farazian, and F. P. Chan, "High Resolution Images of Venus from Ground-Based Radar," *Geophysical Research Letters*, Vol. 15, pp. 577-580, June 1988.
- Jurgens, R. F., S. Brokl, C. Franck, G. A. Morris, L. Robinett, R. S. Saunders, and M. A. Slade, "New Evidence for Highly Reflecting Materials on the Surface of Venus from High Resolution Ground-Based Radar Images," in *Lunar and Planetary Science XIX*, pp. 577-578, Houston, Texas: Lunar and Planetary Sciences Institute Publications Office, 1988.

Jurgens, R. F., R. M. Goldstein, and W. Greiner, "Dual Polarization Radar Cross Sections of Mercury and Venus at 3.53 CM Wavelength," in *Lunar and Planetary Science XX*, pp. 492-493, Houston, Texas: Lunar and Planetary Sciences Institute Publications Office, 1989.

Jurgens, R. F., C. Franck, W. Greiner, D. Howard, L. Robinett, M. A. Slade, K. Wyss, R. E. Arvidson, and J. Plaut, "Radar Observations of Tinatin Planitia: Goldstone 1988 Observations of Venus," *Lunar and Planetary Science XXI*, pp. 593-594, Houston, Texas: Lunar and Planetary Sciences Institute Publications Office, 1990 (abstract).

Arvidson, R. E., J. J. Plaut, R. F. Jurgens, R. S. Saunders, and M. A. Slade, "Geology of Southern Guinevere Planitia, Venus, Based on Analyses of Goldstone Radar Data," *Proceedings of the 20th Lunar and Planetary Science Conference*, pp. 557-572, Houston, Texas: Lunar and Planetary Sciences Institute Publications Office, 1990.

Plaut, J. J., R. E. Arvidson, and R. F. Jurgens, "Radar Characteristics of the Equatorial Plains of Venus from Goldstone Observations: Implications for Interpretation of Magellan Data," *Geophysical Research Letters*, Vol. 17, no. 9, pp. 1357-1360, August 1990.

Slade, M. A., S. Zohar, and R. F. Jurgens, "Venus: Improved Spin Vector from Goldstone Radar Observations," *Astronomical Journal*, Vol. 100, 4, pp. 1369-1374 (plates 1396-1401), October 1990.

Tryka, D. A., D. O. Muhleman, B. Butler, G. Berge, M. A. Slade, and A. Grossman, "Correlation of Multiple Reflections from the Venus Surface with Topography," *Lunar and Planetary Sciences XXII*, pp. 1417-1418, Houston, Texas: Lunar and Planetary Sciences Publications, 1991.

IX.3 Moon

Muhleman, D. O., "Radar Scattering from Venus and the Moon," *The Astronomical Journal*, Vol. 69, no. 1, pp. 34-41, February 1964.

Higa, W. H., "Time Synchronization via Lunar Radar," *Proceedings of the IEEE*, Vol. 60, no. 5, pp. 552-557, May 1972.

Thompson, T. W., R. S. Saunders, and D. E. Weissman, "Lunar and Venusian Radar Bright Rings," *Earth, Moon, and Planets*, Vol. 36, pp. 167-185, 1986.

IX.4 Mars

Goldstein, R. M., and W. F. Gillmore, "Radar Observations of Mars," *Science*, Vol. 141, pp. 1171-1172, 1963.

- Goldstein, R. M., "Preliminary Mars Radar Results," *Radio Science*, Vol. 690, no. 12, pp. 1625-1627, Paper 69D12-611.
- Goldstein, R. M., "Mars: Radar Observations," *Science*, Vol. 150, pp. 1715-1717, December 24, 1965.
- Sagan, C., J. B. Pollack, and R. M. Goldstein, "Radar Doppler Spectroscopy of Mars. I. Elevation Differences between Bright and Dark Areas," *The Astronomical Journal*, Vol. 72, no. 1, pp. 20-34, February 1967.
- Pettengill, G. H., C. C. Counselman, L. P. Rainville, and I. I. Shapiro, "Radar Measurements of Martian Topography," *Astronomical Journal*, Vol. 74, pp. 461-482, April 1969.
- Goldstein, R. M., W. G. Melbourne, G. A. Morris, G. S. Downs, and D. A. O'Handley, "Preliminary Radar Results of Mars," *Radio Science*, Vol. 5, pp. 475-478, February 1970.
- Downs, G. S., R. M. Goldstein, R. R. Green, and G. A. Morris, "Mars Radar Observations, a Preliminary Report," *Science*, Vol. 174, pp. 1324-1327, 1971.
- Standish, E. M., Jr., "The Figure of Mars and its Effect on Radar-Ranging," *Astronomy and Astrophysics*, Vol. 26, no. 3, pp. 463-466, August 1973.
- Downs, G. S., R. M. Goldstein, R. R. Green, G. A. Morris, and P. E. Reichley, "Martian Topography and Surface Properties as Seen by Radar: The 1971 Opposition," *Icarus*, Vol. 18, pp. 8-21, 1973.
- Pettengill, G. H., I. I. Shapiro, and A. E. Rogers, "Topography and Radar Scattering Properties of Mars," *Icarus*, Vol. 18, p. 22, 1973.
- Downs, G. S., P. E. Reichley, and R. R. Green, "Radar Measurements of Martian Topography and Surface Properties: The 1971 and 1973 Oppositions," *Icarus*, Vol. 26, pp. 273-312, 1975.
- Tyler, G. L., D. B. Campbell, G. S. Downs, R. R. Green, and H. J. Moore, "Radar Characteristics of Viking 1 Landing Sites," *Science*, Vol. 193, pp. 812-815, August 27, 1976.
- Downs, G. S., R. R. Green, and P. E. Reichley, "Radar Studies of the Martian Surface at Centimeter Wavelengths: The 1975 Opposition," *Icarus*, Vol. 33, pp. 441-453, 1978.
- Schaber, G. G., "Radar, Visual and Thermal Characteristics of Mars: Rough Planar Surfaces," *Icarus*, Vol. 42, pp. 159-184, 1980.
- Roth, L. E., G. S. Downs, R. S. Saunders, and G. Schubert, "Radar Altimetry of South Tharsis, Mars," *Icarus*, Vol. 42, pp. 287-316, 1980.

- Zisk, S. H., and P. J. Mouginis-Mark, "Anomalous Region on Mars: Implications for Near-Surface Liquid Water," *Nature*, Vol. 288, no. 18, pp. 735-738, December 25, 1980.
- Downs, G. S., P. J. Mouginis-Mark, S. H. Zisk, and T. W. Thompson, "New Radar-Derived Topography for the Northern Hemisphere of Mars," *Journal of Geophysical Research*, Vol. 87, no. B12, pp. 9747-9754, November 30, 1982.
- Muhleman, D. O., B. J. Butler, A. W. Grossman, M. A. Slade, and R. F. Jurgens, "Very Large Array/Goldstone Radar Response from the Mars South Polar Residual Cap," *Fourth International Conference on Mars*, Tucson, Arizona: January 10-13, 1989 (abstract).
- Butler, B., D. Muhleman, A. Grossman, and M. Slade, "Global Radar Mapping of Mars: Surface and Subsurface," *EOS*, Vol. 70, no. 43, p. 1171, 1989.
- Ostro, S. J., R. F. Jurgens, D. K. Yeomans, E. M. Standish, and W. Greiner, "Radar Detection of Phobos," *Science*, Vol. 243, pp. 1584-1586, March 24, 1989.
- Roth, L. E., R. S. Saunders, G. S. Downs, and G. Schubert, "Radar Altimetry of Large Martian Craters," *Icarus*, Vol. 79, pp. 289-310, 1989.
- Thompson, T. W., and H. J. Moore, "A Model for Depolarized Radar Echoes from Mars," *Proceedings of the 19th Lunar and Planetary Science Conference*, pp. 409-422, Houston, Texas: Lunar and Planetary Institute, 1989.
- Zisk, S. H., M. A. Slade, R. F. Jurgens, and P. J. Mouginis-Mark, "New Goldstone Radar Measurements of Martian Volcanoes," *Transactions American Geophysical Union*, Vol. 70, no. 43, p. 1182, October 24, 1989 (abstract).
- Harmon, J. K., and M. A. Slade, "S/X-Band Radar Observations of Mars at Arecibo and Goldstone During the 1988 Opposition," *Transactions American Geophysical Union (EOS)*, Vol. 70, no. 43, p. 1183, October 24, 1989 (abstract).
- Zent, A. P., F. P. Fanale, and L. E. Roth, "Possible Martian Brines: Radar Observations and Models," *Journal of Geophysical Research*, Vol. 95, no. B9, pp. 14531-14542, August 30, 1990.
- Jurgens, R. F., S. D. Howard, M. A. Slade, L. Robinett, and D. Strobert, "A Preliminary Study of the Potential for High Resolution Parametric Radar Imaging of Mars by Ground Based Radar," *Lunar and Planetary Science XXII*, pp. 671-672, 1991 (abstract).
- Moore, H. J., T. C. O'Brien, R. F. Jurgens, M. A. Slade, and T. W. Thompson, "Preliminary Comparison of 3.5 CM and 12.6 CM Wavelength Continuous Wave Observations of Mars," *Lunar and Planetary Science XXII*, pp. 917-918, Houston, Texas: Lunar and Planetary Sciences Institute, 1991 (abstract).

Slade, M. A., L. E. Roth, and S. H. Zisk, "Mars Topography from Earth-Based Radar," Ch.2.2, in *Mars*, Space Science Series, University of Arizona, in press, 1992.

Moore, H. J., and T. W. Thompson, "A Radar-Echo Model for Mars," *Proceedings of Lunar and Planetary Science*, Vol. 21, pp. 457-472, Houston, Texas: Lunar and Planetary Institute, 1991.

Jurgens, R. F., M. A. Slade, and S. H. Zisk, "Normal Incidence Radar Observations of the 'Stealth' South Tharsis Region," *Lunar and Planetary Science XXII*, pp. 673-674, Houston, Texas: Lunar and Planetary Sciences Institute, 1991.

O'Brien, T. C., R. F. Jurgens, M. A. Slade, S. D. Howard, H. J. Moore, and T. W. Thompson, "Observations of Mars During the 1990 Opposition from the Goldstone Solar System Radar Facility at 3.53 CM Wavelength," *Lunar and Planetary Science XXII*, pp. 991-994, Houston, Texas: Lunar and Planetary Sciences Institute, 1991.

Muhleman, D. O., B. J. Butler, A. W. Grossman, and M. A. Slade, "Radar Images of Mars," *Science*, Vol. 253, pp. 1508-1513, September 27, 1991.

Zisk, S. H., P. J. Mouginis-Mark, J. M. Goldspiel, M. A. Slade, and R. F. Jurgens, "Valley Systems on Tyrrhena Patera, Mars: Earth-Based Radar Measurements of Slopes," *Icarus*, Vol. 96, pp. 226-233, 1992.

Harmon, J. K., M. A. Slade, and R. S. Hudson, "Mars Radar Scattering: Arecibo/Goldstone Results at 12.6- and 3.5-cm Wavelengths," *Icarus*, Vol. 98, pp. 240-253, 1992.

IX.5 Asteroids

Goldstein, R. M., "Radar Observations of Icarus," *Science*, Vol. 162, no. 3856, pp. 903-904, November 22, 1968.

Lieske, J. H., and G. W. Null, "Icarus and the Determination of Astronomical Constants," *The Astronomical Journal*, Vol. 74, no. 2, pp. 297-307, March 1969.

Goldstein, R. M., "Radar Observations of Icarus," *Icarus*, Vol. 10, pp. 430-431, May 1969.

Goldstein, R. M., D. B. Holdridge, and J. H. Lieske, "Minor Planets and Related Objects. XII. Radar Observations of (1685) Toro," *The Astronomical Journal*, Vol. 78, no. 6, pp. 508-509, August 1973.

Jurgens, R. F., and R. M. Goldstein, "Radar Observations at 3.5 and 12.6 CM Wavelength of Asteroid 433 Eros," *Icarus*, Vol. 28, pp. 1-15, May 1976.

Jurgens, R. F., and D. F. Bender, "Radar Detectability of Asteroids: A Survey of Opportunities for 1977 through 1987," *Icarus*, Vol. 31, pp. 483-497, 1977.

- Pettengill, G. H., and R. F. Jurgens, "Radar Observations of Asteroids," in *Asteroids*, pp. 206–211, edited by T. Gehrels, University of Arizona Press, 1979.
- Goldstein, R. M., R. F. Jurgens, and D. K. Yeomans, "Radar Observations of Apollo," *Icarus*, Vol. 48, no. 1, pp. 59–61, October 1981.
- Jurgens, R. F., "Radar Backscattering from a Rough Rotating Triaxial Ellipsoid with Applications to the Geodesy of Small Asteroids," *Icarus*, Vol. 49, pp. 97–108, 1982.
- Ostro, S. J., "Radar Observations of Asteroids and Comets," *Publications of the Astronomical Society of the Pacific*, Vol. 97, no. 596, pp. 877–884, October 1985.
- Yeomans, D. K., S. J. Ostro, and P. W. Chodas, "Radar Astrometry of Near-Earth Asteroids," *The Astronomical Journal*, Vol. 94, no. 1, pp. 189–200, July 1987.
- Ostro, S. J., R. R. Connelly, and L. Belkora, "Asteroid Shapes from Radar Echo Spectra: A New Theoretical Approach," *Icarus*, Vol. 73, no. 1, pp. 15–24, January 1988.
- Ostro, S. J., D. K. Yeomans, P. W. Chodas, R. M. Goldstein, R. F. Jurgens, and T. W. Thompson, "Radar Observations of Asteroid 1986 JK," *Icarus*, Vol. 78, no. 2, pp. 382–394, April 1989.
- Ostro, S. J., J. F. Chandler, A. A. Hine, K. D. Rosema, I. I. Shapiro, and D. K. Yeomans, "Radar Images of Asteroid 1989 PB," *Science*, Vol. 248, pp. 1523–1528, June 22, 1990.
- Ostro, S. J., K. D. Rosema, and R. F. Jurgens, "The Shape of Eros," *Icarus*, Vol. 84, pp. 334–351, 1990.
- Yeomans, D. K., "A Comet Among the Near-Earth Asteroids?" *The Astronomical Journal*, Vol. 101, no. 5, pp. 1920–1928, May 1991.
- Ostro, S. J., "Radar Reconnaissance of Near-Earth Asteroids," *International Proceedings Symposium on Radars and Lidars in Earth and Planetary Sciences*, Cannes, France, ESA SP-238, pp. 9–13, September 2–4, 1991.
- Ostro, S. J., D. B. Campbell, J. F. Chandler, I. I. Shapiro, A. A. Hine, R. Velez, R. F. Jurgens, K. D. Rosema, R. Winkler, and D. K. Yeomans, "Asteroid Radar Astrometry," *The Astronomical Journal*, Vol. 102, no. 4, pp. 1490–1502, October 1991.
- Yeomans, D. K., P. W. Chodas, M. S. Keesey, S. J. Ostro, J. F. Chandler, and I. I. Shapiro, "Asteroid and Comet Orbits Using Radar Data," *The Astronomical Journal*, Vol. 103, no. 1, pp. 303–317, January 1992.
- McLaughlin, W. I., "Radar Tracking of Asteroids," *Spaceflight*, Vol. 34, pp. 167–169, May 1992.

IX.6 Jupiter and the Galilean Satellites

Goldstein, R. M., "Radar Observations of Jupiter," *Science*, Vol. 144, pp. 842–843, May 15, 1964.

Goldstein, R. M., and G. A. Morris, "Ganymede: Observations by Radar," *Science*, Vol. 188, pp. 1211–1212, June 20, 1975.

Goldstein, R. M., and R. R. Green, "Ganymede: Radar Surface Characteristics," *Science*, Vol. 207, pp. 179–180, January 11, 1980.

Ostro, S. J., and E. M. Shoemaker, "The Extraordinary Radar Echoes from Europa, Ganymede and Callisto: A Geological Perspective," *Icarus*, Vol. 85, no. 2, pp. 335–345, June 1990.

Ostro, S. J., "Radar Properties of the Icy Galilean Satellites," *EOS Transactions, AGU*, Vol. 73, no. 14, p. 180, Spring Meeting Suppl., 1992.

IX.7 Saturn's Rings and Moons

Goldstein, R. M., and G. A. Morris, "Radar Observations of the Rings of Saturn," *Icarus*, Vol. 20, pp. 260–262, January 1973.

Goldstein, R. M., R. R. Green, G. H. Pettengill, and D. B. Campbell, "The Rings of Saturn: Two Frequency Radar Observations," *Icarus*, Vol. 30, pp. 104–110, January 1977.

Ostro, S. J., G. H. Pettengill, D. B. Campbell, and R. M. Goldstein, "Delay–Doppler Radar Observations of Saturn's Rings," *Icarus*, Vol. 49, pp. 367–381, 1982.

Muhleman, D. O., A. W. Grossmann, B. J. Butler, and M. A. Slade, "Radar Echoes from the Surface of Titan," *Transactions American Geophysical Union (EOS)*, Vol. 70, 43, p. 1182, 1989 (abstract).

Muhleman, D. O., A. W. Grossman, B. J. Butler, and M. A. Slade, "Radar Reflectivity of Titan," *Science*, Vol. 248, pp. 975–980, May 25, 1990.

IX.8 Comets

Goldstein, R. M., R. F. Jurgens, and Z. Sekanina, "A Radar Study of Comet IRAS–Araki–Alcock 1983d," *The Astronomical Journal*, Vol. 89, pp. 1745–1754, November 1984.

Jurgens, R. F., "Seeing Comet IRAS with a Radar Eye," *Spaceflight*, Vol. 27, pp. 221–224, May 1985.

Sekanina, Z., "Nucleus of Comet IRAS-Araki-Alcock (1983 VII)," *The Astronomical Journal*, Vol. 95, no. 6, pp. 1876-1894, June 1988.

Yeomans, D. K., P. W. Chodas, M. S. Keesey, S. J. Ostro, J. F. Chandler, and I. I. Shapiro, "Asteroid and Comet Orbits Using Radar Data," *The Astronomical Journal*, Vol. 103, no. 1, pp. 303-317, January 1992.

IX.9 General

Higa, W. H., "A Maser System for Radar Astronomy," in *Low Noise Electronics, Fifth Agard Avionics Panel Conference*, pp. 296-303, Oslo, July 31-August 2, 1961, edited by K. Endresen, Oxford: Pergamon Press, 1962.

Victor, W. H., "Radar Astronomy," in *Proceedings of the NASA-University Conference on Science and Technology of Space Exploration*, Chicago, IL, November 1-3, 1962, Vol. 1, pp. 95-103, Washington, D.C. : Office of Scientific and Technical Information, NASA, December 1962.

Goldstein, R. M., "Radar Investigations of the Planets," *IEEE Transactions on Military Electronics*, MIL-8, pp. 199-206, July-October 1964.

Goldstein, R. M., "Radar Studies of the Planets," *Reviews of Geophysics*, Vol. 2, no. 4, pp. 579-592, November 1964.

Tausworthe, R. C., "A Precision Planetary Range-Tracking Radar," *IEEE Transactions on Space Electronics and Telemetry*, Vol. SET-11, no. 2, pp. 78-85, June 1965.

Muhleman, D. O., R. M. Goldstein, and R. L. Carpenter, "A Review of Radar Astronomy—Part I," *IEEE Spectrum*, Vol. 2, no. 10, pp. 44-55, October 1965.

Muhleman, D. O., R. M. Goldstein, and R. L. Carpenter, "A Review of Radar Astronomy—Part II," *IEEE Spectrum*, Vol. 2, no. 11, pp. 78-89, November 1965.

Muhleman, D. O., "Relationship between the System of Astronomical Constants and the Radar Determinations of the Astronomical Unit," *Bulletin Astronomique*, Vol. XXV, pp. 153, 1965.

Muhleman, D. O., "Planetary Characteristics from Radar Observations," in *Space Science Reviews*, Vol. VI, pp. 341-364, edited by C. de Jager, Utrecht, Holland: D. Reidel Publishing, 1966.

Ostro, S. J., "Planetary Radar," to be published in *The Encyclopedia of the Solar System*, New York: Academic Press.

- Jurgens, R. F., "Earth-Based Radar Studies of Planetary Surfaces and Atmospheres," *IEEE Transactions on Geoscience and Remote Sensing*, Vol. GE-20, no. 3, pp. 293-305, July 1982.
- Reid, M. S., "Radar and the DSN," *39th Congress of the International Astronautical Federation*, Bangalore, India, Vol. IAF-88-417, pp. 1-6, October 8-15, 1988.
- Anderson, J. D., M. A. Slade, R. F. Jurgens, E. L. Lau, X. X. Newhall, and E. Myles Standish Jr., "Planetary Ranging Experiments," *IAU 5th Asian-Pacific Astronomy Meeting*, Comets and the Solar System, 20, Sydney: University of New South Wales, July 1990.
- Anderson, J. D., "Recent Developments in Solar-System Tests of General Relativity," in *Proceedings of the Sixth Marcel Grossman Meeting on General Relativity*, Kyoto, Japan, June 23-29, 1991 (abstract).
- Jurgens, R. F., M. A. Slade, and S. H. Zisk, "Normal Incidence Radar Observations of the 'Stealth' South Tharsis Region," *Lunar and Planetary Science XXII*, pp. 673-674, Houston, Texas: Lunar and Planetary Sciences Institute, 1991 (abstract).

TECHNICAL REPORT STANDARD TITLE PAGE

1. Report No. JPL Pub. 92-29		2. Government Accession No.		3. Recipient's Catalog No.	
4. Title and Subtitle The Goldstone Solar System Radar: A Science Instrument for Planetary Research				5. Report Date December 15, 1993	
				6. Performing Organization Code	
7. Author(s) J. D. Dvorsky, N. A. Renzetti, and D. E. Fulton				8. Performing Organization Report No.	
9. Performing Organization Name and Address JET PROPULSION LABORATORY California Institute of Technology 4800 Oak Grove Drive Pasadena, California 91109				10. Work Unit No.	
				11. Contract or Grant No. NAS7-918	
				13. Type of Report and Period Covered JPL Publication	
12. Sponsoring Agency Name and Address NATIONAL AERONAUTICS AND SPACE ADMINISTRATION Washington, D.C. 20546				14. Sponsoring Agency Code RE211 BG-314-40-31-30-07	
15. Supplementary Notes					
16. Abstract The Goldstone Solar System Radar (GSSR) station at NASA's Deep Space Communications Complex in California's Mojave Desert is described. A short chronological account of the GSSR's technical development and scientific discoveries is given. This is followed by a basic discussion of how information is derived from the radar echo and how the raw information can be used to increase understanding of the solar system. A moderately detailed description of the radar system is given, and the engineering performance of the radar is discussed. The operating characteristics of the Arcibo Observatory in Puerto Rico are briefly described and compared with those of the GSSR. Planned and in-process improvements to the existing radar, as well as the performance of a hypothetical 128-m-diameter antenna radar station, are described. A comprehensive bibliography of refereed scientific and engineering articles presenting results that depended on data gathered by the instrument is provided.					
17. Key Words (Selected by Author(s)) Communications Electronics and Electrical Engineering Lunar and Planetary Exploration (Advanced)			18. Distribution Statement Unclassified -- Unlimited		
19. Security Classif. (of this report) Unclassified		20. Security Classif. (of this page) Unclassified		21. No. of Pages 116	22. Price